Experimental Studies on Electrical and Lift-force Models of the Ionic Flyer with Wire-plate Electrode Configuration

CHUNG, Chor Fung

A Thesis Submitted in Partial Fulfillment
of the Requirements for the Degree of
Master of Philosophy
in
Automation and Computer-Aided Engineering

September 2007

Thesis/Assessment Committee

Professor Yam, Yeung (Chair)

Professor Li, Wen Jung (Thesis Supervisor)

Professor Liao, Wei-Hsin (Committee Member)

Professor Tung, Steve Chao-Hung (External Examiner)

Experimental Studies on Electrical and Lift-force Models of the Ionic Flyer with Wire-plate Electrode Configuration

submitted by

CHUNG Chor Fung

for the degree of Master of Philosophy
at The Chinese University of Hong Kong

Abstract

Miniaturized helicopters and planes embedded with sensors and cameras are widely used for indoor and outdoor surveillance missions. However, the mechanical vibration and the noise generated by the moving mechanical parts and aero-acoustic phenomenon can greatly degrade the video quality and thus the surveillance performance. We have developed a novel indoor flyer, called the Ionic Flyer to solve these problems. The Ionic Flyer is basically an asymmetrical capacitor, which uses high voltage (usually higher than *10kV*) to produce thrust. It works without mechanical moving parts and converts electrical energy directly to mechanical energy for propulsion.

In this thesis, firstly, the principles of the corona discharge, which govern the electrical properties of the Ionic Flyer, are reviewed in details. Then, the Ionic Flyers with wire-plate electrode configuration were designed based on the criteria of positive corona discharge. Then, experimental studies have been parametrically carried out to understand and evaluate the performance of the Ionic Flyer. The five structural parameters of the Ionic Flyer, including the electrode length (L), the gap distance between the wire-emitter and the plate-collector (d), the radius of the wire-emitter (r_w), the height of the plate-collector (h) and the enclosed area of the electrodes (A) have been investigated systematically. Finally, theoretical models of a quadratic current to voltage and a third-order lift-force to power are derived based on the experimental results. Based on our results, we proved that Ionic Flyers based on engineering requirement and optimal force/power ratio can also be designed by using the derived models.

離子飛行器的電流電壓模型與推進力模型的實驗研究

鍾楚峰

香港中文大學
自動化與計算機輔助工程學課程
哲學碩士論文

2007年8月

摘要

裝有傳感器和攝影機的微型直昇機及微型飛機早已被廣泛應用於室內和室外的監視任務。可是，機械運轉部件所產生的振動和噪音，以及氣動聲學現象往往會大幅度降低這些飛行器拍攝到的影片質素，從而影響監視性能。爲了解決上述的問題，我們研發了一種創新的室內飛行器，名爲“離子飛行器”。從結構上來說，離子飛行器相等於一個擁有非對稱電極的電容器，他使用高壓電源（通常高於十萬伏特）來產生推進力。這種飛行器沒有任何機動配件，即沒有馬達和螺旋槳，故此在飛行時不會製造噪音，而將電能直接轉化爲機械能以產生推進力。

電暈放電原理(The principles of corona discharge)是離子飛行器的電學性能的基礎，故本文將首先詳細論述正、負極電暈放電的特性。我們設計了線板電極配置的離子飛行器，並將這個飛行器置於正極電暈放電的環境下運作。透過一系列固定參數的實驗，我們了解和評估了飛行器的工作性能，並有系統地分析了它的五個結構參數（分別爲電極長度(L)，正負電極距(d)，正電極半徑(r_w)，負電極高度(h)與電極關閉面積(A)），最後根據實驗結果衍生出一個二次方電流與電壓模型和一個三次方推進力與輸入能量模型。透過這兩個模型，我們可以根據工程需求來設計離子推進器，從而得出優化的推進力與功率比。

Acknowledgements

This thesis would not be completed without the help of many people.

I would like to express my first and foremost gratitude to my Master Degree supervisor, Professor Li Wen Jung, for his tireless guidance in the past two years. He provided me creative ideas for my research work and explores my interest in the Ionic Flyer project.

I also want to thank Dr Zhang Guanglie and Mr Luo Yilun. They taught me so much from the expertise in hardware development and the approach in solving different problems in my research work. I benefited a lot from their selfless and inspiring advice. Appreciations are also due to my post-project partner Mr Chan Cheung Shing for his kind assistance in solving many mechanical problems of the Ionic Flyer project. Some of the experimental setups would not be finished without his help and advices. Although I only worked as a one-man team in this project, I never felt I am alone in doing my experiments because of their advices and invaluable discussion.

Special thanks are also due to Miss Mandy Sin, Kwok Sze Yin and Dr Qu Yanli for assisting in my grammatical proof-reading of this thesis and made the completion of this thesis possible.

I am also grateful to my colleagues Mandy Sin, Kwok Sze Yin, Gary Chow and Tony To. They played tennis with me at vacation times to help keep my life in balance. I would also like to thank all my labmates in the *CMNS* for their support to my research and for bringing me a comfortable working atmosphere.

Last but not least, I would like to thank my parents for all their trust, love, and care.

Table of Contents

List of Figures

List of Tables

Nomenclature

L	Electrode length of the Ionic Flyer
d	Gap distance between the emitter and the collector of the Ionic Flyer
h	Plate-collector height of the Ionic Flyer
r_w	Wire-emitter radius of the Ionic Flyer
K_e	Electrical environment constant of the Ionic Flyer
V	Applied voltage
I	Measured current
V_0	Onset voltage
C	Current gain
m_0	Roughness factor of the wire-emitter
δ	Air density factor
g_0	Break down field strength of air
G	Modification factor of the Peek's formula
g_v	Electric field strength at the surface of the wire during corona discharge
r_v	Effective wire radius of the wire-emitter during corona discharge
F	Lift-force acting on the Ionic Flyers
J	Force gain
V_f	Barrier voltage
P_f	Initial Power Dissipation
K_f	Lift-force environment constant

Chapter 1

Introduction

1.1 Development of Micro Indoor Surveillance Flyers

1.1.1 Overview

Helicopters and airplanes use conventional aerodynamic principles to produce lift and thrust. These principles are based on fluidic dynamics, which are governed by Newtonian physical laws and have been extensively researched and understood for almost one hundred years now [1], [2]. Aerodynamic systems are now pervasive in our lives – from commercial jets, police helicopters to hydrofoil ferries. Furthermore, another category of flying machines called the micro air vehicles (MAV) were under fast development in recent ten years based on its wide range of applications in military, civilian or commercial sectors. For most military applications, MAVs are usually installed with motion sensors and actuators. They can be remotely controlled by the users at a far away base station to carry out surveillance mission [3]. In the recent years, research activities on micro indoor flyers gain momentum worldwide, one of the reasons is that they can solve the problems of limited mobility and field of view of ground-based robots [5], [6]. With the advance development in MEMS technology, lithium-poly batteries and microprocessors, the size and weight of these MAVs can now be greatly reduced. For instance, MEMS-based wing technologies have been applied to fabricate the wing-frame and the wing-membrane of flapping-wing micro aerial vehicles [4]. Thus, there are now miniaturized helicopters and planes embedded with sensors and cameras, and are widely used for indoor surveillance

missions. In many indoor surveillance applications, small helicopters are preferred because they provide "levitated" flight, i.e., hovers in air at fixed location to provide surveillance information. In addition, unlike winged-aeroplanes, they also provide up, down, forward, and backward thrust capabilities in allowing a ground controller to position them at a desired location in space [7]. Thus, it is now possible to demonstrate autonomous micro helicopters that are able to survey an indoor environment and transmit live video broadcast to a ground station.

1.1.2 Intrinsic Problem of Surveillance Helicopters

Conventional helicopters basically contain rotating mechanical parts in order to move the air around them to create lift and thrust forces, and this may cause damages to objects or endanger human subjects around them, in additional to the noise generated by moving mechanical parts and aeroacoustic phenomenon [11]. Moreover, from a ground observer's point of view, the mechanical vibrations of a helicopter could cause extremely undesirable affects on the real-time video information transmitted to the ground station. Moreover, since the dynamic systems of helicopters are nonlinear, approximated models have usually been applied during the development of autonomous strategies. Thus, by using the conventional *IMU* (gyros or accelerometers) alone usually cannot give satisfaction results in term of stabilized and autonomous (take-off and landing) flight. [8]. Recently, a wide range of vision-based control strategies were developed to achieve autonomous hovering control, guidance control or collision avoidance (for example, [9], [10]), but the results were only suited for certain applications since those vision-based control always need to operate in designed environments.

1.2 Proposed Non-moving Parts and Noiseless Flyers

Based on the above intrinsic problems of the traditional indoor surveillance flyers, we proposed a new kind of indoor surveillance flyers that does not require any moving mechanical parts to provide thrust, and does not produce any noise i.e., it uses ionic

momentum exchange to provide lift and thrust. We refer to these flyers as Ionic Flyers. The Ionic Flyer is basically an asymmetrical capacitor which uses high voltage (usually higher than *10kV*) to produce thrust. It works without moving parts and convert electrical energy directly to mechanical energy for propulsion. The working principle is not aerodynamics but probably related to electrohydrodynamics, i.e., its exact operational principles are unknown to researchers around the world at this time to the best of our knowledge.

The idea of ions propulsion has been proposed since *1964* by *Alexander P. de Seversky*. He developed and patented an ion-propelled aircraft called the *Ionocraft* [12]. The *Ionocraft* has a wire-to-mesh electrode structure and they do not contain any mechanical moving parts. It can levitate in mid-air to certain height when a high voltage is applied to the wire-mesh electrode and achieve a lift-force/power ratio of about *0.63 gram/Watt*. Instead of using a motor and blades, *Ionocraft* create the downward air flow electrically by means of ionic discharge. *Seversky* attempted to explain the operation principle by using the "wind" generated by the ions flow. This phenomenon has been later described as the "ionic-wind" effect [13]. The Ionocraft amazed many people at that time. However, *Seversky* did not release any further information on the *Ionocraft,* either theoretical explanations or experimental data regarding the operation principles.

Based on the idea of ions propulsion that is suggested by *Seversky*, many researchers have tried to develop similar flying machines. By imitating the electrode structure of the *Ionocraft,* it is possible to demonstrate a lift-up effect. And this kind of flyers was commonly called *"Lifters"* on the internet. On the other hand, debates are raised by some scientists and hobbyists on a theory called the *Biefeld-Bown effect*, which was proposed by Dr. Biefeld and Dr. Bown around 1950s, to explain the operation principles of the *Lifters*. Currently, there is still no universally accepted explanation to the *Biefeld-Bown effect*, which cannot be explained by the laws of conventional Newtonian mechanics.

Nevertheless, due to the very simple implementation to test the *Biefeld-Bown effect* or ionic-wind effect of the *Lifters*, many amateur enthusiasts have conducted sporadic

experiments in the past five years, for example, to demonstrate a basic 'levitation flight'. Since the construction method and materials are rather simple and cheap, one only needs some balsa woods and aluminum foil that can be obtained from a supermarket easily. And they can obtain a high voltage power by modifying an old computer monitor. This makes *Lifters* become a "hot" topic to some of the flyers' hobbyists. There are some online forums discussing and sharing their recent flying experiences and experimental data (e.g., [16], [17]), but are very unsystematic, with some hypotheses formed without any theoretical basis. Investigative work of the operational principles and applications of the Lifter are now worldwide. However, as stated before, many of them are hobbyists, so that the experiments were usually performed sporadically with no clear results, since systematic analysis required knowledge on high voltage engineering and fluid mechanics, in addition to precise and professional equipments are expensive and hard to obtain. Existing research publications are also limited to some hypothesis explaining the working principles of the *Lifters* [18], [19], [20], i.e., no optimization design rules are offered by existing literature. Simply put, no autonomous *Lifters* now exist with its own onboard control/sensing circuits and power sources due to the limit experimental results and the extremely low load/power ratio of the *Lifters*.

We will refer to these flying machines, that use high voltage supply and with special designed wire-plate electrodes, as Ionic Flyers because our experimental results suggested that the lift-force is generally generated by ions. We propose to build the Hybrid Ionic Flyer (*HIF*) embedded with its own power source, control electronics and sensors, and it will provide real-time video feed to a ground station. The *HIF* will maneuver in midair using no moving mechanical part and will generate no noise. This requires the understanding of the relationship between the thrust/lift force and the input electrical power, electronics to control and regulate input energy, and energy requirement for a durable flight. Figure 1.1 explains the development procedures of the Hybrid Ionic Flyer and the works that were done in this dissertation.

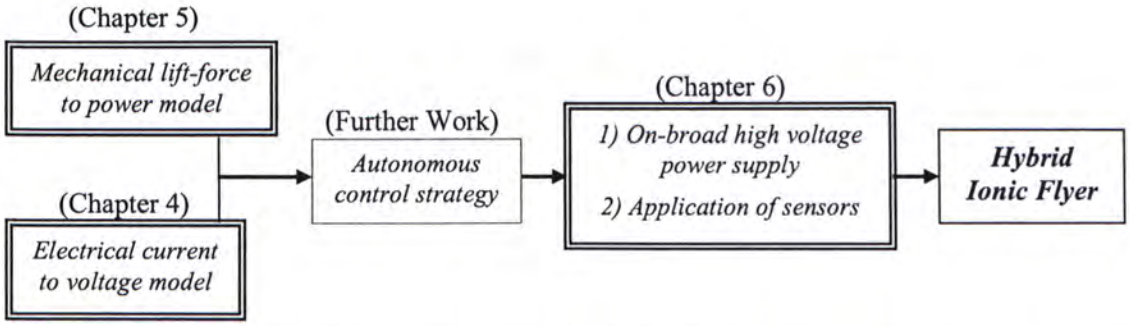

Figure 1.1: The development milestone of the Hybrid Ionic Flyer and the work done of this dissertation

Unlike helicopters that have well developed and comprehensive theories and dynamic models, there is no existing model describing the electrical and mechanical properties of the Ionic Flyer. So, formal scientific researches were done to study and evaluate the working performance of the Ionic Flyer. We have found out a very systematic explanation of the 'Ionic Flying' mechanism, and can confidently design Ionic Flyers based on engineering requirements. Moreover, our current experimental results have also successfully proved that instead of the Biefeld-Bown effect, a pure ionic momentum exchange can generally be used to explain the lift force for the Ionic Flyers. Through systematically experimental investigation on the structural parameters of the Ionic Flyer, an electrical current to voltage and a mechanical lift-force to power relationship have been developed. Based on these two models, an optimization design rule regarding the force/power ratio of the Ionic Flyers can be used to analyze the performance of the system. As far as we know, we are the first group in the world to systematically conduct conclusive experiments and explain the basic lifting force versus input electrical power.

1.3 Organization of the remaining dissertation

The remaining chapters of the dissertation are organized as follows. In Chapter 2, the architecture and some important structural parameters of the Ionic Flyers are introduced. Two proposed operational principles of the Ionic Flyers, i.e. the electrohydrodynamic

effect and the Biefeld-Bown effect are also reviewed. Chapter 3 illustrates the theory of electrical discharge. The properties of uniform field electrical breakdown are first described. Then, corona discharge which governs the electrical properties of the Ionic Flyers is briefly explained. We will analyze different properties of both positive and negative corona discharge. Thereby figure out the reason of applying positive corona discharge in the Ionic Flyers. In Chapter 4, the experimental setup in deriving the current to voltage relationship of the Ionic Flyers has been illustrated. Based on the experimental results, a basic quadric *I-V* equation is derived. We will investigate the relationship between the structural parameters of the Ionic Flyers and the *I-V* model. A general *I-V* model will be formulated accordingly. In Chapter 5, the lift-force to input power relationship of the Ionic Flyers is discussed. We will explain the experimental setup which is used to determine the relationship between the lift-force acting on the Ionic Flyers and the corresponding power input. A linear equation regarding the lift-force to applied voltage (*F-V*) is derived. Then the lift-force model is developed based on the *F-V* equation and the *I-V* model. Analysis on the effect of the structural parameters of the Ionic Flyers is also included. The maximum force/power ratio of the Ionic Flyers under certain engineering criteria is derived based on the results of Chapter 3 and Chapter 4. Chapter 6 demonstrates experimentally the possibility of generating multi-directional force by the Ionic Flyers. A μ-IMU with an accelerometer and a Bluetooth modulus embedded is implemented to test the feasibility of applying sensor and wireless transmission on the Ionic Flyers under ultra high electric field. Chapter 7 presents a new design of the Ionic Flyer which has a single-emitter to multi-collector electrode configuration. Experimental results show that this design has a higher force/power ratio. A light-weight-high-voltage power supply was implemented by using a piezoelectric transformer. The circuit is proved feasible for activating an Ionic Flyer with designed structural parameters. These are the suggested future work for others. Finally, we present conclusions in Chapter 8.

Chapter 2

The Basic Structure of the Ionic Flyers

2.1 The Components and the Structural Parameters of the Ionic Flyers

A basic Ionic Flyer contains two primary elements that are essential for its proper functioning. They are an emitter and a collector. For the Ionic Flyers with wire-plate electrical configuration that were studied in this dissertation, the emitter is usually a thin metal wire (usually with radius less than *0.2mm*) that is connected to high voltage and the collector is typically a plate foil that is connected to ground. Insulating materials such as balsa wood is used to create the frame in order to isolate the wire-emitter and the plate-collector. Thus, basic Ionic Flyers can be considered as capacitors with two asymmetrical electrodes and using the air as the dielectric material. The power input should be in high voltage in order to create a high electric field between the asymmetrical electrodes and constitute the corona discharge and this is the essential requirements for the operation of the Ionic Flyers. There are two kinds of corona discharge, positive-type or negative-type, and they are both applicable to the Ionic Flyers. If the wire-emitter is connected to high positive voltage, the Ionic Flyers will work under positive corona discharge. If the emitter wire is connected to negative high voltage, it will work under negative corona discharge. More details on the corona discharge will be discussed in the next chapter.

Figure 2.1 illustrates the basic structure of the Ionic Flyer with the structural parameters L, d, h, r_w, A represent the electrode length (either the emitter or the collector), the gap

distance between the emitter and the collector, the collector height, the emitter radius and the electrode enclosed area (either the emitter or the collector). These structural parameters can quantitatively change the geometric size of the electrode, and therefore affect the corona discharge and the lift-force. In Chapter 4 and Chapter 5, experiments were carried out to investigate the current to voltage relationship and the lift-force to power relationship based on these structural parameters.

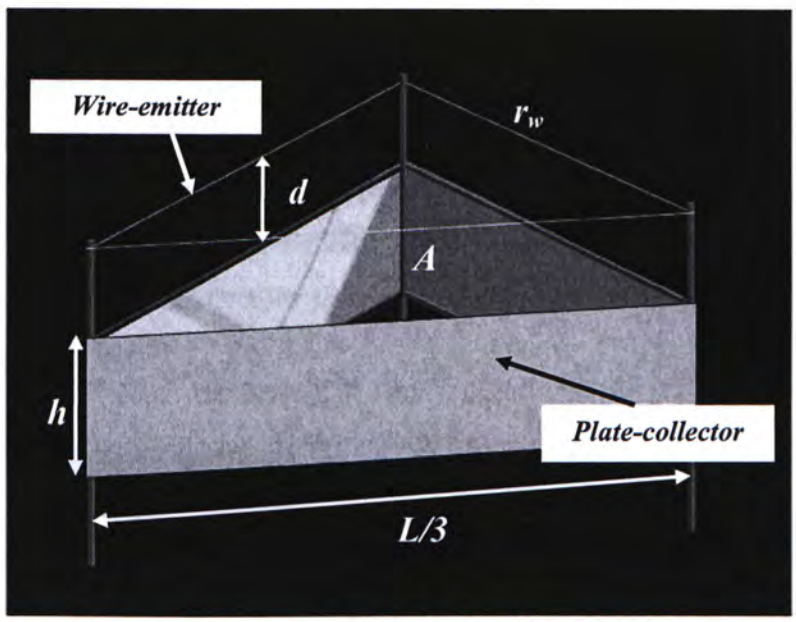

Figure 2.1: The structure of a basic Ionic Flyer with the five structural parameters: the electrode length L, the gap distance between the emitter and the collector d, the collector height h, the emitter radius r_w and the electrode enclosed area A

2.2 Proposed Operational Principles

A complete theory to explain the working principle of the Ionic Flyers is still under investigation by the scientist. There are two prepositions, the electrohydrodynamic effect and the Biefeld-Brown effect, which are described below.

2.2.1 The Electrohydrodynamic Effect

By applying a high voltage between the two electrodes of the Ionic Flyers, the electric corona discharge could occur because of the sufficiently different radii of curvature [24]. The high electric field generated by the emitter causes gaseous ionization and its partial breakdown to produce a high density of ions. As a result, ions with the same polarity of the emitter are drifted to the collector and this cause an electric current flow between the emitter and the collector. The movement of ions is probably under high-frequency collision with the electrically neutral air molecules [25]. Momentum transfer from the ions to the air can be assumed to take place. Therefore, the Coulomb force acting on the ions becomes an electric body force on the air molecules. By Newton's third law, there is an upward reaction force acts on the Ionic Flyer. Figure 2.2 illustrate the microscope view of the ions and neutral molecules under the high electric field generated by the Ionic Flyers.

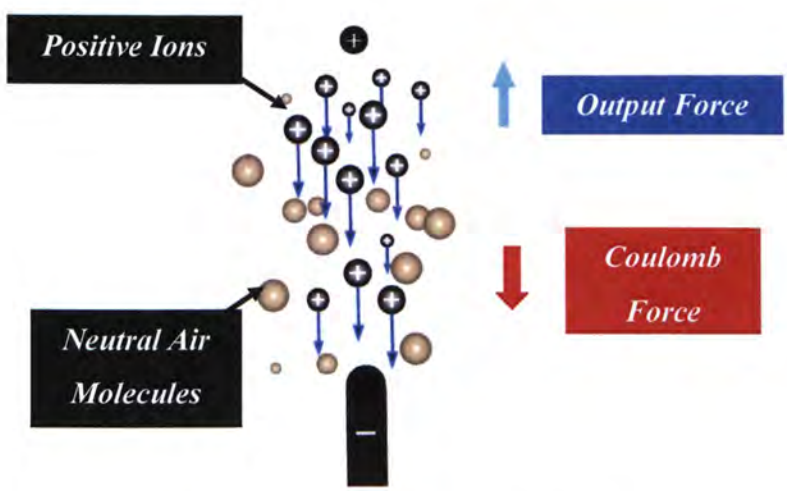

Figure 2.2: The microscopic view between the electrodes of the Ionic Flyers under positive corona discharge

2.2.2 The Biefeld-Brown Effect

The Biefeld-Brown effect is a hypothetic theory and it was proposed by Thomas Townsend Brown (USA) and Dr. Paul Alfred Biefeld (CH). They conducted high voltage experiments and discovered that asymmetrical electrodes can generate a directional force under the strong electric field. They explain such effect as a kind of antigravity effect and it cannot be explained by the conventional physics. According to the theory, there will be an induced gravitational field when a strong uneven electric field is generated by a device. The induced gravitational field can interact with the Earth's gravitational field and either increase or decrease its strength. If the induced gravitation field is in the opposite direction and its strength is stronger than the Earth's gravitational field, the device will lift up. This effect can be experimental studied by applying high voltage to a capacitor which is placed inside a plastic casing to reject the influence of electric wind. The weight of capacitor is measured to be reduced as Biefeld Bown effect exists to reduce the gravity strength on the capacitor [27]. In Chapter 6, experiments were carried out to show that the largest part of the lift-force generated by the Ionic Flyers is not based on the Biefeld-Brown principle.

Chapter 3

Overview of Corona Discharge

3.1 The Gaseous Discharge

At normal temperature and pressure, gases are excellent insulators. However, basically any gas under the indoor or outdoor environments is expected to contain a number of ions and electrons. For example, the atmosphere contains an average in the order of 1000 positive and negative ions per cm^3 because of the ultraviolet and cosmic radiation at the ground level. And the rate of ionization which maintains this number is generally in the range 2-10$cm^{-1}s^{-}$, if there are no other external radioactive substances [28].

Normally, in the absence of electric field, the production rate of these ions and electrons can be balanced by the recombination rate to maintain a constant density. If a small voltage is applied to the electrodes and producing electric field strength of about 1V/cm, the movement of the existing ions and electrons will constitute the current flowing through the electrodes. Therefore, the gas becomes an ohmic conductor, and its conductivity depends upon the rate of ion and electron production, the recombination coefficient and the mobilities [28]. As long as the current is small enough, the equilibrium of the existing charged particles can be maintained. However, if the applied voltage reaches a certain high level, the electric field strength will be strong enough to ionize the air molecules. As a result, gas discharges and electrical breakdown will occur because of the prompt increase of the ions density.

3.2 Uniform Fields, Electrical Breakdown

During gas discharges, existing electrons are accelerated and upon collisions with the neutral molecules. If the electrons gain enough energy from the electric field, which exceeds the ionization threshold, they will ionize neutral molecules during collisions and thus produce ions and additional electrons. The processes will be repeated by the additional electrons and this phenomenon is called the electron avalanche. As a result, a large density of ions and electrons will be produced. Compared to massive positive or negative ions, electrons have a much higher mobility. So by the time the electrons reach the anode, the ions are still virtually in their original positions and thus forming a space charge concentrated at the anode and taper toward the cathode. For uniform field, the space charge developed by electron avalanche is capable of constituting long streamers that lead to rapid development of electrical breakdown. The properties of uniform field electrical discharge were extensively studied by Townsend. He formulated a discharge model called "Townsend Discharge" based on his experiments to describe the avalanche of electrons or the space charges [22].

3.3 Non-uniform Fields, Corona Discharge

In uniform field and quasi-uniform field gaps, the onset of streamers usually leads to complete breakdown of the gas rapidly. However, various manifestations of luminous and audible discharges are observed long before the complete breakdown occurs in non-uniform fields. These discharges may be transient or steady state and are known as "coronas". Corona discharge is a low energy electrical discharge with non-thermal ionization that takes place in the pressure close to the atmospheric, if at least one of the electrodes is of low radius of curvature, such as a wire with small radius in order to generate a non-uniform electric field. This kind of discharge is self-sustained and no external energy, other than the electrical, is needed to sustain the ionization processes and to maintain the current flow. Light emission and a hissing sound are the manifestations of corona discharge and its particular characteristics are determined by the shape of the

electrodes, the polarity, the size of the gap, and the nature of the gas. In the following, we will discuss two types of corona discharge: the positive-type and the negative-type, and they govern two different types of operation of the Ionic Flyers

3.3.1 Positive Corona Discharge

For positive corona discharge, the wire-emitter of the Ionic Flyer is connected to positive high voltage. The ionization by electron collision takes place in the high field region near the wire-emitter. Electrons because of their higher mobility will be readily drawn into the plate-collector, leaving the positive ions behind. The ions will cause a reduction in the field strength close to the wire-emitter and at the same time will increase the field further away from it. Figure 3.1 (b) illustrate the field distortion caused by the positive ions. The dotted curve represents the original undistorted field across the gap while the solid curve shows the distorted field. The distortion causes the high field region further move into the gap (i.e. toward the collector) and extends the region for ionization. As a result, the positive ions dominate the space charged particles and constitute a direction flow from the wire-emitter to the plate-collector and produce the corona current.

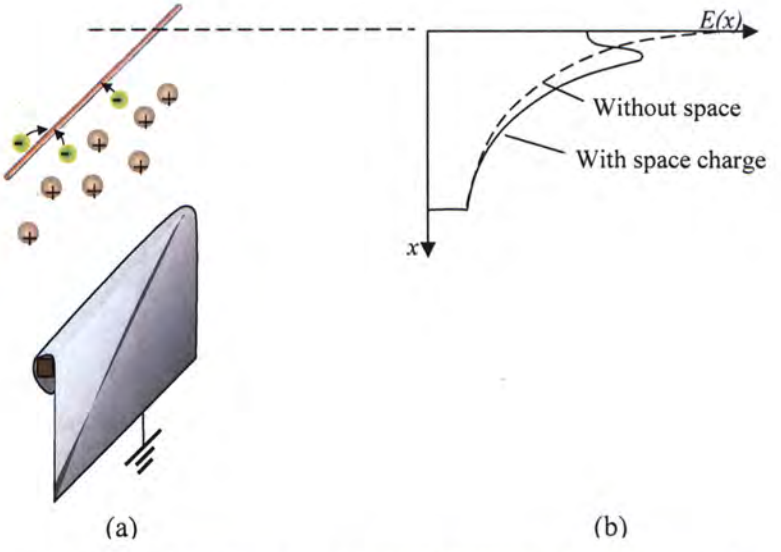

Figure 3.1: (a) Space charge build-up between the positive wire-emitter and the ground plate-collector. (b) Electric field distortion by space charge

3.3.2 Negative Corona Discharge

For negative corona discharge, the wire-emitter of the Ionic Flyer is connected to negative high voltage. The electrons are repelled into the low field region that they cannot gain enough energy for ionization. The electrons drift with a relatively low speed and become attach to the gas molecules, forming slowing moving negative ions and trend to hold back the positive ions which remain in the space between the electrodes (see Figure 3.2 (a)). In the vicinity of the wire-emitter the field is grossly enhanced, but the ionization region is significantly reduced (see Figure 3.2 (b)). This effect terminates ionization and once the ionization ceases, the applied field sweeps away the negative and positive ions space charge from the vicinity of the electrodes. The effect starts again after the clearing time for the space charge. Because this recovery is only dependent on the time the negative ions need to reach the positive electrode, corona is observed as bursts of ionization that are equidistant in time.

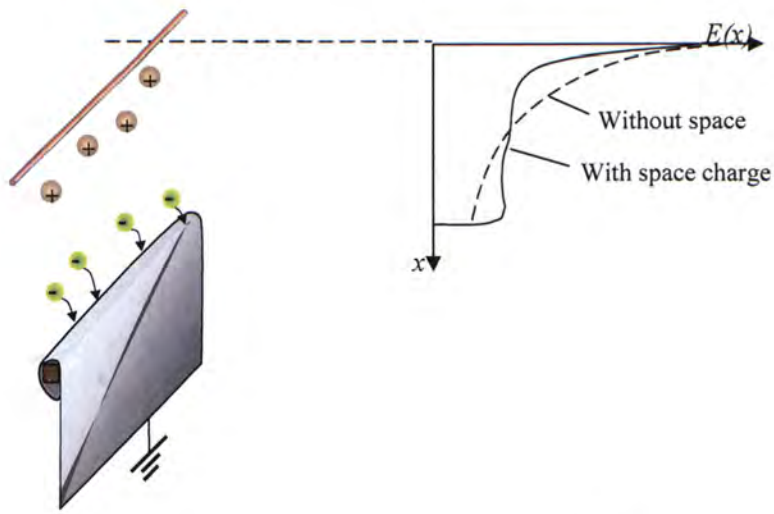

(a) (b)

Figure 3.2: (a) Space charge build-up between the negative wire-emitter and the ground plate-collector. (b) Electric field distortion by space charge

3.4 Conclusion

In both for positive and negative coronas, positive space charge near the emitter wire dominates the discharge because the mobility of electrons is much higher than that of positive ions. Two regions are formed between the wire-emitter and the plate-collector: 1) the ionization region which is confined to a small cylindrical volume around the wire and is found to be larger for positive corona; 2) the charge accumulation region, which is the remaindering region in inter-electrode gap, in which the ions drift due to the electric field without additional ionization. The observations of the current output for positive and corona discharges are as follows: 1) during positive corona there is always a significant current flowing due to the motion of positive ions, the process is relatively continuous and steady; and 2) for negative pulsed corona, the current is due to electron motion and the discharge occurs in form of discrete pulses with very little current flowing between pulses, the process is intermittent [26], [22].

Thus, Ionic Flyers work better under positive corona is based on the following criteria:

1. a directional flow of positive ions dominates the charge flow
2. the process is continuous and smooth

Chapter 4

Electrical Current-Voltage Model

The electrical properties of the Ionic Flyers are the first concern in this dissertation. Instead of studying or modeling the complex electric field distribution between the electrodes, we focused on the current to voltage relationship of the Ionic Flyers. Since in electrical and mechatronic systems, the current to voltage characteristic is one of the most basic but important property for analyzing the power consumption and also the efficiency of the system. As discussed in the previous chapter, the electrodes of the Ionic Flyers have substantially different radii of curvatures and electric corona discharge usually occurs when the applied voltage reaches certain high level. In the case of positive corona, the repeating generation and transportation of positive ions between the emitter and collector constitutes a continuous current flow. Thus, an electrical model was sought for the Ionic Flyers by obtaining the current to voltage relationship. Actually, the current waveform commonly shows a "saw-tooth" shape with an average DC level and the oscillation of the current is usually in very high frequency of about *1 MHz* [26]. In most studies regarding the current to voltage characteristic of corona discharge, the mean total current is usually adopted for analysis and it can be obtained directly by using some common measurement equipments like an ammeter or a multimeter.

4.1 Experimental Setup and Measurement

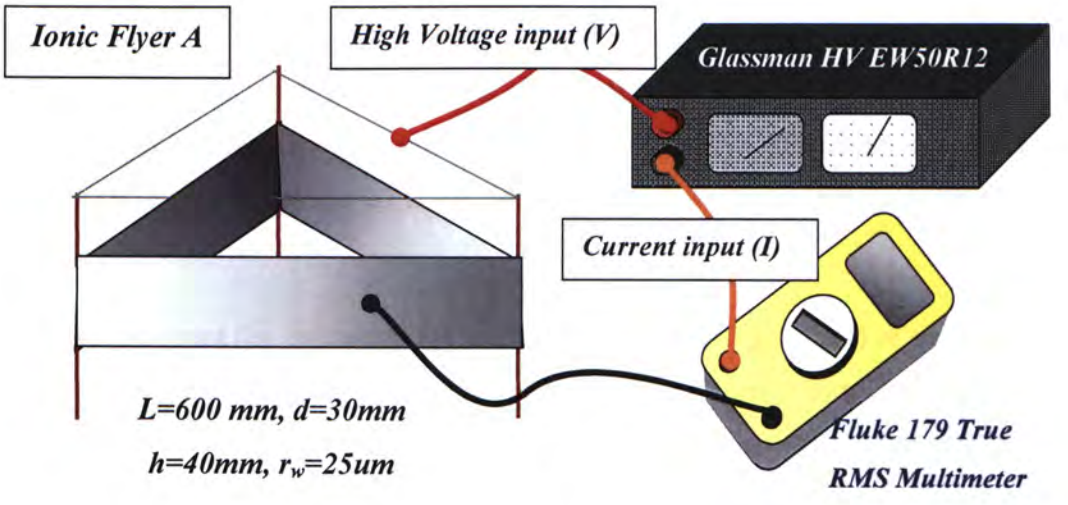

Figure 4.1: Schematic representation of the experimental setup for the measurement of the current-voltage relationship of the Ionic Flyers

Figure 4.1 describes the experimental setup that is used to obtain the current-voltage relationship of the Ionic Flyers. The experiments are conducted by increasing the input voltage at *1kV* increments to the Ionic Flyers and record the current consumption at the same time. The high-voltage power supply is *Glassman HV EW50R12* that has the maximum voltage output of *50kV* and maximum power output of *500W*. A *Fluke 179 True RMS Multimeter* is connected electrically in series with the Ionic Flyers to measure the current output and the minimum measurable current is $10\mu A$. All the experiments were conducted at the *CMNS* clean room with controlled environmental temperature of 25 ± 2 °C and pressure of 1atm. Thus, all the experimental results are valid under standard temperature and pressure (i.e. 25°C and 1atm [30]). Moreover, all the experiments were repeated for at least three times and at different days. Since the repeated experimental results for all the prototypes achieve standard deviations of less than 10%, average data is used as representative data for analysis and modeling.

4.2 Basic Current to Voltage Relationship

For the ease of explanation, *Ionic Flyer A* which has $L = 600mm$, $h = 40mm$, $d = 30mm$ *and* $r_w = 25\mu m$, as shown in Figure 4.1, is taken as a representative Flyer in the following discussion. Table 4.1 shows the five sets of experimental data of *Ionic Flyer A* with the experiment date and the corresponding temperature. As stated in the table, the temperature is kept at around 25°C and the standard derivation for the each data is less than *0.02 (2%)*.

The average current (by averaging the five measurements of each data) of the *Ionic Flyer A* was plotted with the applied voltage in Figure 4.2. The current to voltage relationship, that obtained experimentally, shows a typical square-law form that is a common property for corona experiments in many electrode geometries [31],[32],[33],[34], especially for positive-corona experiments. The Least absolute residuals (*LAR*), that is one of the Least Square Fitting Method, has been used to determine the best fitting equation for the experimental current to voltage data [35]. Figure 4.2 shows a quadratic equation of the form $I = 0.001176(V - 6.169)^2$, where I is in micro-amperes and V is in kilovolts, used to fit the experimental data for the range of *6.169-26kV* of *Ionic Flyer A*. R-square, with a values from zero to one, measures how good the fit is in explaining the variation of the data. The quadric equation achieves an R-squared of 0.9983 (A value closer to 1 indicating that a greater proportion of variance is accounted for by the model) that is acceptable in our applications.

V in kV	*I in mA Day 1* (24.5°C, 46%)	*I in mA Day 2* (24.2°C, 50%)	*I in mA Day 3* (25°C, 48%)	*I in mA Day 4* (24°C, 50%)	*I in mA Day 5* (25.3°C, 48%)	*AVER.*	*STDEV.*
7.4	0.01	0.01	0.01	0.01	0.01	0.01	0
9	0.01	0.01	0.01	0.01	0.01	0.01	0
10	0.02	0.02	0.02	0.02	0.02	0.02	0
11	0.03	0.03	0.03	0.03	0.03	0.03	0
12	0.04	0.04	0.04	0.04	0.04	0.04	0
13	0.06	0.06	0.06	0.06	0.06	0.06	0
14	0.08	0.08	0.07	0.07	0.07	0.072	0.0055
15	0.1	0.1	0.09	0.09	0.09	0.092	0.0055
16	0.12	0.12	0.11	0.12	0.11	0.114	0.0055
17	0.14	0.13	0.14	0.14	0.14	0.138	0.0045
18	0.16	0.15	0.16	0.16	0.16	0.158	0.0045
19	0.19	0.19	0.18	0.19	0.19	0.188	0.0045
20	0.22	0.21	0.22	0.22	0.22	0.218	0.0045
21	0.25	0.25	0.26	0.26	0.26	0.256	0.0055
22	0.29	0.28	0.29	0.29	0.29	0.288	0.0045
23	0.33	0.31	0.33	0.33	0.33	0.326	0.0089
24	0.38	0.35	0.39	0.37	0.39	0.376	0.0167
25	0.45	0.41	0.45	0.44	0.45	0.44	0.0173
26	0.52	0.52	0.56	0.54	0.56	0.54	0.02

Table 4.1: Five sets of *I-V* experimental data, which was taken at different days, for *Ionic Flyer A*. The second last column shows the averaged experimental data and last column shows the standard derivation of the experimental data

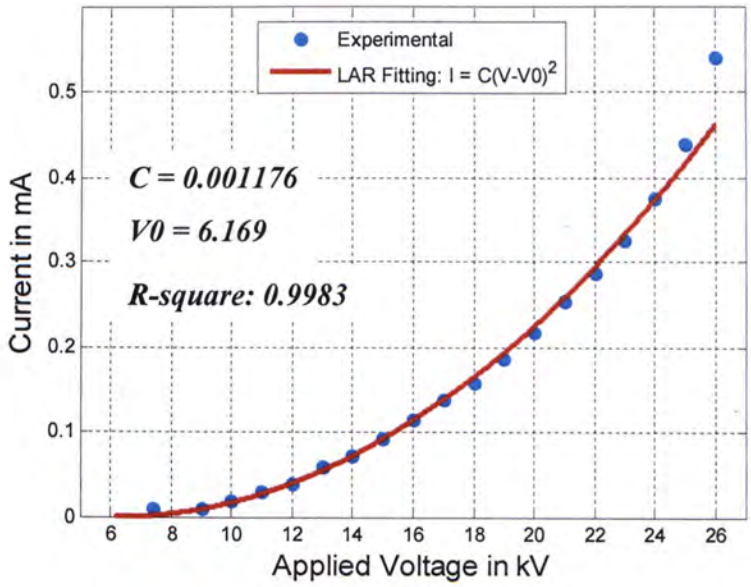

Figure 4.2: The variation of positive corona current with applied voltage for Ionic Flyer A: experimental points (blue circle), the derived quadratic equation $I = 0.001176\ (V - 6.169)^2$ (full line)

4.2.1 The Three Electrical Stages of the Ionic Flyers

All Ionic Flyers go through three stages as the applied voltage increase gradually. Again, Ionic Flyer A is used as the representative flyer in this discussion.

When the applied voltage is in the range of *0kV* to about *6kV*, no measurable current is record by the multimeter. This is the *"Insulating Stage"* of the Ionic Flyer since the electric field generated by the Ionic Flyer is not strong enough to initiate the corona discharge of the air (In order to initiate the corona discharge, the electric field strength on the emitter should reach 30kV/cm [31]). The Ionic Flyer can than be considered as an insulator as the power consumption is equal to zero

As voltage input becomes greater than *6kV*, there is measurable current record by the multimeter. The voltage at which current starts to flow through the Ionic Flyers is called the *corona onset voltage* and the details were discussed in the following sections. The Ionic Flyer becomes conductive at this stage (i.e., *conducting stage*) because the electric field strength is strong enough to break down the air and initiate corona between the

electrodes. The corona discharge create avalanche of electrons and also leads to large amount of positive ions accumulate in the space. As the mobility of electrons is far larger than the positive ions in positive corona, so the current measured by the multimeter is mostly due to the positive ions. As the applied voltage increases, the degree of electrons avalanche increase and therefore create more positive ions. This results in the reduction of the electrical resistance of the air. In this stage, the Ionic Flyer is just like an asymmetrical capacitor that have very low capacitance and work under the breakdown voltage of the dielectric material (i.e., air).

When the voltage input is further increase from the onset voltage, more streamers appears. There is a transformation from corona discharge to complete breakdown of the air when the applied voltage reaches about *26kV* (*threshold voltage*). Sparking signaling the complete break and it can be observed randomly at the gap between the electrodes. The breakdown is due to the high density of ions constitute breakdown streamers, that their length is long enough to complete an ionic path between the positive and the negative electrodes. This number of breakdown streamers increase as the applied voltage increase beyond the threshold voltage. Moreover, the position of sparking is random and cannot be predicted. Breakdown streamers make the Ionic Flyer temporary short-circuited and a large current is flowing through the Ionic Flyer. The supply current of the power supply should be limited so as to protect the Ionic Flyer. As all the energy is release to the air as heat, light and sound energy, Ionic Flyers are not able to generate thrust. This is called the *breakdown stage* since the Ionic Flyer may be possibly damaged by the sparking.

All Ionic Flyers can be defined with an *operating range* that they can work properly. The *operating range* is defined between the *onset voltage* and the *break-down voltage* (6KV to 26kV in this case). At this range, the Ionic Flyer can fly silently and relatively stable. The *lift-up voltage* is the minimum voltage input to lift up the Ionic Flyer (the weight of the electrode and the basic wooden frame to support the electrodes). For a proper Ionic Flyer, the lift-up voltage should be in the range of the operation stage.

4.2.2 Proposed Quadratic Equation for the Current to Voltage Relationship

The current-voltage characteristic for all the Ionic Flyers with the wire-plate configuration in our experiments has the typical square-law current-voltage relationship. Based on our experimental results, we derived a general *I-V* relationship that has R-squared values of greater than 0.9 to all experimental data. The general *I-V* relationship is described by equation (4.2.1) with two parameters, the current gain C and the onset voltage V_0. Since these two parameters reflect the properties of the corona discharge, they depend on the structural parameters (as described in Chapter 2) of the Ionic Flyers and the environment factors. The details of these two parameters are discussed in the next session.

$$I = C(V - V_0)^2 \qquad \textbf{(4.2.1)}$$

where I is the input current in *micro-ampere*; V is the input voltage in *kilovolt*, V_0 is the *onset voltage* of the Ionic Flyer in *kilovolt* and C is the Current Gain in mA/kV^2.

The onset voltage V_0 and the current gain C determine the electrical properties of the Ionic Flyers. Ionic Flyers with different configurations can be determined by the values of C and V_0. Based on our experimental results, Ionic Flyers with the same values of C and V_0 can be considered to have the same electrical model, although they may have different geometric appearance. The details are discussed in the next session.

4.3 Determination of the Current Gain *C* and the Onset Voltage V_0 by the Structural Parameters of the Ionic Flyers

Bases on the basic *I-V* relationship of the Ionic Flyers, there are two theoretical parameters, the current gain C and the onset voltage V_0 that can be varied by changing quantitatively the structural parameters of the Ionic Flyer. As Ionic Flyers are basically capacitors, although work under break down status of the dielectric material, they are expected to have similar electrical properties. For instance, the current gain C has a similar role as the capacitance of a parallel plate capacitor in the current to voltage

relationship. In case of parallel plate capacitor, the current to voltage characteristic is $I = C\frac{dV}{dt}$ with the capacitance depends on the area and the gap distance of the plates. The current gain C and the onset voltage V_0 is characterized by the particular properties of corona discharge and thus can are determined by the shape of the electrodes, the size of the gap, and the nature of the gas. Experimental studies have been carried out to find out the relationship between these two parameters with six primitive structural parameters of the Ionic Flyer. They are 1) the electrode length of the Ionic Flyer (L); 2) the gap distance between the wire-emitter and the plate-collector (d); 3) the radius of the wire-emitter (r_w); 4) the height of the plate-collector (h); 5) the area enclosed by the electrode (A) and 6) the Electrical environmental constant (K_e) which is probably determined by the temperature and pressure of the air.

Experiments have been carried out systematically based on the five structural parameters to figure out their effects to the current gain C and the onset voltage V_0. As all the six structural parameters are not interrelated to each other, their effect can be considered independently and the total effect can be summarized by the equation (4.3.1).

$$I = f(L, d, r_w, h, A, K_e)(V - V_0(r_w, d))^2 \qquad \textbf{(4.3.1)}$$

where the function $f(L, d, r_w, h, A, K_e)$ is equal to the current gain C and $V_0(r_w, d)$ is the onset voltage

During the analysis of the experimental results, LAR fitting is adopted to formulate the current gain C and the onset voltage V_0 by using the structural parameters. If C or V_0 result in very similar values, the following criterion is adopted. The maximum variation of the parameter (C or V_0) is being calculated by equation (4.3.2). If a value of less than *10%* is obtained, that structural parameter will be considered as a non-effective parameter. Since *10%* is an acceptable variation for the derived values and the experimental values. In that case, that structural parameter would not be modeled in the final *I-V* model.

$$Var. = \frac{|p_{Aver.} - p|}{p_{Aver.}} \times 100\% \qquad \textbf{(4.3.2)}$$

where $p_{Aver.}$ is the mean value of experimental parameter p (i.e. C or V_0)

4.3.1 The Electrode Length (*L*)

For a parallel plate capacitor, the capacitance is proportional to the area of the electrodes. One way to change the electrode area of the Ionic Flyers is by changing the electrode length. In this section, experiments were carried out to test for the effect of the electrode length to the current gain C and the onset voltage V_0. Five triangular Ionic Flyers with the electrode length L =*300mm, 600mm, 750mm, 900mm and 1200mm* respectively, have been constructed for this experiment as shown in Figure 4.3. They are all have h = *40mm* and r_w = *25μm*, the reason for choosing these value is the conclusion after several preliminary tests. The five prototypes have been test for two times. In the first test, all the Ionic Flyers has been set with the electrodes' separation distance d = *30mm*. While in the second test, the electrodes' separation distance is set at *50mm*. The experimental procedure as described in session 4.2 has been adopted to obtain the current-voltage relationship of each of the Ionic Flyers.

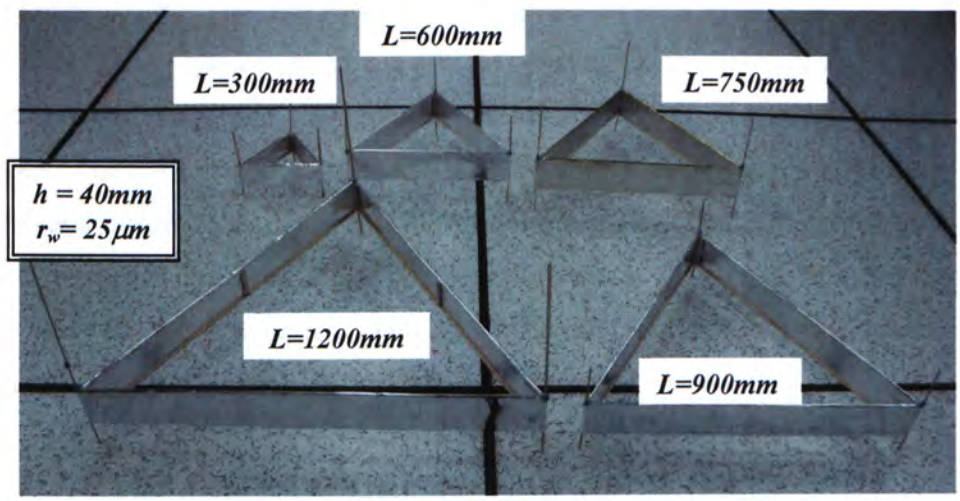

Figure 4.3: Five triangular Ionic Flyers with *L= 300, 600mm, 750mm, 900mm and 1200mm.* The other structural configurations are described in the box

The experimental data and the derived *I-V* characteristic equation for the five Ionic Flyers have been plotted in Figure 4.4, with (a) shows the results for $d = 30mm$ and (b) shows the results for $d = 50mm$.

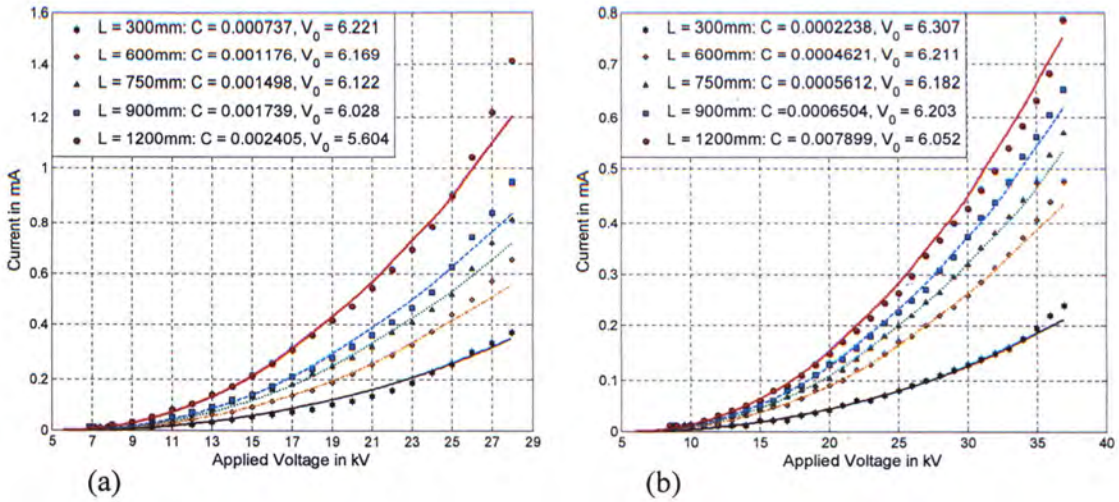

Figure 4.4: Experimental and derived *I-V* relationship for the Ionic Flyers with the configurations as stated in Figure 4.3. The gap distances for (a) is *30mm* and (b) is *50mm*

By considering the results as shown in Figure 4.4 (a), the current gains C are found to be $0.0007368mA/kV^2$ for the *300mm* model, $0.001176mA/kV^2$ for the *600mm* model, $0.001498mA/kV^2$ for the *750*mm model, $0.001739mA/kV^2$ for the *900*mm model and $0.002405mA/kV^2$ for *1200*mm model. Experimental results show that as the electrode length of the Ionic Flyers increase, the current consumption is also increase with the same applied voltage. In addition, the experimental results show at Figure 4.4(b) has the same properties. The current gain C of the two set of experimental results have been plotted with the total electrode length as shown in Figure 4.5. As stated in the figure, the current gain can basically fitted by the linear equation which is passing through the origin. Results showed that the current gain C of the Ionic Flyers is proportional to their electrode length and this property can be formulated by

$$\frac{I_M(V_i)}{L_M} = \frac{I_N(V_i)}{L_N} \qquad \textbf{(4.3.3)}$$

where I_M and L_M are the input current and the total perimeter length of the Ionic Flyer M; I_N and L_N are the input current and the perimeter length of the Ionic Flyer N; V_i is any applied voltage in the operating range.

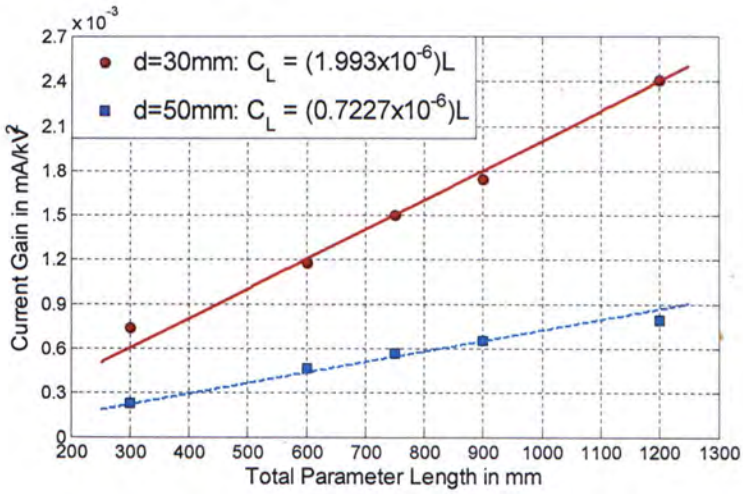

Figure 4.5: The variation of current gain C with the electrode length, blue square is the experimental point for the prototypes with d=30mm and red circle is the experimental point for the prototypes with d = 50mm. Linear equations are applied to fit the experimental points accordingly.

The experimental result suggested that although in wire-plate configuration, the current pulse would not be triggered in unison along its length (it triggered at random points along the wire at different times) [36], the total effect on the current consumption can be expect to be proportional to the length of the wire (i.e. the total electrode length of the Ionic Flyers in our case).

To conclude from the experimental results, when Ionic Flyers are supplied with the certain voltage, their conductivity is basically proportional to its electrode length. The current gain can than be represent by $f(L,d,r_w,h,A,K_e)=L\cdot f_1(d,r_w,h,A,K_e)$

On the other hand, the onset voltage V_0 did not show significant changes and keep at *~6kV* as observed in Figure 4.4. The largest variation is found to be 7% for the first experiment and 4.2% for the second experiment. The experimental results show that when the electrode length is varied from *300mm* to *1200mm*, the largest variation is within *10%*, we conclude that the electrode length is not a significant parameter to affect

the onset voltage V_0. Actually, the value of V_0 can be well predicted by the Peek's equation and that will be explained in details in the next session.

4.3.2 The Gap Distance between the Wire-emitter and the Plate-collector *(d)*

Another important parameter that affects the current gain C and the onset voltage V_0 is the gap distance between the emitter and the collector. For parallel plate capacitor, it is well known that the electric field strength and thus the capacitance are inversely proportional to gap distance. For Ionic Flyers, as long as the field is highly non-uniform, the effect of the gap distance is expected to be more significant than the uniform field case.

The investigation is done by using two prototypes, one has $L = 1200mm$ and the second one has $L = 900mm$, while both of them have $r_w = 25\mu m$ and $h = 40mm$. The experiments were carried out by adjusting the gap distance of the two prototypes to *30mm, 40mm, 50mm, 60mm and 90mm*. The experimental data and the derived *I-V* characteristic equation for the two Ionic Flyers have been plotted in Figure 4.6, with (a) and (b) show the results for the *1200mm*-flyer and the *900mm*-flyer respectively.

The experiments results suggest that as long as the gap distance increase, the current consumption is decrease at a same applied voltage. By considering Figure 4.6 (a), the current gain C is found to be $0.002405mA/kV^2$ for the *30mm*-distance, $0.001215mA/kV^2$ for the *40mm*-distance, $0.0007899mA/kV^2$ for the *50mm*-distance, $0.0005186mA/kV^2$ for the *60mm*-distance and $0.0002271mA/kV^2$ for *90mm*-distance. Obviously, the current gain C is not only inversely proportional to the gap distance, but show a faster decreasing rate. In many physic systems, like the electrostatic field between two charges, the relation to the gap distance is in inverse square law. Figure 4.7 shows a plot on the current gains of the two prototypes with the gap distances. A LAR fitting curve, which is in inverse square law, is being fitted independently to the two sets of experimental data. The inverse square curve which is in the form of $C(d)=(k/d^2)$, where *C(d)* is the current gain; d is the separation distance and k is a proportional constant that depends on other parameters. By combining the results of the previous section, the proportional constant k is varied

linearly with the electrode length of the Ionic Flyers. In conclusion, the total current gain $f(L,d,r_w,h,A,K_e)$ is equal to $\frac{L}{d^2}\cdot f_2(r_w,h,A,K_e)$

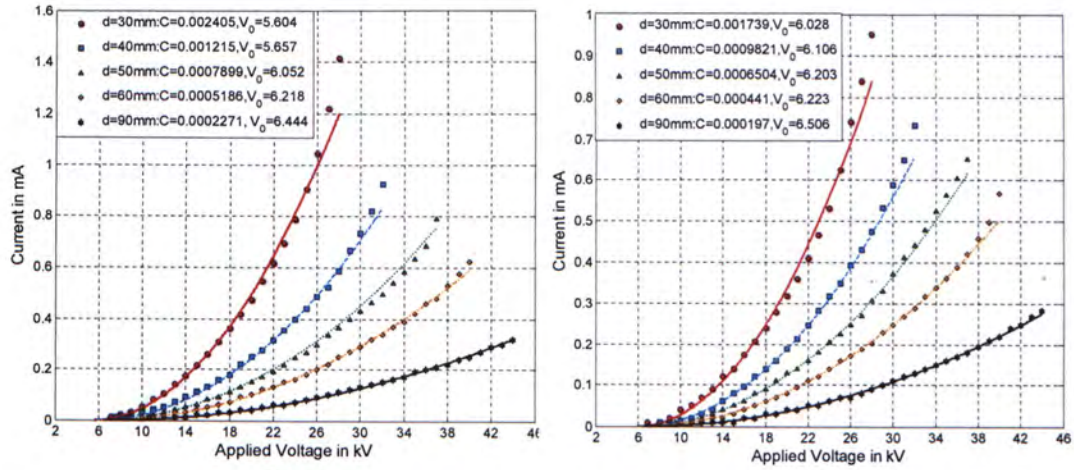

(a) (b)

Figure 4.6: Experimental and derived *I-V* relationship for the Ionic Flyers with $r_w = 25\mu m$ and *h=40mm.* The five sets of points and curves are corresponding to gap distance *of 30mm, 40mm, 50mm, 60mm and 90mm* respectively. The electrode length of the Ionic Flyers in *(a) is 1200mm and (b) is 900mm*

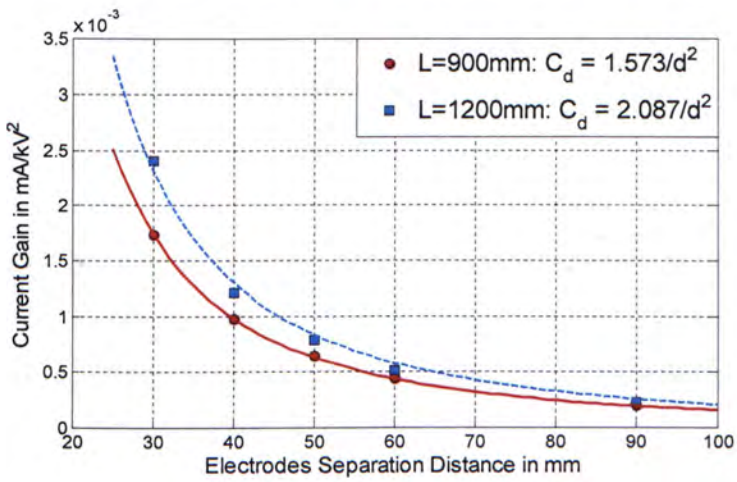

Figure 4.7: The variation of current gain C with the gap distance, blue square is the experimental point for the prototype with *L=1200mm* and red circle is the experimental point for the prototype with L = *900mm*. Linear equations are applied to fit the experimental points accordingly.

4.3.2.1 Introduction to the onset voltage V_0 and the Peek's equation

While the current gain C has an inverse square relationship with the gap distance, the onset voltage V_0 is found to be increase with the increase in gap distances. By comparing the onset voltage V_0 for the five Ionic Flyers as shown in Figure 4.6 (a), it found to be *5.604kV* for the *30mm*-distance, *5.657kV* for the *40mm*-distance, *6.052kV* for *50mm-distance*, *6.218kV* for *60mm-distance* and *6.444kV* for *90mm-distance*. Since the Ionic Flyers start to conduct electricity at the initiation of corona discharge, so the onset voltage V_0 of the Ionic Flyers should be equal to the corona onset voltage (or corona inception voltage). The corona onset voltage has been extensively studied by Peek and some mathematical models commonly called the Peek's formulas has been developed which are proved experimentally applicable to many electrodes configuration during the corona discharge [26], [37].

During the corona discharge, the electric field at the surface of the high voltage electrode is equal to the value obtained from equation developed by Peek [23], [31]. The onset voltage V_0 of the Ionic Flyers as calculated by the Peek's equation can be described as follows [37]:

$$V_0 = m_0 g_0 \delta \left(1 + \frac{0.0301}{\sqrt{\delta \cdot r_w}}\right) r_w \cdot \ln\left(\frac{d}{r_w}\right) \tag{4.3.4}$$

where m_0 represent the wire roughness factor and should be equal to one in case that all wires used in the experiments were bare polished wire; δ is the air density factor which is equal to one as all the experiments were conducted at atmospheric pressure; g_0 equals to a constant of *2.98*; d is the gap separation distance in meter and r_w is the radius of the wires in meter

The Peek equation is proved to be a good approximation for the surface electric field and the corona onset voltage for many high voltage experiments with some common electrode configuration like wire-cylinder arrangement [37]. However, it is not guaranteed that the Peek's equation is applicable to any electrode configurations. Currently, many researches

on high voltage experiments used Peek's equation as a reference in their simulation and experimental results. In our experiments, the results (refer to Figure 4.6) show that the onset voltage V_0 (that should be equal to the corona onset voltage) of the Ionic Flyers has a constant derivation as calculated by the Peek's equation (4.3.4). The derivation can be explained by the studies carried out by Dan Rafiroiu. In many wire electrodes corona discharge, the Peek's equation can be used to predicted the corona onset voltage and achieve the maximum relative error of 5% if the radius of wire is greater than *0.25mm*. However, it is suggested than for thinner wires, a modification factor should be applied to the Peek's formula. As the electric field strength at corona onset was found to be lower than the values predicted by Peek, a higher value of corona onset voltage can be expected as compare to the Peek's calculation [37].

The experimental results that we obtained can be used as an evidence of Rafiroiu's findings because the wire-emitter radius of the testing prototypes is $25\mu m$ which is smaller than *0.25mm*. Figure 4.8 shows the values predicted by the Peek's equation and the experimental results on the onset voltage V_0. The constant derivation of the experimental values and the Peek's formula is found to be *1.508 (the modification factor)* by using *LAR* fitting. The modified Peek's equation that suited the onset voltage V_0 of the Ionic Flyers is:

$$V_0 = Gm_0 g_0 \delta \left(1 + \frac{0.0301}{\sqrt{\delta \cdot r_w}}\right) r_w \cdot \ln\left(\frac{d}{r_w}\right) \qquad \textbf{(4.3.5)}$$

where G a the correction factor which is equal to *1.508* for the wire radius r_w equal to $25\mu m$.

The modified Peek's equation is plotted in Figure 4.8, which fitted well with the experimental values. More details on the onset voltage V_0 and the Peek's equation are discussed in the next section.

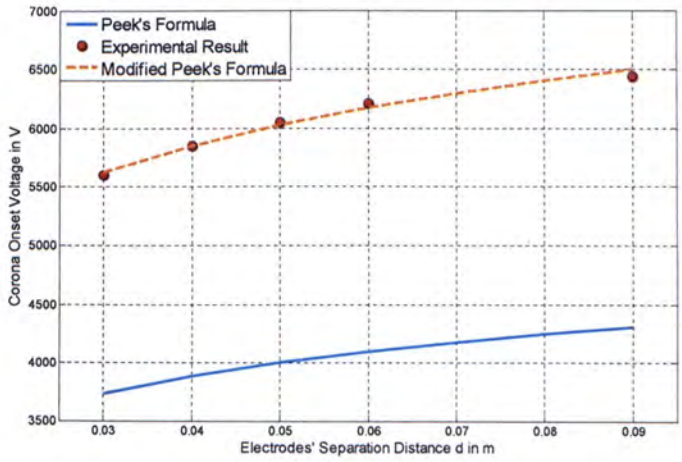

Figure 4.8: The variation of the onset voltage V_0 with the gap distance for the Ionic Flyers with electrode length $L=1200mm$ and $r_w = 25\mu m$. Blue solid line shows the values as calculated by the Peek's formula , red circle shows the experimental values and orange broken line shows the modified Peek's formula.

4.3.3 The Wire-emitter Radius (r_w)

As introduced in Chapter 3, the wire-emitter plays an importance role in ionization process and its radius governs the corona onset voltage. By equation (4.3.5), the onset voltage V_0 of the Ionic Flyers is determined by the gap distance d and the radius of the wire-emitter. In the last section, detailed experiments been carried out by focusing on the gap distance and the experimental results suggest that the Peek's equation should be modified by a factor when applying to wire with radius smaller than $0.25mm$. In this section, experiments have been carried out by focusing on the radius of the emitter. The experimental prototype was an Ionic Flyer with $L = 1200mm$, $h = 40mm$. On the other hand, four wires with radius r_w equal to $0.01mm$, $0.025mm$, $0.075mm$, $0.12mm$, respectively, have been taken as the testing sample. The experiments are carried out by testing each wire with five values of gap distance d, which is $30mm$, $40mm$, $50mm$, $60mm$ *and* $90mm$. The five sets of experimental results have been shown in Figure 4.9. Basically, all the experimental results follow the simple rules of the Peek's equation that the corona onset voltage is lower for wires with smaller radii.

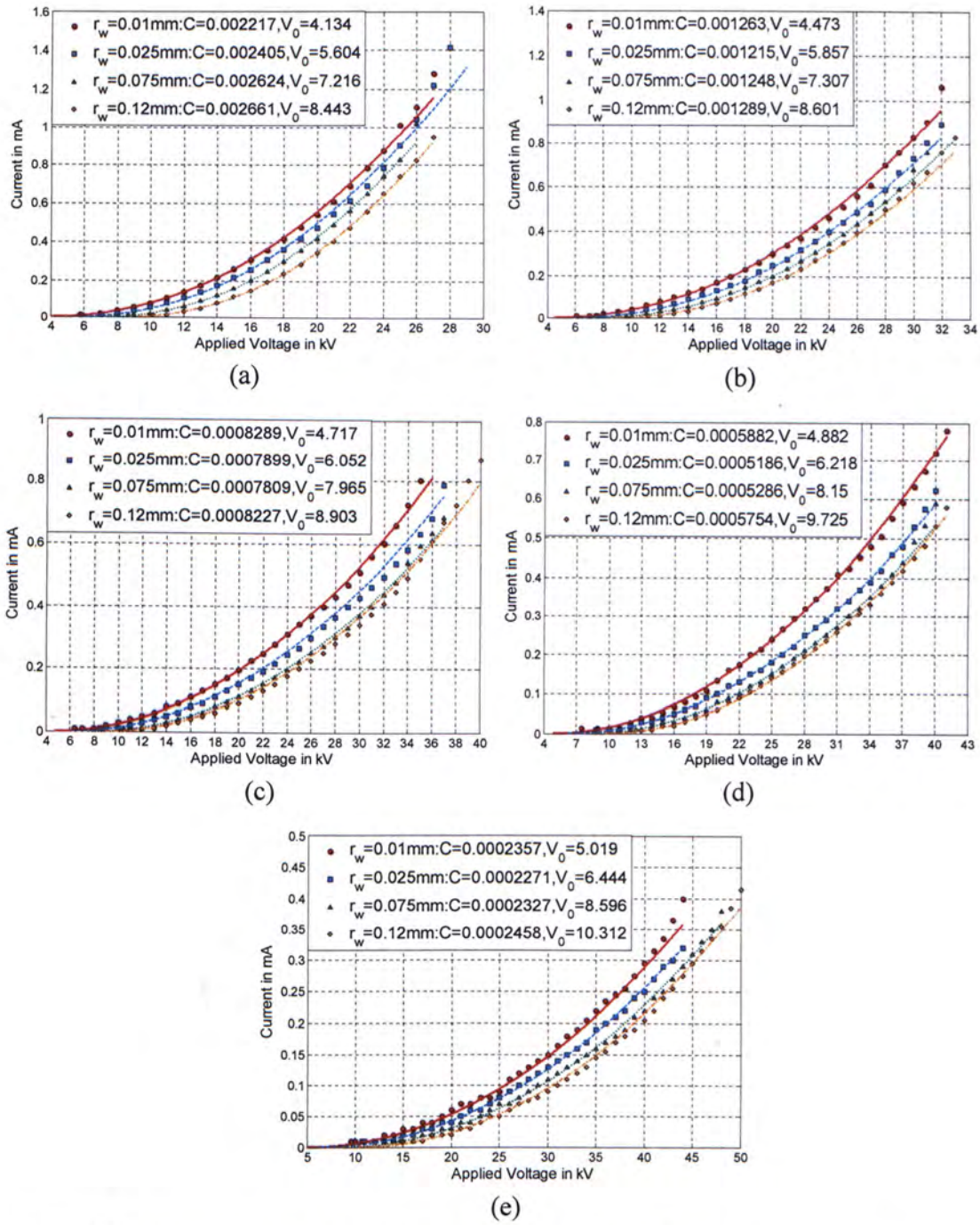

Figure 4.9: Experimental and derived *I-V* relationship for the Ionic Flyers with *L=1200mm* and *h = 40mm*. The four sets of points and curves are corresponding to the wire radii *of 0.01mm, 0.025mm, 0.075mm, 0.12mm.* The gap distance of the Ionic Flyers in *(a) is 30mm; (b) is 40mm; (c) is 50mm; (d) is 60mm and (e) is 90mm*

Based on the experimental and application requirement, all the wire-emitter that used in the Ionic Flyers should have radii smaller than *0.25mm*. This is because the increasing of the wire radius will increase the onset voltage and shit the operating ranges of the Ionic Flyers to a higher applied voltage. The application criteria of the Ionic Flyers suggest that the maximum applied voltage should be kept as low as possible. In fact, the higher the voltage, the higher the difficulties in developing electrical and electronic circuits in the future development of the Ionic Flyers project. So basically, applied voltage in all of our experiments is kept under *50kV*. Due to the above reason and also the experimental results, the thickest wire that used in the experiments is *0.12mm*.

As stated in the previous section, the modification factor for wire with radius r_w = *0.025mm* is a constant which is equal to *1.508*. In this section, the results further suggest that the modification factor is also related to the wire radius r_w. Figure 4.10 contains five graphs, with each graph shows the experimental onset voltage that is extracted from Figure 4.9 and the predicted values as obtained by the original Peek's equation. While the five graphs are corresponding to different gap distance of the Ionic Flyers as described before. As shown in the graphs, the derivations between the experimental values and the Peek's equation increase as the radii of the wires decrease. The general modification factor is deduced by calculating the derivations for each radius and an approximation equation is used to represent those values. And the derivations are interpreted as the ratio of the experimental values and the Peek's predicted values. Figure 4.11 shows the modification factors for all the values of the wire radii and the gap distances. As expected, the general modification factor decays from the small values of wire radius. As reference to Rafiroiu's results, the modification factor should be stabilized at one for r_w greater than *0.25mm* [37]. So, the general modification factor decay from a high value of about *1.7* at r_w=*0.01mm* to one at r_w=*0.25mm* and stabilized afterward. By using LAR fitting method with a standard exponential decay equation, the correction factor is:

$$G(r_w)=1+e^{-\left(\frac{r_w}{4x10^{-5}}\right)} \qquad \textbf{(4.3.6)}$$

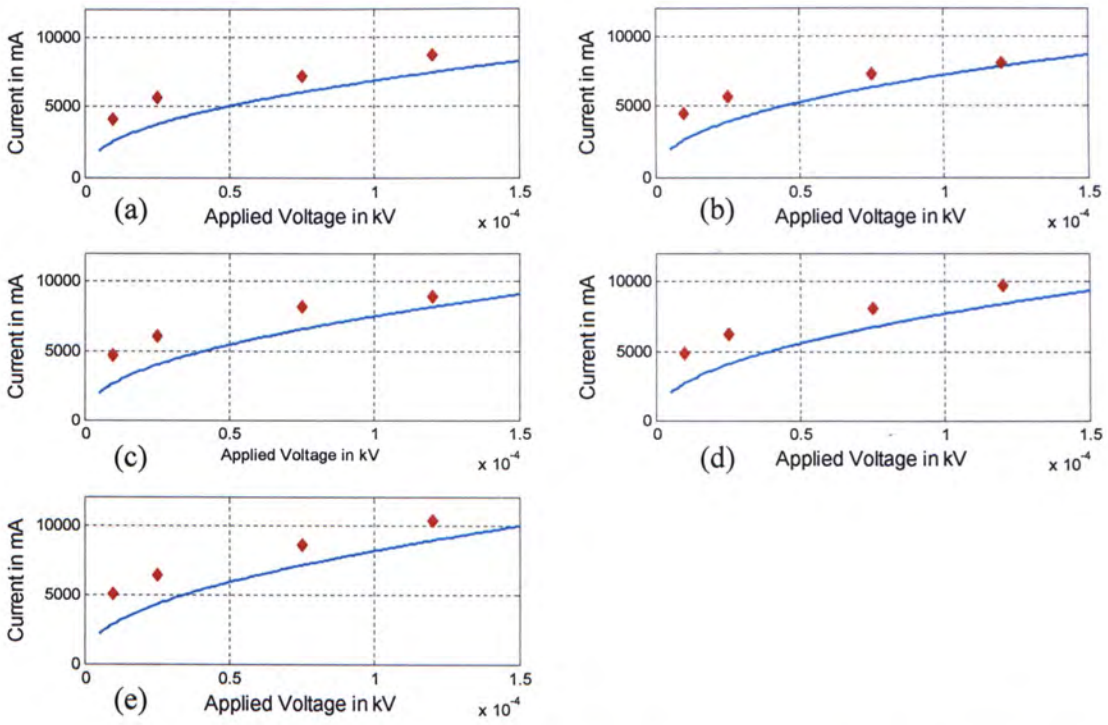

Figure 4.10: Experimental and the Peek's predicted values of the onset voltage for the testing wire radii. The gap distance *for (a) is 30mm; (b) is 40mm; (c) is 50mm, (d) is 60mm and (e) is 90mm.*

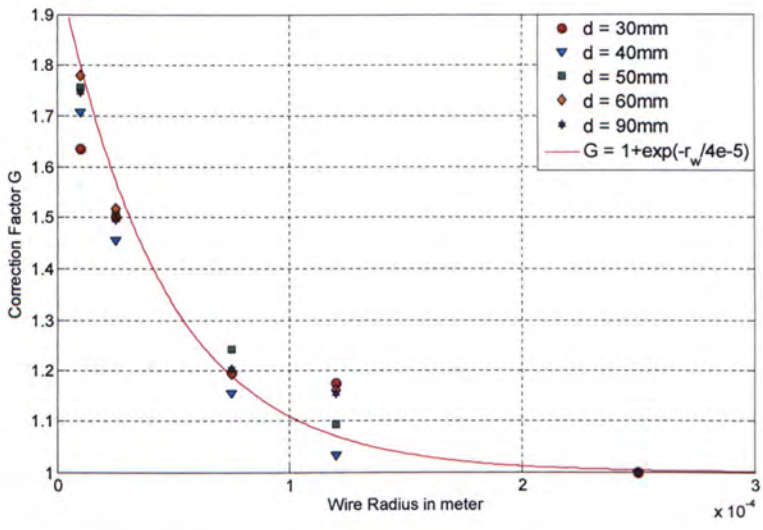

Figure 4.11: Experimental and derived modification factor *G* for the Peek's equation based on the experimental results as shown at Figure 4.10 and Figure 4.11

4.3.3.1 Conclusion on onset voltage V_0

The experimental results suggest that the onset voltage of the Ionic Flyers is dependent on the gap distance and the radius of the wire-emitter. The values are further tested that can be well predicted by the Peek's equation on the corona onset voltage. While on the other hand, the radii of the emitter wires that suited our application should be smaller than *0.25mm,* thus the Peek's equation should have a modification factor which is determined experimentally with the form of equation (4.3.6). So, the general equation for the prediction of the onset voltage V_0 for the Ionic Flyers is in the form of a modified Peek's equation:

$$V_0 = G(r_w) m_0 g_0 \delta \left(1 + \frac{0.0301}{\sqrt{\delta \cdot r_w}}\right) r_w \cdot \ln\left(\frac{d}{r_w}\right) \tag{4.3.7}$$

where m_0 and δ equal to one and g_0 equals to a constant of *2.98* as discussed above; *d,* in meter, is the gap distance between the emitter and the collector two wires r_w is the radius of the wires in meter; $G(r_w)$ is the derived modification factor with equation of (4.3.6).

Moreover, two important features of the corona discharge can be further defined based on equation (4.3.7):

$$g_v = g_0 \delta \left(1 + \frac{0.0301}{\sqrt{\delta \cdot r_w}}\right) \tag{4.3.8}$$

$$r_v = r_w \left(1 + \frac{0.0301}{\sqrt{r_w}}\right) \tag{4.3.9}$$

where g_v, in *V/m* is the corona field strength at the surface of the wire-emitter and it is depends on the radius of the wire only; r_v is the effective radius of the wire-emitter during corona such that the ionization region (for details, please refer to section 3.3.1 of Chapter 3) is define within a cylinder within inner radius r_w and outer radius r_v.

Finally, the experimental results as shown at Figure 4.9 (from (a) to (e)) suggest that the current gain *C* of the Ionic Flyers is almost unaffected by the wire radius. The variation of

the current gains for (a) is *7.4%*; (b) is *3.1%*; (c) is *2.9%*; (d) is *6.2%* and (e) is *4.5%*. Since all the results show the variation of less than *10%*, the radius of the emitter wire is considered as one of the non-effective structural parameters for the current gain C. Actually, the similar results has been obtained on the high voltage experiment on other electrode configurations of the electrostatic precipitator [37].

4.3.4 The Plate-collector Height (h)

As we mentioned before, for parallel plate capacitors, the capacitance is only geometrically related to the area of the electrode and the gap distance between the two electrodes. The experimental results shown in section 4.3.1 (section for L) and 4.3.2 (section for d) have proved that, as similar to the case of parallel plate capacitors, the current gain C and the onset voltage V_0 of the Ionic Flyers are significantly affected by their electrode length and the gap distance between their emitter and collector. And it was expected that the current gain C of the Ionic Flyers would not be affected much by other two structural parameters related to the electrodes, which are the radius of the wire-emitter and the height of the plate-collector. In the previous section, we have already verified that the radius of the wire-emitter can be classified as a non-effective structural parameter to the current gain C. In this section, we will further demonstrate the insignificancy of the last parameter, which is the height of the plate-collector.

The experiments were carried out by investigating two sets of Ionic Flyers. The first set consisted of four Ionic Flyers, all have $L = 600mm$, $d = 30mm$, $r_w = 25\mu m$ and constructed with collector heights of *30mm, 40mm, 50mm, 60mm,* respectively, as shown in Figure 4.12. The second set also contained four Ionic Flyers, the only different was that they were all constructed with electrode length $L = 1200mm$.

Figure 4.13 shows the experimental results, with (a) corresponding to the first set with $L = 600mm$ and (b) corresponding to the second set with $L = 1200mm$. In both graphs, the experimental results display repeatable trend and results for the four Ionic Flyers. Based on the derived quadratic *I-V* equation, it was indicated that they have similar current gain C and onset voltage V_0. From the results shown in Figure 4.13, we can deduce that the

variations of the current gain C and the onset voltage V_0 for (a) is 9.4% and 3.5%, and (b) is 7.6% and 4.3%, respectively. As expected, the variations of the two set of data are both within 10%. So, it is obvious that the height of the plate-collector plays no crucial role in affecting the current gain C and the onset voltage of the Ionic Flyers.

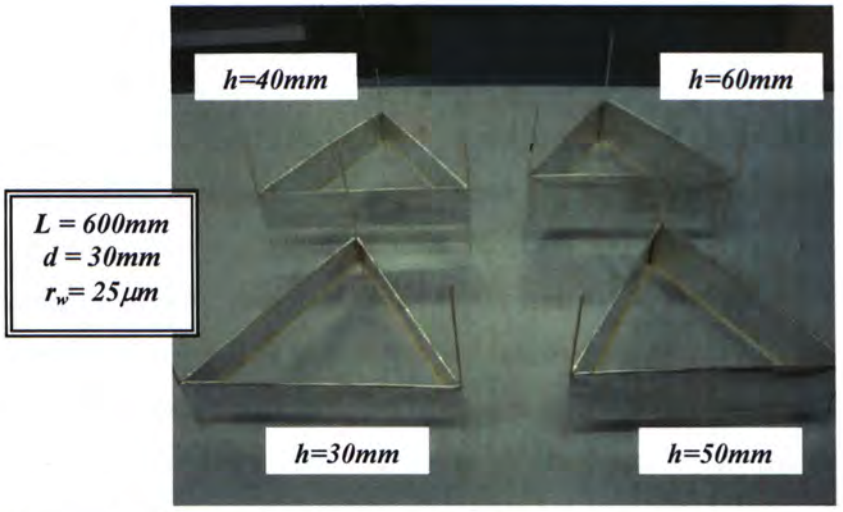

Figure 4.12: Four triangular Ionic Flyers with *h= 30, 40mm, 50mm and 60mm*.The other structural configurations are described in the box

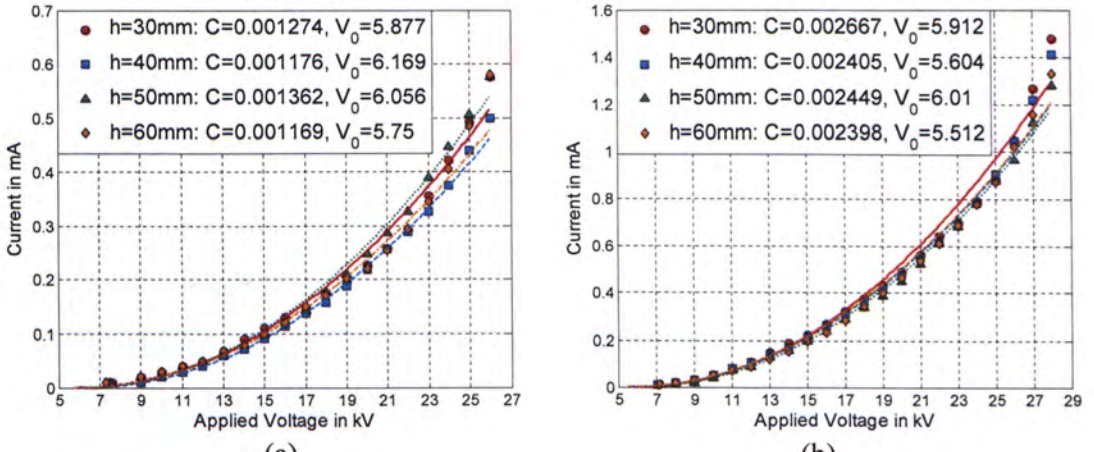

Figure 4.13: Experimental and derived *I-V* characteristic for the Ionic Flyers with the configuration as described in Figure 4.12 . The electrode length L for (a) is *600mm* and (b) *is 1200mm*

4.3.5 The Electrode Enclosed Area (*A*)

Someone may wonder why all the Ionic Flyers tested in the previous sections were constructed in triangular shape. This is because triangular structure is nearly the simplest and most stable structure. In fact, the Ionic Flyers can be lifted up even they are not in triangular shapes since the lifted force acted on them mainly depends on conditions of ions generation and transportation by the pairs of emitters and collectors but not their geometric shapes. In the view of constructions, the geometrical shape is only the way of arranging the electrode pairs, to form the Ionic Flyers. Nevertheless, the electrode's enclosed area will be different with different geometric shapes even they have the same structural parameters, which are *L, d, h* and r_w. As long as the size (i.e. the enclosed area) of the Ionic Flyers is large enough (the smallest one that we ever test is a triangular Ionic Flyer with electrode length of *300mm*), abnormal effect is not observed based on our previous experimental results. Thus, the sizes of the Ionic Flyers are expected to be irrelevant to the *I-V* characteristic of the Ionic Flyers provided that they have the same structural parameters. This hypothesis has been proved experimentally and the results will be shown in the following.

The experiments involved six Ionic Flyers and they have been categorized into two groups. Each group contains three Ionic Flyers and they were constructed in square-shape, hexagonal-shape and triangular-shape, respectively. We choose square-shape and hexagonal-shape for comparison with triangular-shape because of the ease of construction. Because of their symmetrical geometry, the chance for us to misalign the electrodes will be greatly reduced or else the experimental results will be seriously affected. For the first group, the three Ionic Flyers were constructed with L= *900mm*, d=*30mm*, h=*40mm*, r_w=*25mm* as illustrated in Figure 4.14, while those in the second set has similar configurations except they all have L=*1200mm*.

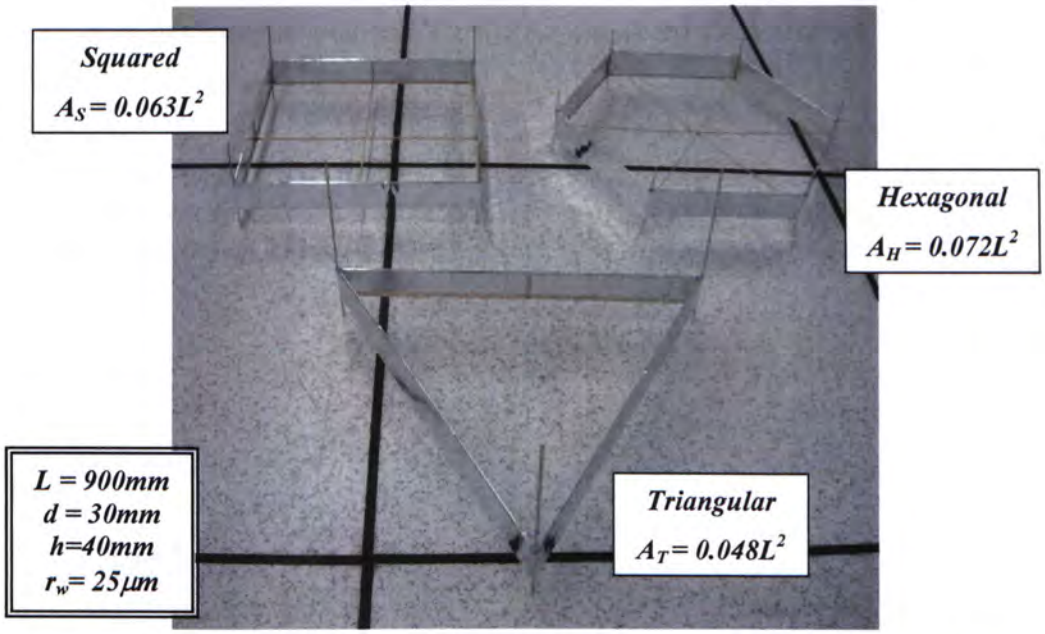

Figure 4.14: Three Ionic Flyers constructed with three kinds of geometric shape, square-shaped in the upper-right corner, hexagonal in the upper-left corner and triangular in the lower row. All three Ionic Flyers were constructed with $L=900$, $d=30mm$, $h= 40$ and $r_w = 25\mu m$

According to basic geometry, the enclosed area for the triangular, square and hexagonal Ionic Flyers with electrode length L is equal to $A_t = \frac{\sqrt{3}}{36}L^2$, $A_s = \frac{1}{16}L^2$ and $A_h = \frac{\sqrt{3}}{24}L^2$, respectively. The triangular one has the smallest area which is equal to about *76%* the area of the square one and *67%* of the hexagonal one. The experimental results have been presented in Figure 4.15 with (a) reporting the results of the *900mm-length* prototypes and (b) the *1200mm-length* prototypes. Basically, those results resemble the collector height experiment as discussed in the previous section. By considering the current gains and the onset voltages in (a), the variations are calculated to be *1.7%* and *1.3%* respectively. While for the results in (b), the variations are 4.4% and 4.3% respectively. By concluding from experimental results of the three different shapes of Ionic Flyers, the current gain C and the onset voltage V_0 do not display noticeable derivations as the variations are all within *10%*. This conforms to the basic assumption that the geometrical shape of the Ionic Flyers is nothing but only the way of arranging the electrodes. As long as the area is large enough (area greater than a triangle with *300mm* in total length is

grantee from our experimental results), the *I-V* characteristic would not be affected by the electrodes' enclosed area of the Ionic Flyers.

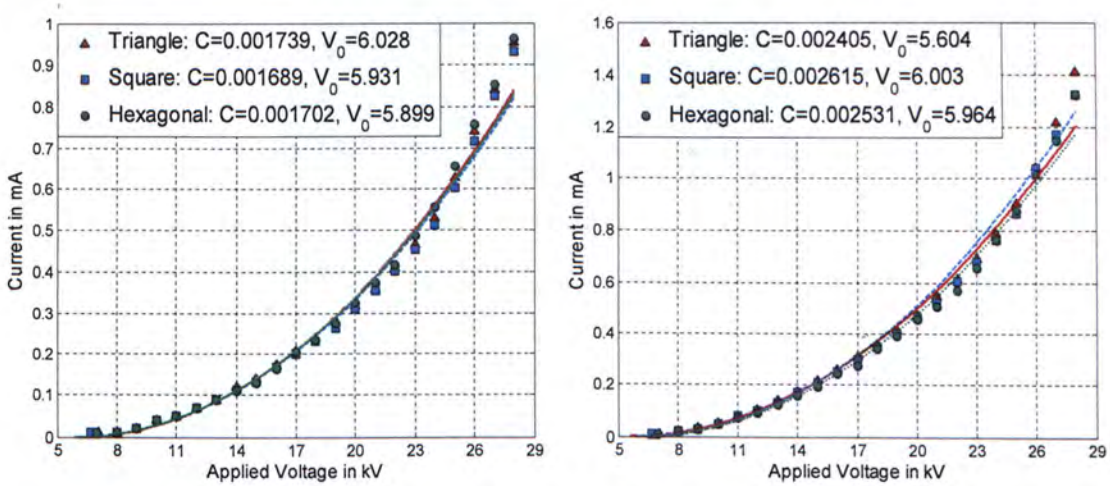

(a) (b)

Figure 4.15: Experimental and derived *I-V* characteristic for the Ionic Flyers with the configuration as described in Figure 4.14 . The electrode length *L* for (a) is *900mm* and (b) *is 1200mm*

Based on the above experimental results, we further investigate the effect of the size of the Ionic Flyer by filling the inner space of the Ionic Flyer with extended electrodes.

Figure 4.16 shows three triangular Ionic Flyers with the inner space occupied by the extending electrodes. Actually, they can be considered as two Ionic Flyers, with one in half electrode length of another one, connected electrically in parallel. For the ease of explanation, they were referred to "Composite Ionic Flyers" in the following in the following discussion. This new structure is similar to the case of a few parallel plate capacitors connected in a parallel circuit. Simply put, the capacitance of two parallel connected capacitors is equal to the summation of their individual capacitance and this law can be applied to the current gains of the Ionic Flyers. Also, the electrode length of the Composite Ionic Flyers is proposed to be equal to the summation of the outer and inner electrode length as described in Figure 4.16. In the following discussion, experimental results have proved that the properties that described in all those previous section can be basically applied to the Composite Ionic Flyers.

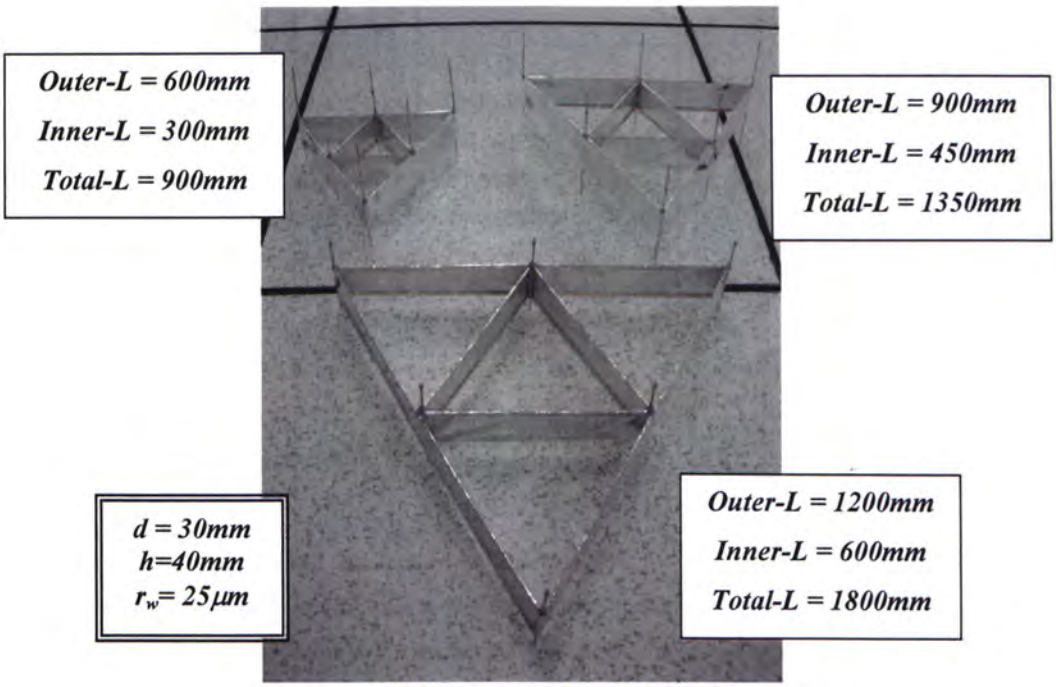

Figure 4.16: Three triangular Composite Ionic Flyers, which contain extending parallel connected electrodes being occupy in their inner space. The total electrode length is equal to the addition of the outer length and the inner length. All three Ionic Flyers were constructed with $d=30mm$, $h= 40$ and $r_w = 25\mu m$

As shown in Figure 4.17, we have compared the *I-V* characteristics of three "Normal" Ionic Flyers with other three "Composite" Ionic Flyers. The electrode lengths of the Composite Ionic Flyers were made to be comparable with "Normal" Flyers while all the other structural parameters were being kept constant in both cases. As indicated in the figure, the three Composite Ionic Flyers have onset voltage V_0 of *6.123kV, 6.1kV* and *5.876kV* respectively. These results can be well predicted by the modified Peek's formula as discussed in section 4.3.3.1 as the values of the gap distance (*30mm*) and the wire-emitter radius ($25\mu m$) are all known. Also, the current gains of the composite Ionic Flyers obtained in the experiments were *0.001705* mA/kV^2, *0.002555* mA/kV^2 and *0.003237* mA/kV^2 for the *900mm-length, 1350mm-length* and *1800mm-length* prototypes respectively and these experimental values were also fitted within *10%* variations by equation (4.3.3). So, it is apparent that both "Normal" and "Composite" Ionic Flyers have analogous properties, which can be evaluated based on similar assumptions and equations.

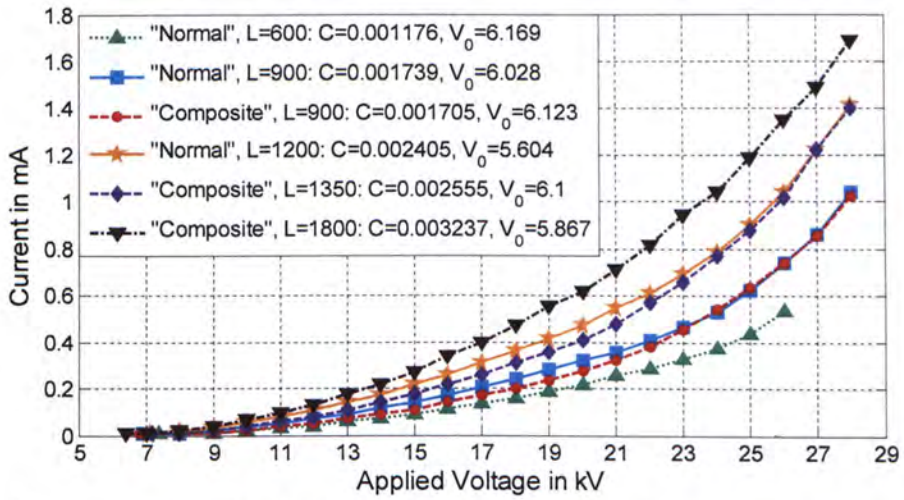

Figure 4.17: Experimental and derived *I-V* characteristic for the Composite Ionic Flyers as described in Figure 4.16. The experimental results of three "Normal" Ionic Flyers with comparable length and same other structural parameters were used to compare the results

From the experimental results above, it can be concluded that the inner space structure of the Ionic Flyers will not affect their *I-V* characteristics. Thus, effectively expanding the electrodes inside the inner space can result in size reduction of the Ionic Flyers, while on the other hand, achieving the same *I-V* characteristic. Nevertheless, these Composite Ionic Flyers should achieve the same gap distance for their inner and outer electrodes. Since experiments show that if the inner and outer electrodes were not parallel to each other in the horizontal level, the whole system will consume large power (in the order of two to three times larger than the normal one) and have vigorous vibration, instead of directional upward-force, which can be observed on the "abnormal" Ionic Flyers. It is suggested that the interference may exist in the directional flow of ions. As the electric field strength is different for the inner and outer electrode pairs, the ions, which are supposed to be attracted to the plate-collector, are being deviated by another force generated by the inner wire-emitter. Thus the ions will scatter instead of move directly to the collector. These multi-directional forces make the Ionic Flyers vibrate and as a result, affect the lift-up process. But further investigation is needed so that a more detailed explanation can be made.

To conclude, the results shown in this section suggest that the pair of electrodes (the wire-emitter and the plate-collector) can be considered as infinitesimal pairs of electrodes being connected in parallel and different geometrical arrangements will not affect the total *I-V* characteristics of the Ionic Flyers provided that their structural parameters are the same.

4.3.6 The Electrical Environmental Constant (K_e)

The discussions in all the previous sections focus on the effects of the five structural parameters to the current-voltage relationship, which is characterized by the current gain C and the onset voltage $V_{0,}$ of the Ionic Flyers. However, based on the theory of corona discharge, the ionic generation and the ionic diffusion are also depend on environmental factors like temperature, pressure and the background radiation, etc. Thus, the current-voltage characteristic of the Ionic Flyers is also expected to be responsive to different environmental conditions. As stated in the beginning of this chapter, all of the experiments regarding the Ionic Flyers were performed in the *CMNS* laboratory of the Chinese university of Hong Kong. In the laboratory, the environmental conditions are under controlled, thus all the experimental results are valid in standard temperature and pressure (*STP*) of 25^oC and $1atm$. For the calculation of the onset voltage V_0 of the Ionic Flyers, the modified Peek's equation has been developed based on the original Peek's equation. The equation consists of an air density factor, which is equal to one when the equation is applied for the discharge at *STP*.

In the following discussion, we would define an electrical environment constant K_e for the current gain C by using the experimental results in previous sections. By concluding the results from the experiments on the structural parameters, the current gain C of the Ionic Flyers can be summarized by the following equation:

$$K_e \cdot \frac{L}{d^2} \qquad \textbf{(4.3.10)}$$

where L and d are the electrode length and the gap distance in *mini-meter*; K_e is the electrical environmental constant which depends on the environmental conditions.

By collecting all the experimental results obtained in previous sections, the current gains have been plotted against $\frac{L}{d^2}$ as shown in Figure 4.18. A linear equation is used to fit the experimental data and the slope of the equation is equal to the electrical environmental constant under standard temperature and pressure. As indicated in the figure, the slope is equal to $0.001755 mA/mm \cdot kV^2$. In fact, this value reflects the changes of the environmental conditions and it should be valid under standard temperature and pressure. Recalibration of this value is needed if the environmental condition changes.

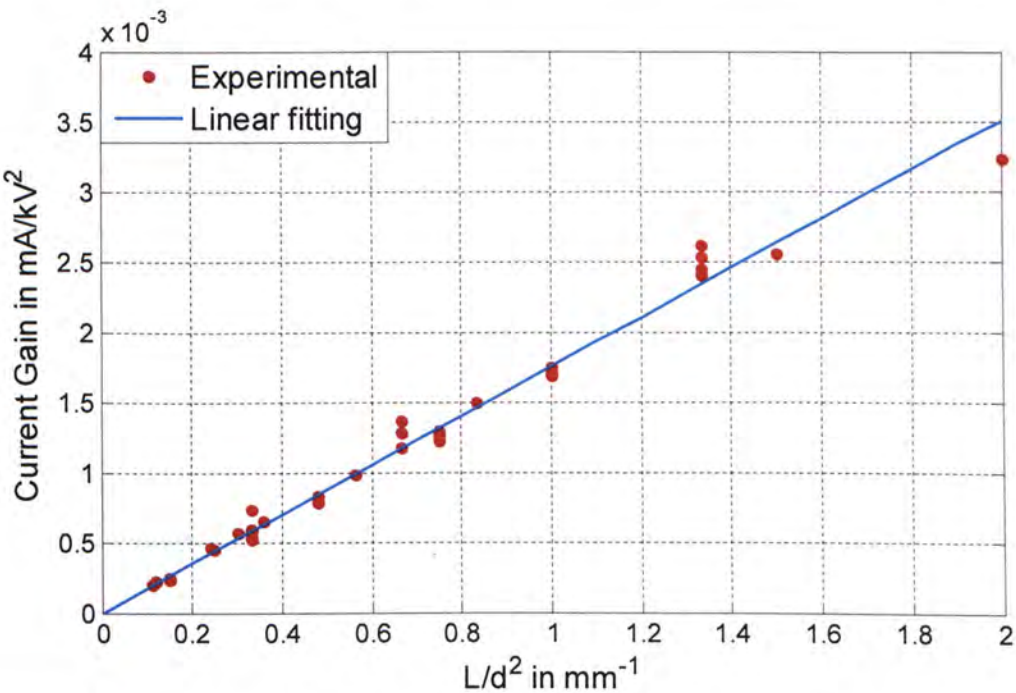

Figure 4.18: The experimental results on the current gain, which obtained in the previous sections, are plotted against $\frac{L}{d^2}$, with the corresponding electrode length L and gap distance d in mm. The data is fitted by a linear curve that is passing through the origin with the slope of $0.001755 mA/mm.kV^2$.

4.4 Summary of the Experimental Derived Current-Voltage Model

By summarizing the experimental results of the five structural parameters, including L, d, r_w, h and A, a general current-voltage model has been developed and presented in the following table.

Table 4.2: The experimental derived current-voltage model for the Ionic Flyers

$$I = C(L,d)(V - V_0(r_w,d))^2$$

with $$C(L,d) = 0.001755\frac{L}{d^2}$$

and $$V_0(r_w,d) = G(r_w)m_0 g_0 \delta\left(1 + \frac{0.0301}{\sqrt{\delta \cdot r_w}}\right) r_w \cdot \ln\left(\frac{d}{r_w}\right)$$

where $G(r_w) = 1 + e^{-\left(\frac{r_w}{4x10^{-5}}\right)}$

The current to voltage characteristic of the Ionic Flyer with wire-plate configuration and working under standard temperature and pressure can be predicted within 10% variation by equation as state at Table 4.2.

Chapter 5

Mechanical Lift-force Models

During positive corona discharge, a layer of positive ions will accumulate near the wire-emitter. These ions will accelerate by the electric field and force to move along the electric field line in the direction from the wire-emitter to the plate-collector. As long as the first layer leave the wire-emitter and on their way of moving to the plate-collector, another layer of positive ions is formed near the wire-emitter. The whole process repeats as long as the high voltage is kept applying to the electrodes and this kind of discharge is classified as self-sustaining discharge [26]. According to the electrohydrodynamic effect, when these layers of ions are transporting to the plat-collector, they will impart to the neutral molecules in the air and this generate a direction flow of air. The collision between the ions and the air molecules create the upward force to lift-up the Ionic Flyers. The energy is transfer directly from electrical energy of the high voltage power supply to the mechanical energy of the Ionic Flyers.

In the following discussion, experimental studies were carried out to investigate the magnitude of the lift-force acting on the Ionic Flyers. The organization of this chapter is similar to the previous one. The lift-force model, which is the relationship between the power input and the lift-force output of the Ionic Flyers, is first experimentally derived. Then, the five structural parameters described in the previous chapter are being test for their effects to the lift-force model. Finally, an equation regarding the lift-force to power ratio (F/P) of the Ionic Flyers is derived by concluding the results of this chapter and the previous chapter. The F/P equation can be effectively applied to optimize the F/P ratio of the Ionic Flyers under certain engineering requirement and constrain.

5.1 Experimental Setup and Measurement

The experiments regarding the lift-force model is done by applying high voltage electricity to Ionic Flyers and measure the corresponding weights that the Ionic Flyers can lift-up. Figure 5.1 illustrate the experimental setup. The Ionic Flyer is hanged *600mm* above a table by using a tripod. A *15*-gram "blu tack", which acts as an additional weight to the Ionic Flyer, is connected by a non-metal wire to the Ionic Flyer. The *15*-gram "blu tack" is then put on the pan of the electronic balance, which is the OHAUS Scout Balance with resolution of *10mg*. A transparent box, as indicated in the figure, is used to shell the balance in order to prevent air flow, which is generated by the Ionic Flyer, from hitting the pan of the electronic balance or else the measurement will be seriously affected. The transparent box contains a small hole to allow the wire-connection between the Ionic Flyers and the "blu tack". So, at the beginning of the experiments, the electronic balance should give a reading of *15 gram* and that is the weight of the "blu tack".

The experiments are performed by increasing the applied high voltage, which is starting from the onset voltage V_0, at *1kV* increments to the Ionic Flyers. The Ionic Flyer has to be able to lift up its own weight, which includes the electrodes and the wooden frame, first. When the Ionic Flyer is able to generate excessive force for lifting up additional weights by the increasing of applied voltage, the reading of the balance begins to drop from *15 gram*. The amount of reduction from the reading of the balance plus the own weight of the Ionic Flyer represents the lift-force generated by the Ionic Flyer.

The applied voltage and current is recorded for every *0.5 gram* reduction (i.e. that represents *5mN* increment in lift-force) of the reading on the electronic balance. All the experiments in this chapter, as discussed in the previous chapter regarding the *I-V* model, were preformed at the *CMNS* laboratory at standard temperature and pressure (*STP*). All the experiments were repeated for five times at different days. The results show that for all the Ionic Flyers that have been tested in this project, the output force measured at different days vary less than *10%*. Since the variation is very small, the average data of the five sets of data has been used as the representative data for analysis and modeling.

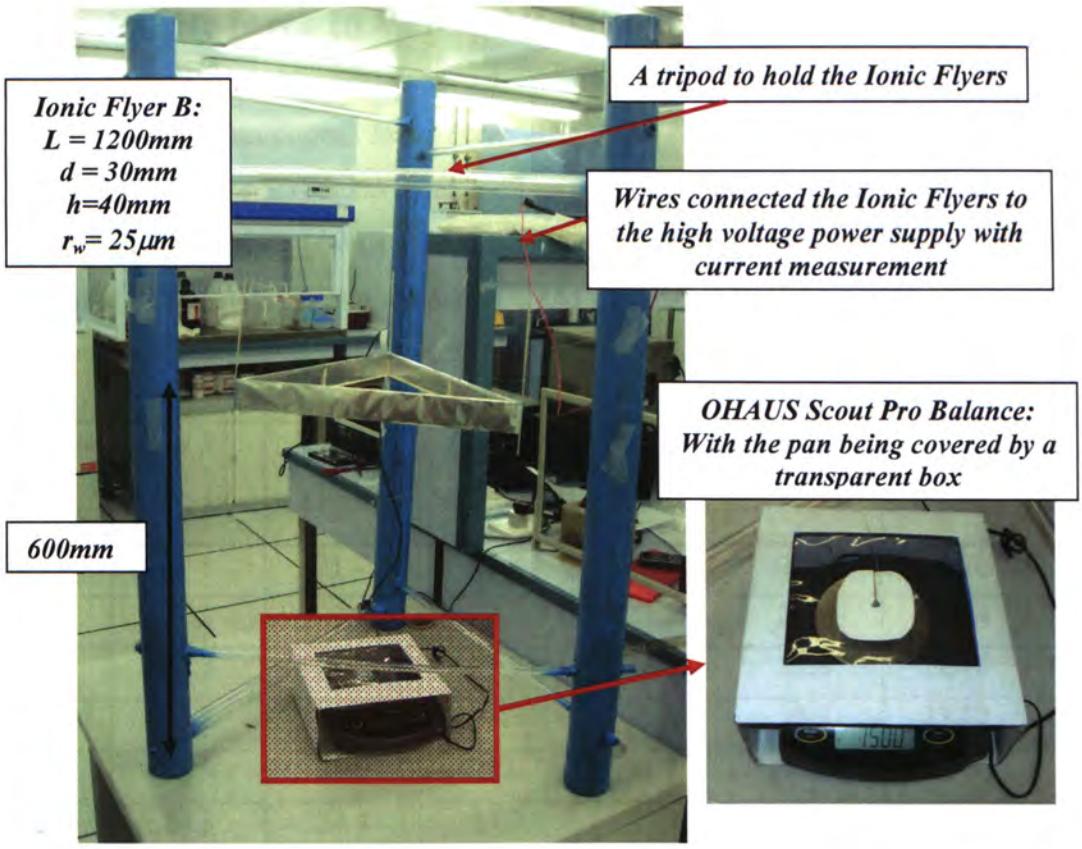

Figure 5.1: The experimental set-up used to measure the lift-force to voltage relationship, and also the lift-force to power relationship of Ionic Flyers

The organization for the following discussion is similar to that of the *I-V* model. Firstly, a basic lift-force model has been derived and the Ionic Flyer *B* (that is described below) was used as a representative flyer to explain the properties of the lift-force model. Also, there are two important parameters relating the lift-force and the power input and they were studied experimentally with respect to the five structural parameters (i.e. *L, d, r_w, h, A*) of the Ionic Flyers. Finally, a general lift-force model is developed based on the effects of the structural parameters of the Ionic Flyers.

5.2 Basic Lift-force to Voltage Relationship

In the following discussions, *Ionic Flyer B* with $L=1200mm$, $h=40mm$, $d=30mm$ and $r_w=25\mu m$ (see Figure 5.1) is taken as a representative flyer to discuss the results of the lift-force experiments. Table 4.1 shows the five sets of experimental data that they were recorded at different days. The temperature and humidity has been stated in the table for reference.

Force in gram	***V in kV*** (24.3°C, 45%)	***V in kV*** (24.2°C, 50%)	***V in kV*** (24.8°C, 49%)	***V in kV*** (24.9°C, 53%)	***V in kV*** (24.9°C, 50%)	***AVER.***	***STDEV.***
9.24	21.8	21.7	21.8	21.7	21.8	21.76	0.05477
9.74	22.2	22.2	22.3	22.3	22.2	22.24	0.05477
10.24	22.8	22.8	22.7	22.8	22.8	22.78	0.04472
10.74	23.3	23.4	23.3	23.3	23.3	23.32	0.04472
11.24	23.9	23.9	23.9	23.9	23.9	23.9	0
11.74	24.3	24.4	24.3	24.4	24.3	24.34	0.05477
12.24	24.8	24.8	24.7	24.7	24.8	24.76	0.05477
12.74	25.2	25.2	25.2	25.2	25.2	25.2	0
13.24	25.5	25.6	25.6	25.5	25.6	25.56	0.05477
13.74	26.2	26.2	26.2	26.2	26.2	26.2	0
14.24	26.7	26.7	26.6	26.6	26.7	26.66	0.05477
14.74	27.2	27.2	27.1	27.2	27.2	27.18	0.04472
15.24	27.6	27.7	27.6	27.6	27.6	27.62	0.04472
15.74	28.2	28.2	28.3	28.2	28.2	28.22	0.04472
16.24	28.7	28.8	28.8	28.7	28.7	28.74	0.05477

Table 5.1: Five sets of lift-force experimental data, which was taken at different days, for *Ionic Flyer B*. The second last column shows the averaged experimental data and last column shows the standard derivation of the experimental data

As stated in the table, all the experimental data have a very small value of standard derivation. The maximum standard derivation of the experimental data for Ionic Flyer *B* is found to be 0.05477. In fact, the experimental results for other Ionic Flyers have the standard derivations of less than *0.1 (i.e. 10%)*. The applied voltage (by using the averaged voltage as the representative voltage) of *Ionic Flyer B* was plotted against the lift-force as shown in Figure 5.2. The lift-force to voltage relationship, that obtained experimentally, has a linear relationship. A linear equation of $F = 1.019(V - 12.98)$, where F is the lift-force in gram and V is the applied voltage in kilovolt, has been derived by using the Least Square Fitting Method based on LAR (refer to Chapter 4 for detailed descriptions). The equation is plotted in the range of 21-*29kV* in Figure 5.2 (the figure did not show the x-intersection) and the R-square of the fitting is found to be 0.9994.

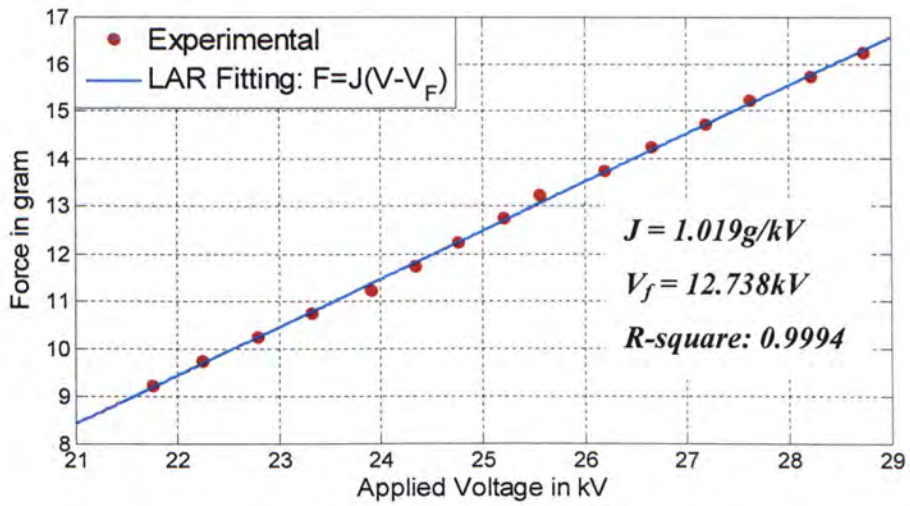

Figure 5.2: The variation of lift-force with the averaged applied voltage for *Ionic Flyer B*: experimental points (red circle), the derived *F-V* equation $F = 1.019(V - 12.738)$ (blue and full line)

5.2.1 The Initial Power Dissipation (*IPD*)

Based on the results of Chapter 4, the *I-V* relationship of the Ionic Flyer consists of the onset voltage V_0 for which indicates the initiation of the corona discharge. As long as the applied voltage exceeds V_0, the Ionic Flyer will consume electrical energy. Nevertheless, experimental results show that the Ionic Flyer does not generate measurable lift-force

even the applied voltage reach V_0 (by referring to section 4.3.1, *V_0 of Ionic Flyer B equals to 5.604kV*). According to the derived lift-force to voltage relationship, there exists a minimum voltage, named the barrier voltage V_f, so that the Ionic Flyer begins to create lift-force. Since the barrier voltage V_f (for *Ionic Flyer B*, $V_f = 12.738kV$) is always greater than the onset voltage V_0, the lift-force generation always occur after the corona discharge. The results suggested that although the Ionic Flyers start to consume electrical energy at V_0, the energy is not responsible for generating lift-force until the applied voltage reaches V_f.

As the applied voltage V is greater than V_0, the Ionic Flyer will dissipate certain power which is equal to $CV(V - V_0)^2$ based on the *I-V* relationship. While the applied voltage keeps increasing from V_0 to V_f, the power dissipation increase but there is still no measurable lift-force. Until the applied voltage reaches V_f, the power dissipation is equal to $P_f = CV_f(V_f - V_0)^2$. We defined P_f as the "Initial Power Dissipation (*IPD*)" as the maximum power loss before the Ionic Flyers is able to generate lift-force.

The ions, heat and light that produce by the Ionic Flyer are a kind of power loss during the initial stage of corona discharge. Also, there may exit air viscosity or friction so that the Ionic Flyers have to be dissipated certain power to overcome them. All these factors are the sources that contribute to the Initial Power Dissipation (*IPD*). *IPD* (or the barrier voltage V_f) can be treated as a limiting factor that the Ionic Flyer should be able to overcome in order to create lift-force. By the experimental results as discussed in the following sections, *IPD* depends on the structural parameters in certain aspects. For *Ionic Flyer B*, the Initial Power Dissipation is *1.55 Watt*

5.2.2 The Maximum Lift-force

Like all mechatronic systems, the lift-force output of the Ionic Flyers has an upper limit. This is because the applied voltage of the Ionic Flyer is limited by the threshold voltage that the maximum input power is deduced. The maximum lift-force can be calculated by the maximum input power in general. When the applied voltage is greater than the

threshold voltage, the lift-force acting on the Ionic Flyer will drop abruptly to zero since all the input power will be dissipated in the complete down of the air.

5.2.3 Proposed Third-order Equation for the Lift-force to Power Relationship

The lift-force to voltage relationship of the Ionic Flyers with the wire-plate configuration, as derived from the experiments, has a linear relationship. Based on our experimental results, we proposed a general *F-V* equation that can fit the experimental results with R-squared values of greater than *0.9*. The linear equation has been described in (5.2.1) with two parameters, the voltage gain J and the barrier voltage V_f. These two parameters have been proved experimentally depending on the structural parameters of the Ionic Flyers and also the environment factors. The details of the experimental results are discussed in the next session.

$$F = J(V - V_f) \tag{5.2.1}$$

where F is the lift-force in gram; V is the applied voltage in *kilovolt*; V_f is the barrier voltage in *kilovolt* and J is the force gain in *gram/kilovolt* .

The barrier voltage V_f and the force gain J characterize the lift-force model of the Ionic Flyers. The *F-V* relationship, together with the *I-V* model as discussed in the previous chapter, are applied to develop the lift-force to power relationship of the Ionic Flyers.

From elementary electrical theory, the power consumption of the Ionic Flyers is:

$$P = IV \tag{5.2.2}$$

where P is the input power in *W*att; I is the current consumption in mini-Ampere and V is the applied voltage in kilovolt.

According to the electrical *I-V* model which is described by the equation (4.2.1), the input power of the Ionic Flyers is related to the applied voltage by the following equation:

$$P = CV(V - V_0)^2 \tag{5.2.3}$$

where C and V_0 are the current gain and the onset voltage as discussed before.

By substituting equation (5.2.1) into equation (5.2.3), the input power to lift-force relationship is described by the following equation:

$$P = C(J^T F + V_f)(J^T F + V_f - V_0)^2 \tag{5.2.4}$$

where P is the input power in *Watt*; F is the force output in *gram;* J^T, in *kilovolt/gram*, is equal to the reciprocal of the voltage gain J; V_f is the barrier voltage in *kilovolt* and V_0 is the onset voltage in *kilovolt*

Figure 5.3 shows the experimental data and the derived lift-force model (equation (5.2.4)) of *Ionic Flyer B*. The current gain C is equal to *0.002405mA/kV* and voltage gain V_0 is equal to *5.604kV* as deduced by the electrical *I-V* model. In addition, as indicated in Figure 5.2, J^T is equal to *0.981kV/g* and V_f is equal to *12.738kV*. The lift-force model has a y-intersect at *1.559W* and this is the Initial Power Dissipation (*IPD*) of *Ionic Flyer B* as discussed in the previous section.

In the remaining discussion regarding the relationship between the lift-force and the input power, figures of lift-force to input power relationship is used to explain the properties instead of the one as shown in Figure 5.3 (i.e., figure of input power to lift-force relationship). The purpose of this is to give a better and ease comparison on the force/power ratio for different Ionic Flyers.

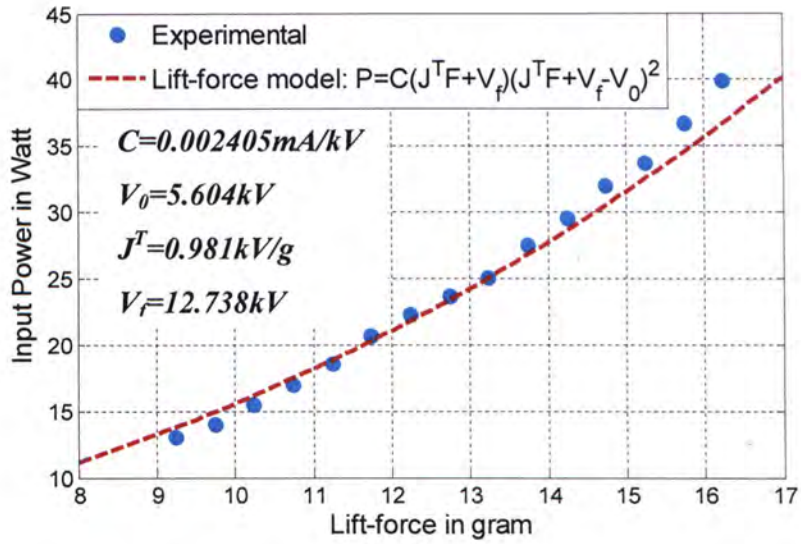

Figure 5.3: The variation of the input power with the lift-force for *Ionic Flyer B*: experimental points (blue circle), the derived lift-force model $P = 0.002405(0.981F + 12.738)(0.981F + 7.134)^2$ (red and broken line)

5.3 Determination of the Voltage Gain J and the Barrier Voltage V_f by the Structural Parameters of the Ionic Flyers

Based on the basic *F-V* relationship (also *F-P* relationship) of the Ionic Flyers, there are two parameters, the force gain J and the barrier voltage V_f, that can be varied by quantitatively changing the structural parameters of the Ionic Flyers. The same experimental procedures as described in chapter 4 were adopted to figure out the relationship between these two parameters and the five structural parameters of the Ionic Flyers. The five structural parameters, as described in the previous sections, are 1) the electrode length of the Ionic Flyer (L); 2) the gap distance between the wire-emitter and the plate-collector (d); 3) the wire-emitter radius (r_w); 4) the plate-collector height (h); 5) the electrode enclosed area (A) and 6) the lift-force environmental constant (K_f) which is determined by the temperature and pressure of the air.

According to the experimental procedures, the same prototypes regarding the current-voltage experiments as descried in Chapter 4 is adopted in the experiments of this chapter. All the experiments were first focused on the force-voltage relationship, then lift-force to power relationship is derived by using the *I-V* model and the *F-V* model. The general lift-force to voltage relationship can be represented by the following equation:

$$F = g(L, d, r_w, h, A, K_f)(V - V_f(V_0)) \tag{5.3.1}$$

where the function $g(L, d, r_w, h, A, K_f)$ is equal to the force gain J and $V_f(V_0)$ is equal to the barrier voltage.

In the following discussion, the rule as characterized by equation (4.3.2) and introduced in the previous chapter is adopted in analyzing the effectiveness of the structural parameters. The maximum variation of the testing parameter (*J or* V_f) is being calculated. If a value of less than *10%* is returned, the structural parameter will be considered as a non-effective parameter.

5.3.1 The Electrical Length (*L*)

In the previous chapter, the experimental results indicate that the current gain C of the Ionic Flyers is proportional to their electrical length. The current consumption thus is proportional to the electrode length at certain applied voltage. And it was expected that the lift-force acting on the Ionic Flyers are linearly related with the current consumption. Thus the force gain J of the Ionic Flyers is expected to be proportional to their electrode length. For this, experiments were carried out by investigating the four triangular Ionic Flyers with common structural parameters of d = *30mm*, h = *40mm*, r_w = *25μm* and the electrode lengths of *300mm, 600mm, 900mm and 1200mm,* respectively as shown in Figure 4.3 (in section 4.3.1).

Figure 5.4 illustrate the experimental results, with the "points" representing the experimental *F-V* data and that the "lines" are the derived *F-V* equation. The results are

consistent with our assumption: given the same input voltage, the lift-force acting on the Ionic Flyers increases with the extension of electrode length. The force gain J of the four Ionic Flyers were *0.2351 g/kV, 0.4474 g/kV, 0.6919 g/kV* and *1.109 g/kV* for the *300mm-length*, *600mm-length*, *900*mm-*length* and *1200*mm-*length* prototypes respectively. Furthermore, the force gains of the four Ionic Flyers were plotted against the electrode length as shown in Figure 5.5. A linear equation is used to fit the data and the R-square is *0.9849*. We can observe that the force gain is proportional to the electrode length of the Ionic Flyer as expected. The relationship between the lift-force and the electrode length of the Ionic Flyers can be represented by:

$$\frac{F_M(V_i)}{L_M} = \frac{F_N(V_i)}{L_N} \qquad \textbf{(5.3.2)}$$

where F_M and L_M are the lift-force and the electrode length of the Ionic Flyer M; F_N and L_N are the lift-force and the perimeter length of the Ionic Flyer N (*M and N represent different Ionic Flyers*); V_i is any applied voltage greater than the barrier voltage V_f

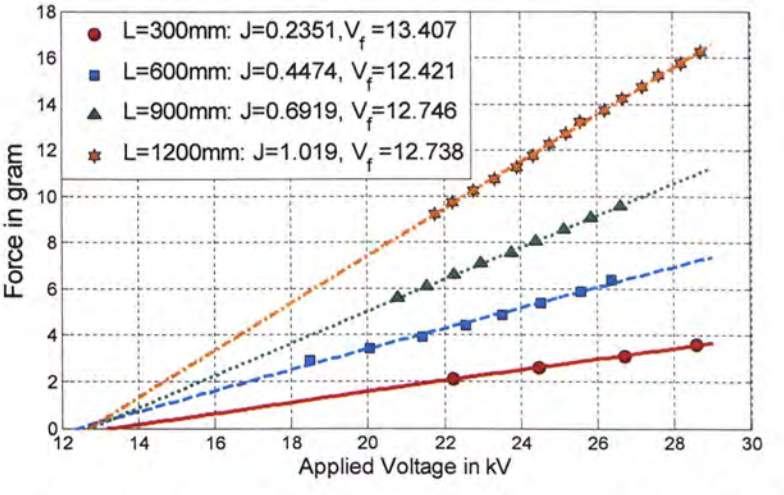

Figure 5.4: Experimental (points) and derived (lines) *F-V* relationship for the Ionic Flyers with the configuration as shown in Figure 4.3

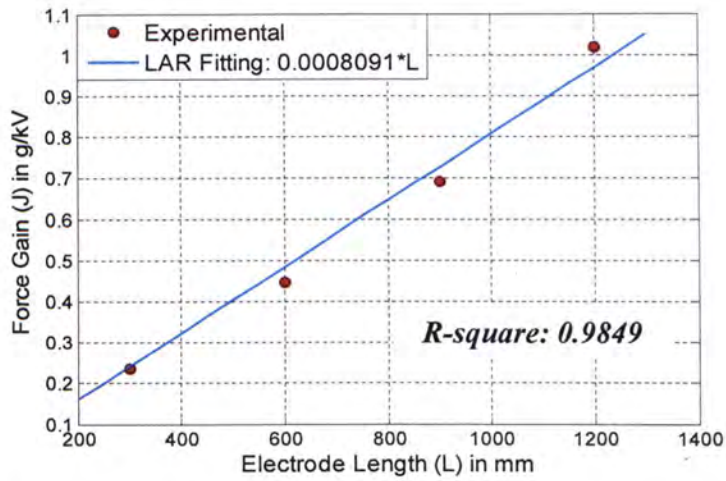

Figure 5.5: The experimental (points) and derived equation (line) for the relationship between the force gain J and the electrode length.

To conclude, given the same applied voltage, the force gain J of the Ionic Flyers is proportional to their electrode length. Thus, the general force gain $g(L,d,r_w,h,A,K_f)$ can be represent by $L \cdot g_1(d,r_w,h,A,K_f)$ with another function $g_1(.)$ that will be discussed in the following sections

In the following discussion, we would explain the relationship between the barrier voltage V_f and the electrode length of the Ionic Flyers. Based on the derived F-V equation, it was indicated that the four Ionic Flyers have similar barrier voltage V_f (see Figure 5.4) with the variation of *4.5%*. So, it is obvious that the electrode length plays no crucial role in affecting the barrier voltage V_f of the Ionic Flyers. On the other hand, by referring the results of section 4.3.1 in Chapter 4, the current gain C is proportional to the electrode length of the Ionic Flyers. Thus, the Initial Power Dissipation (*IPD*), which is equal to $P_f = CV_f(V_f - V_0)^2$ is theatrically proportional to the electrode length of the Ionic Flyers.

As discussed in the previous section, the Initial Power Dissipation use for the initial ions, heat and light generation of the corona discharge (those refer to the corona loss). Also the friction that acts on the Ionic Flyers is another source of the *IPD*. By the theory of corona

discharge, the corona loss occurs at ionization region around the wire-emitter and the power dissipation is proportional to its length [22], [15] (for the Ionic Flyers, the electrode length is equal to the emitter length). On the other hand, it is reasonable that the friction acting on the Ionic Flyer is proportional its length. Hence, the Initial Power Dissipation is expected to be proportional to the electrode length of the Ionic Flyers.

Figure 5.6 shows the experimental and derived lift-force to power relationship for the four Ionic Flyers. As indicated in the figure, the Initial Power Dissipations were *0.39W*, *0.72W*, *1.11W* and *1.55W* for the *300mm-length*, *600mm-length*, *900mm-length* and *1200mm-length* prototypes respectively. So, it is apparent that the *IPD* is proportional to the electrode length of the Ionic Flyers. Moreover, as observed from the figure, the force/ratio increases with the increase of the electrode length as long as the input power greater than about *3W*. The details of the force/power ratio would be briefly discussed in the next chapter.

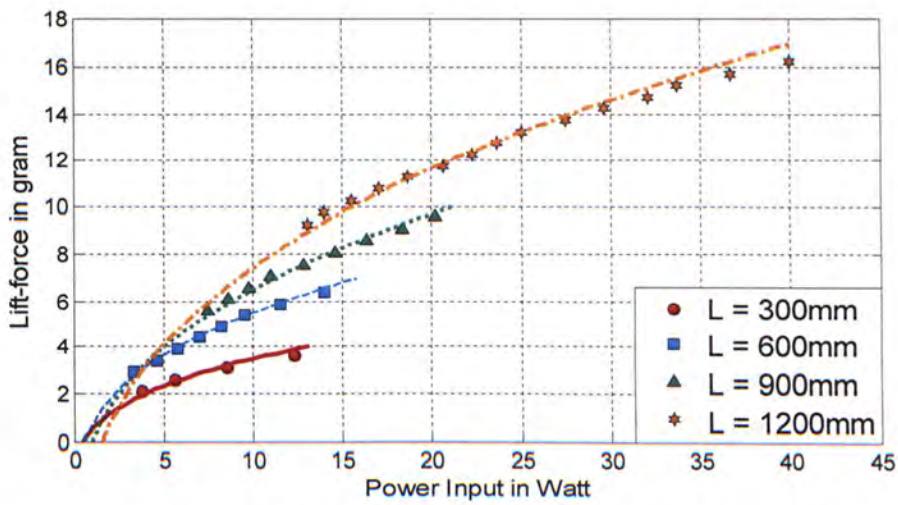

Figure 5.6: Experimental (points) and derived (lines) force to power relationship for the Ionic Flyers with the configurations as described in Figure 4.3

5.3.1.1 The relationship between the lift-up voltage and the electrode length of the Ionic Flyers

Since the lift-force acting on the Ionic Flyers is proportional to the electrode length under constant applied voltage. If we further assume that the weight of the electrodes and wooden-frame are proportional to the electrode length (the length of the Ionic Flyer), then the *lift-up voltage* is expected to be constant for every Ionic Flyers as long as the collector height and the wire radius is kept constant. Nevertheless, it is difficult to construct the wooden-frame with consistent thickness for each Ionic Flyer. Moreover, the size of the vertical pillar of the frame should be kept constant even the length is increase. Thus, the weight of the frame is actually not proportional to the length of the Ionic Flyers. In fact, experimental results also indicate different lift-up voltages (that is the first data points in the *F-V* graph) for the four Ionic Flyers.

5.3.2 The Gap Distance between the Wire-emitter and the Plate-collector (*d*)

As we mentioned in the previous chapter, the gap distance is an important structural parameter to the current to voltage relationship of the Ionic Flyers. The current gain C is proved to obey the inverse square law and the onset voltage V_0 is well predicted by the modified Peek's equation. In this section, we will further demonstrate the significance of the gap distance to the lift-force to power relationship which is quantified by the force gain J and the barrier voltage V_f.

The experiments were carried out by investigating the prototypes as stated previously in section 4.3.2. They were constructed with common parameters of $L = 1200mm$, $r_w = 25\mu m$, $h = 40mm$ and gap distances of *30mm, 40mm, 50mm, 60mm and 90mm,* respectively. The lift-force to voltage relationships of the five Ionic Flyers are illustrated in Figure 5.7. The force gain J displays a similar trend as the current gain in the *I-V* experiments. We can observe that the force gain decrease with the expansion of the gap distance, given the applied input voltage. As the gap distance decrease, the current consumption decrease and thus the lift-force decrease as expected.

In Figure 5.8, force gains of the five Ionic Flyers were plotted against the gap distance. We have verified that the force gain J is decrease at a slower rate as compared to that of the current gain C, as respect to the gap distance. Thus, a general inverse equation of $\frac{p}{d^n}$ (p and n is any constant) is adopted to determine the relationship between J and the d. Based on LAR fitting, the equation describing their relationship of d on J is:

$$J(d) = \frac{p}{d^{0.54}} \tag{5.3.3}$$

where p is a constant which depends on other structural parameters. For the five Ionic Flyers with the structural parameters reported above, p is equal to $6.405g.mm^{0.54}/kV$ as presented in Figure 5.8

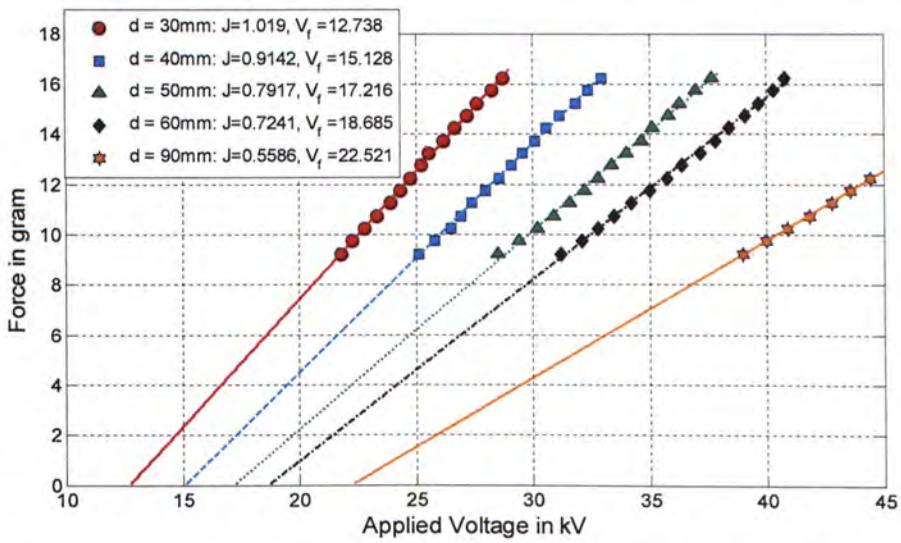

Figure 5.7: Experimental (points) and derived (lines) force to voltage relationship for the five Ionic Flyers with $L=1200mm$, $h=40mm$, $r_w=25\mu m$ and gap distance d of *30mm, 40mm, 50mm, 60mm* and *90mm respectively*

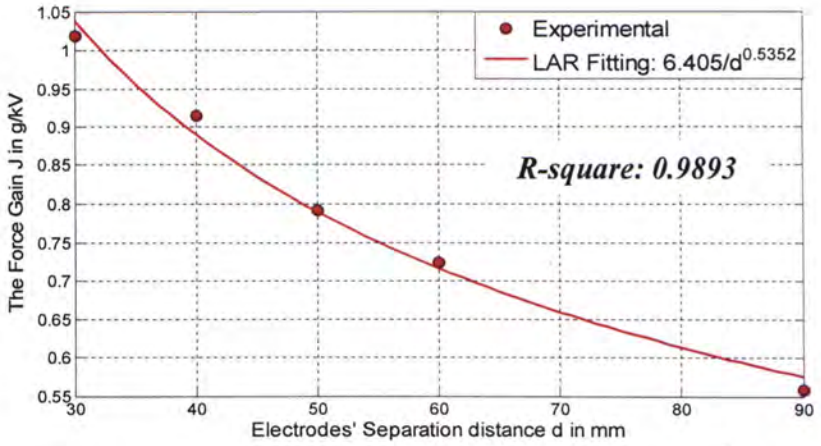

Figure 5.8: The variation of the force gain J with the gap distance (points). Equation (5.3.3) is applied to fit the experimental points with R-square of *0.9893*

In the following discussion, the barrier voltages of the five Ionic Flyers are interpreted by using the Initial Power Dissipation. It can be recognized in Figure 5.7 that the barrier voltages were *12.738kV*, *15.128kV*, *17.216kV*, *18.685kV* and *22.521kV* for the *30mm-gap*, *40mm-gap*, *50mm-gap*, *60mm-gap* and *90mm-gap* prototypes respectively. It is obviously that the arising of the barrier voltage is related to the onset voltage V_0 of the Ionic Flyers. As explained in the previous section, the Initial Power Dissipation is proved to be proportional to the length of the wire-emitter. Hence, the *IPD* should be kept constant as even the gap distance is being changed. This hypothesis has been verified by the experimental results. As deduced from the previous section, the *IPD* for the Ionic Flyers with L = *1200mm* is *1.55W*. Based on the preposition of "constant" *IPD*, the barrier voltage V_f should obey the following equation as long as the electrode length is kept constant:

$$CV_f(V_f - V_0)^2 = P_c \qquad \textbf{(5.3.4)}$$

where C is the current gain and V_0 is the onset voltage as discussed in Chapter 4. P_c is the *IPD* which is proportional to the electrode length of the Ionic Flyers only.

Figure 5.9 shows the experimental data and a curve that represents equation (5.3.3). It can be verified that equation (5.3.3) matched the experimental data with an R-square of

0.9902. Thus, it is apparent that the barrier voltage can be well predicted by the hypothesis which characteristic by equation (5.3.3).

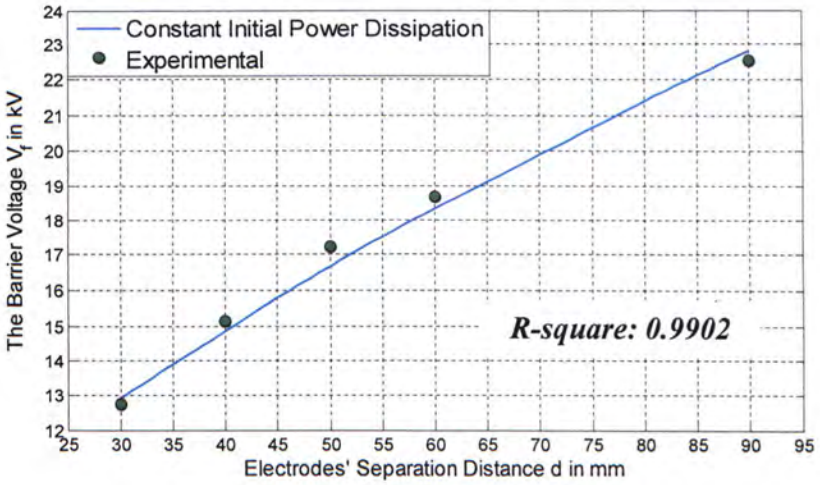

Figure 5.9: The variation of the barrier voltage V_f with the gap distance (points). The blue solid curve represents equation (5.3.3) which is applied to fit the experimental results. The fitting achieve the R-square of *0.9902* which verify the hypothesis.

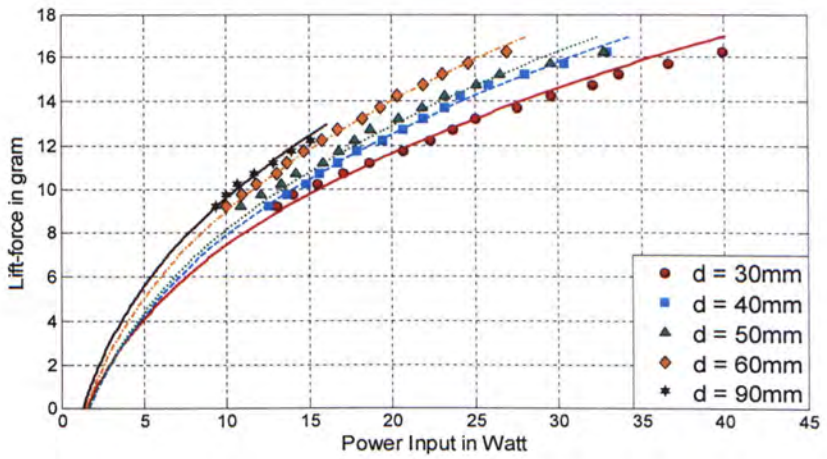

Figure 5.10: Experimental (points) and derived (lines) *F-P* relationship for the Ionic Flyers with *L=1200mm, h=40mm,* r_w*=25*μ*m*. The electrodes' separation distance d for the five data is *30mm, 40mm, 50mm, 60mm* and *90mm*

The lift-force to power relationship is illustrated in Figure 5.10. The experimental results are analyzed and are consistent with the previously proposed theory of constant. It is

apparent that the five curves, that corresponding to the five gap distances in the experiments, intersect at *1.55 W* on the x-axis. As the force gain decrease at a slower rate as compared to that of the current gain (i.e. $\frac{1}{d^{0.54}}$ vs. $\frac{1}{d^2}$), hence the force/power ratio is greater for the Ionic Flyer with gap distance under constant power input.

5.3.3 The Wire-emitter Radius (r_w)

In Chapter 4, it is proved that the onset voltage of the Ionic Flyers depends significantly on the radius of the emitter, which however shows no evidential contribution to the current gain C. In this section, we will further demonstrate that the radius of the wire-emitter is an non-effective structural parameter to the force gain *J*. While the barrier voltage V_f is basically obey the proposition of constant Initial Power Dissipation

The experiments were carried out by investigating three sets of Ionic Flyers. The first set consisted of three Ionic Flyers, with common parameters of $L = 1200mm$, $d = 40mm$, $h = 40mm$ and emitter radii of *0.025mm*, *0.075mm* and *0.12mm* respectively. The second and the third set also contained four Ionic Flyers, the only different was that they were all constructed with gap distance *d* of *50mm and 60mm* respectively.

Figure 5.11 shows the experimental results, with (a), (b) and (c) corresponding to the three sets of Ionic Flyers. In each graph, the three linear curves display similar slopes. Based on the derived quadratic *F-V* equation, it was indicated that they have similar force gain *J* as from the results shown in Figure 5.11. We can observe that the variations of the force gain *J* for each set of data are all within *10%*. So, it is obvious that the force gain *J*, similar to the current gain *C*, does not depend on the emitter radius of the Ionic Flyers.

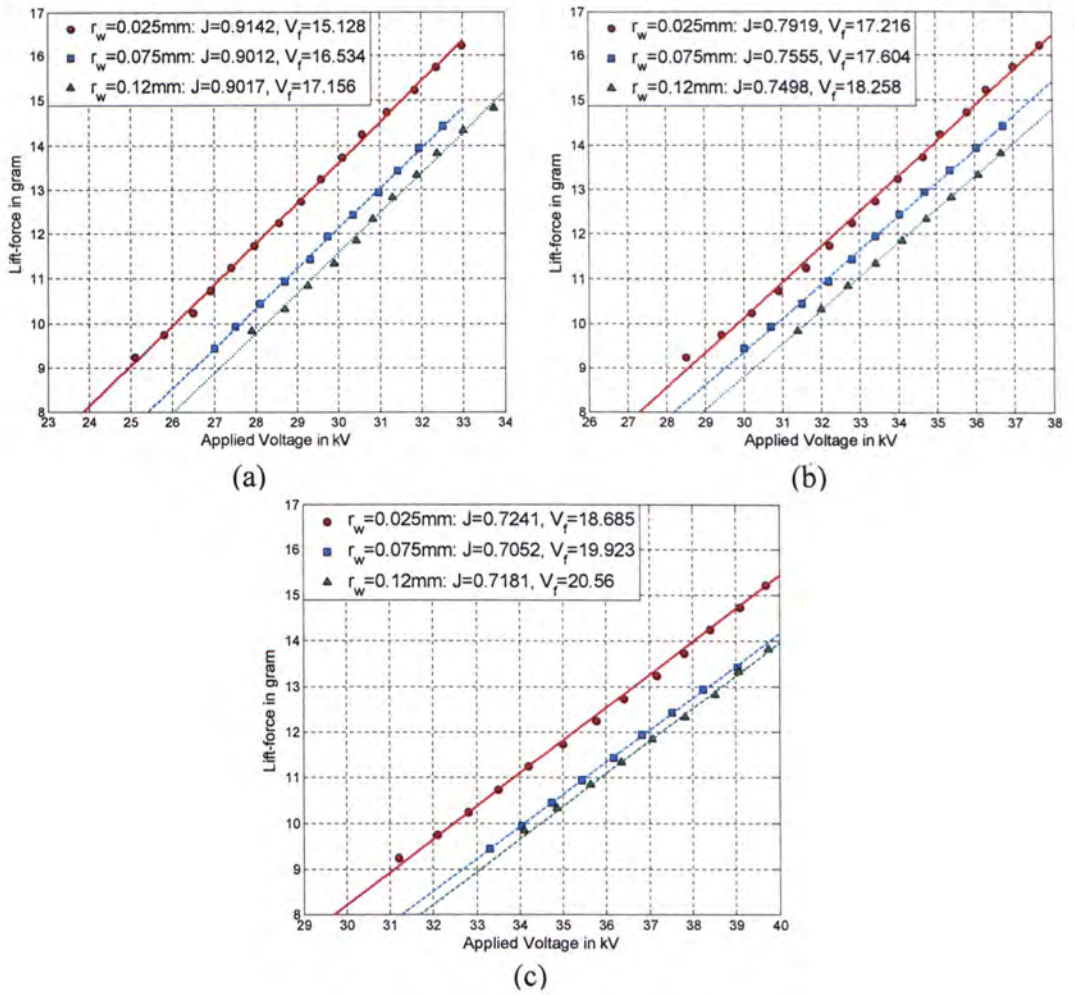

Figure 5.11: Experimental (points) and derived (lines) lift-force to voltage relationship for the three sets of Ionic Flyers with *L=1200mm, h=40mm* and emitter radii of *0.025mm*, *0.075mm* and *0.12mm respectively*. The gap distance for a) is *40mm, b)* is *50mm and c)* is *60mm*

Since the length of the wire-emitter is kept constant at *1200mm* during the experiments, the barrier voltage could be well predicted by the proposition of constant *IPD*. The barrier voltages, at indicated in Figure 5.11, is plotted against the emitter radii as shown in Figure 5.12. We have compared the experimental results with three curves that describe the constant *IPD*. As illustrated obviously in the figure, the experimental data is consistence with the curves (with R-square of *0.9963*, *0.9902* and *0.9881* respectively). So, it is apparent that the barrier voltage V_f, can be evaluated based on the assumption of constant Initial Power Dissipation.

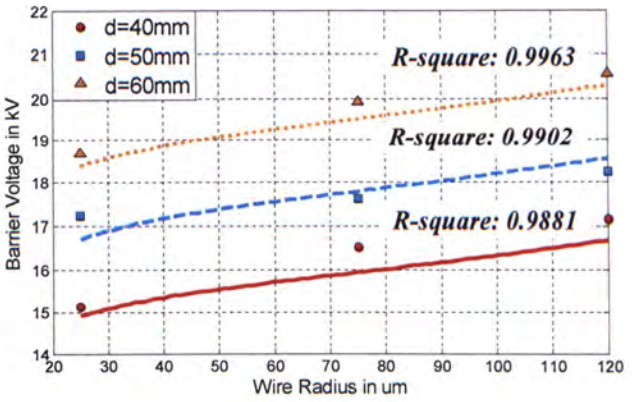

Figure 5.12: The variation of the barrier voltage V_f with the emitter radius (points). The curves represents the constant *IPD* which is applied to compare the experimental results.

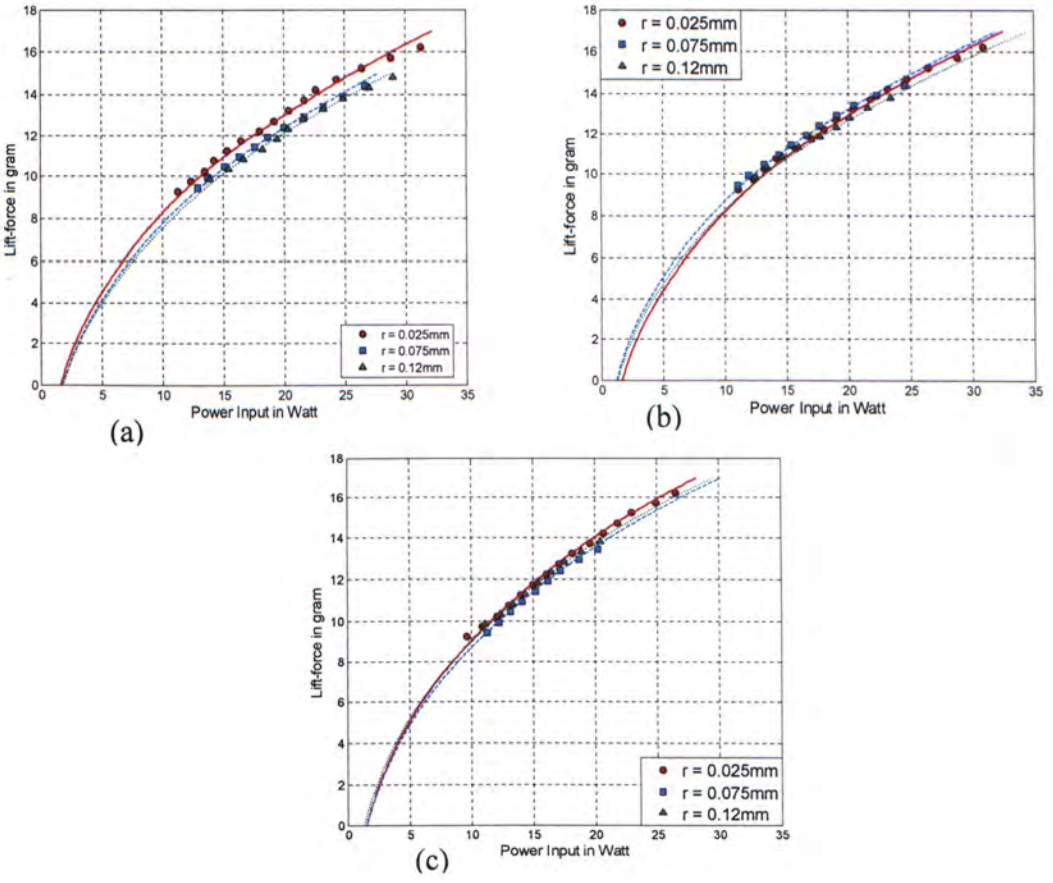

Figure 5.13: Experimental (points) and derived (lines) lift-force to power relationship for the three sets of Ionic Flyers with *L=1200mm, h=40mm* and emitter radii of *0.025mm*, *0.075mm* and *0.12mm* respectively. The gap distance for a) is *40mm, b)* is *50mm and c)* is *60mm*

Figure 5.13 shows the lift-force to power relationship for the three sets of Ionic Flyers. In all the three graphs, they display repeatable trend and results for the three Ionic Flyers. As quantified by the constant *IPD*, those curves pass through *1.55 W* on the x-axis. To summarize, the constant current gain, force gain and *IPD* for the Ionic Flyers with different emitter radius results in an unaffected force/power ratio as indicated in Figure 5.13.

5.3.4 The Plate-collector Height (*h*)

As we mentioned before, it was expected that the height of the plate-collector plays no crucial role in the working performance of the Ionic Flyers. In the previous chapter, we have already verified the insignificancy of the collector height to the *I-V* characteristic, which is quantified by the current gain C and the onset voltage V_0, of the Ionic Flyers. In this section, we will further demonstrate that this structural parameter does not participate in the lift-force to power relationship on the Ionic Flyers.

The experiments were performed by investigating two sets of Ionic Flyers that were stated previously in section 4.3.4 (the *I-V* section, also see Figure 4.12). The lift-force to voltage relationship is illustrated in Figure 5.14, with (a) describing the first set with L = *600mm* and (b) describing the second set with L = *1200mm*. The linear curves, which have the similar situation of the *I-V* curves as discussed before, display congruous trend for the four Ionic Flyers in both graphs. The variations of the current gain C and the onset voltage V_0 for each set of data are both within *10%*. So, it is suggested from the experimental results that the height of the plate-collector can be classified as a non-effective structural parameter to the lift-force to voltage relationship of the Ionic Flyers.

Figure 5.15 shows the lift-force to power relationship, consistent curves can be observe as expected. To conclude, we proved evidentially that the height of the plate-collector (with variation from *30mm* to *60 mm*) will not affect the performance of the Ionic Flyers, which is characterized by the current gain C, the onset voltage V_0, the force gain J and the barrier voltage V_f.

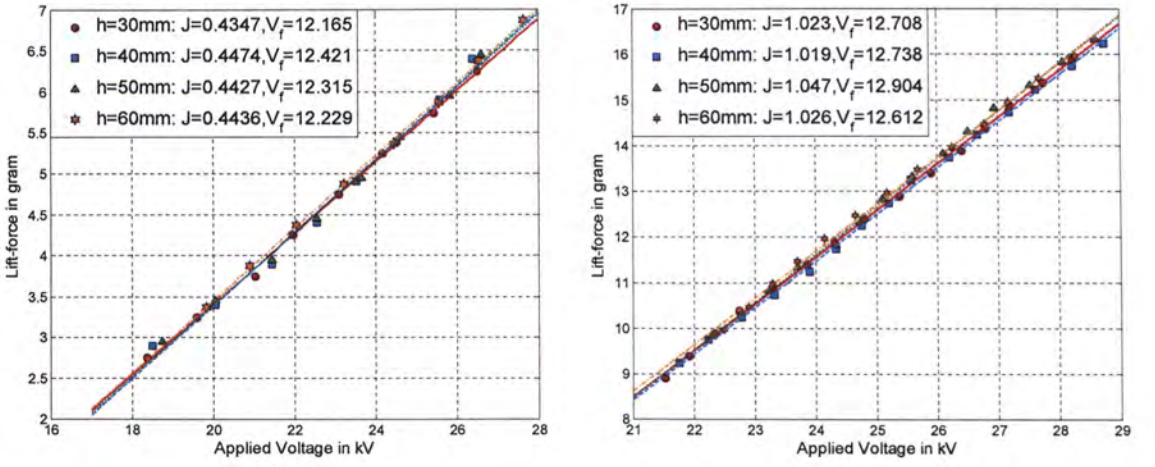

(a) (b)

Figure 5.14: Experimental (points) and derived (lines) lift-force to voltage relationship for the two sets of Ionic Flyers with d=*30mm*, r_w=*25μm* and the collector height of *30mm, 40mm, 50mm and 60mm* respectively. The electrode length for a) is *600mm* and *b)* is *1200mm*

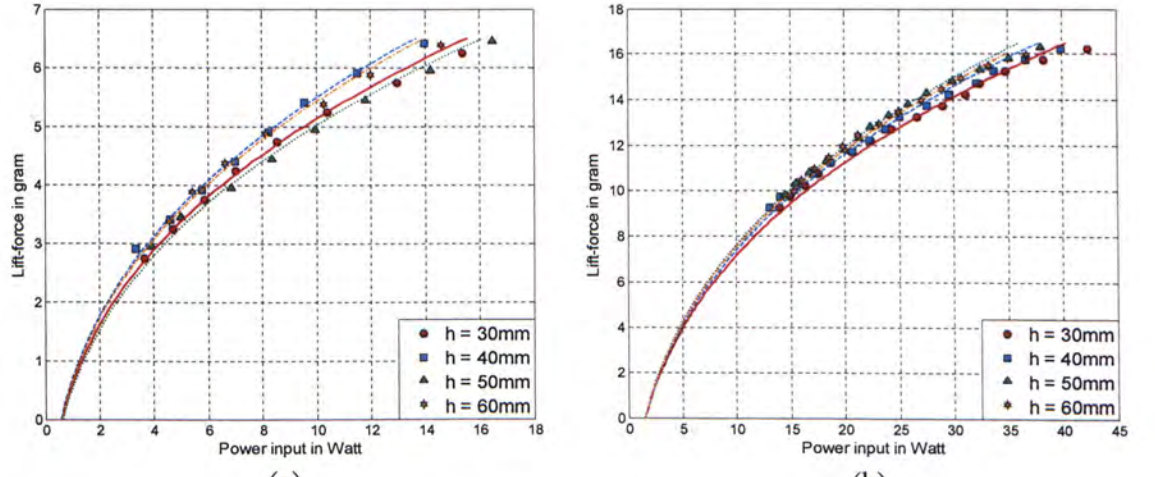

(a) (b)

Figure 5.15: Experimental (points) and derived (lines) lift-force to power relationship for the two sets of Ionic Flyers with d=*30mm*, r_w=*25μm* and the collector height of *30mm, 40mm, 50mm and 60mm* respectively. The electrode length for a) is *600mm* and *b)* is *1200mm*

5.3.5 The Electrode Enclosed Area (A)

We proved in the previous chapter (in section 4.3.5) that, the pair of electrodes (the wire-emitter and the plate-collector) can be treated as infinitesimal pairs of electrodes being

connected electrically in parallel and different geometrical arrangements will not affect the total *I-V* characteristics of the Ionic Flyers provided that their electrode length is kept constant. It is expected that the performance of lift-force generation would not be affected by the arrangement of the electrodes as long as the electrode length is kept constant. In this section, we will further demonstrate that the enclosed area and even the arrangement of electrodes govern insignificantly to the lift-force to power relationship of the Ionic Flyers.

The experiments were divided into two parts. In the first part, two groups Ionic Flyers with square-shape, hexagonal-shape and triangular-shape, as described in section 4.3.5, (see Figure 4.14) have been investigated. The experimental results on the lift-force to voltage relationship are presented in Figure 5.16 with (a) reporting the results of the *900mm-length* prototypes and (b) the *1200mm-length* prototypes. In both graphs, consistence trends and curves can be observed. By considering the force gains and the barrier voltages in (a), the variations are *1.5%* and *0.5%* respectively. While for the results in (b), the variations are *1%* and *1.5%* respectively. The variations are both within *10%*, thereby the lift-force to power relationship, as illustrated in Figure 5.17, can display consistence curves for the three Ionic Flyers with different geometrical shapes. The experimental results manifest the insignificance of the electrode's enclosed area to the working performance of the Ionic Flyers.

In the second part, we further investigated the effect of the electrodes' arrangement of the Ionic Flyer. The experiments were carried out accordingly by analyzing three Composite Ionic Flyers (see Figure 4.16 in section 4.3.5) and comparing the experimental results with three "Normal" Ionic Flyers. Again, as indicated by Figure 5.17 and Figure 5.18, the barrier voltages were consistence with the criteria as stated in section 5.3.1, and the voltage gains were also fitted within *10%* variations by equation (5.3.2). So, it is evidentially proved that both "Normal" and "Composite" Ionic Flyers have analogous properties, which can be evaluated based on similar assumptions and equations.

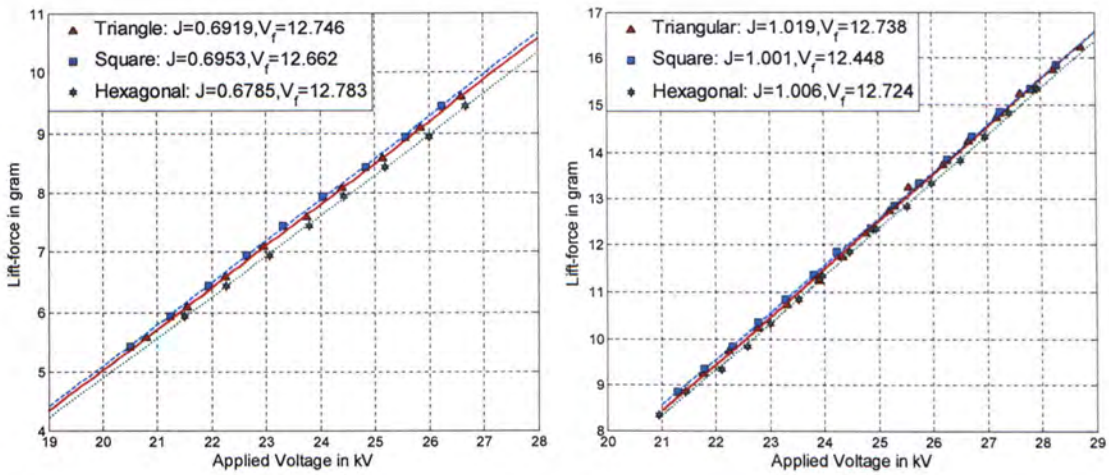

Figure 5.16: Experimental (points) and derived (lines) lift-force to voltage relationship for the Ionic Flyers with the configuration as described in Figure 4.14 . The electrode length L for (a) is *900mm* and (b) *is 1200mm*

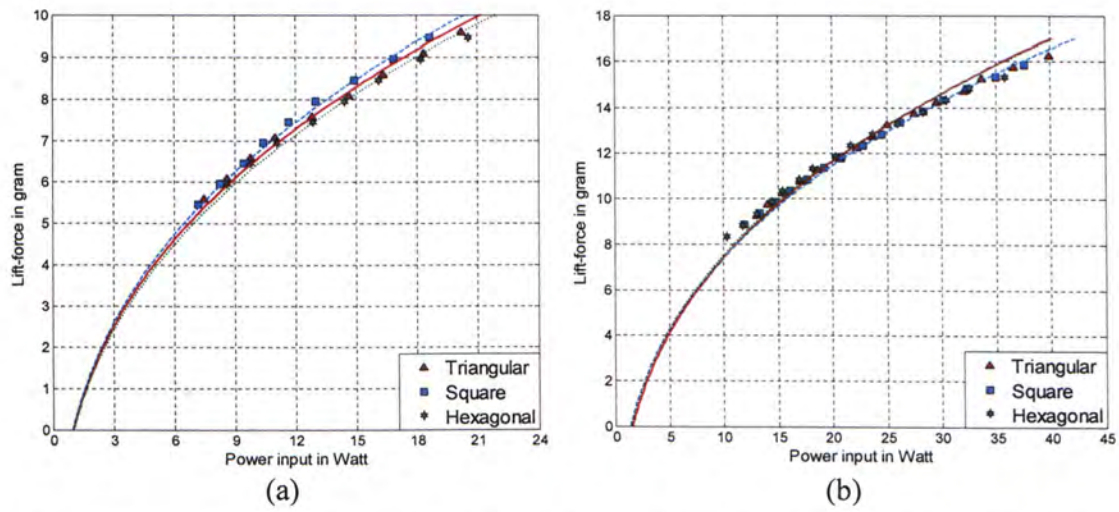

Figure 5.17: Experimental (points) and derived (lines) *F-P* relationship for the Ionic Flyers with triangular, square and hexagonal shape. The total perimeter length is a) *900mm, b) 1200mm*

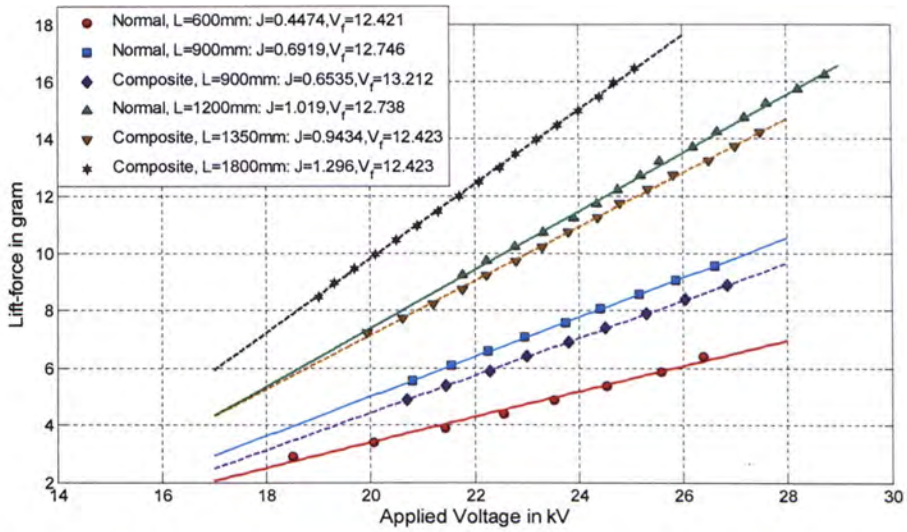

Figure 5.18: Experimental (points) and derived (lines) *F-V* relationship for the Ionic Flyers with triangular, square and hexagonal shape. The total perimeter length is a) *900mm, b) 1200mm*

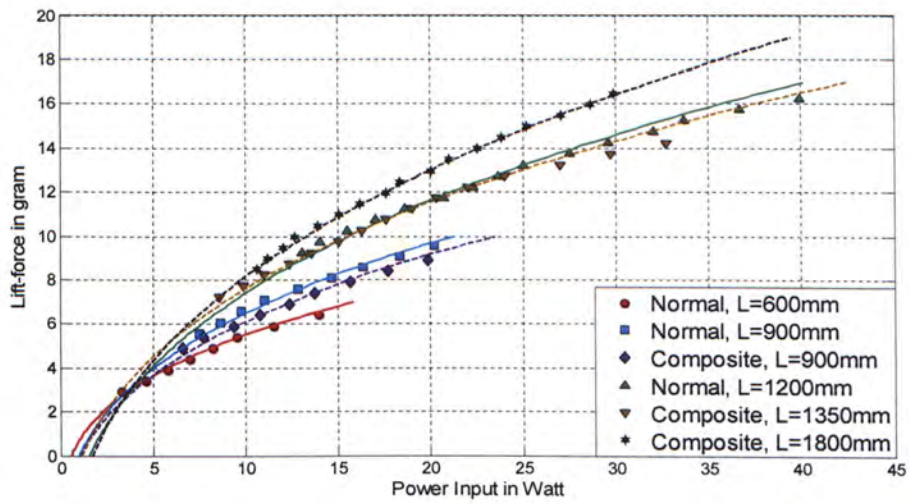

Figure 5.19: Experimental (points) and derived (lines) *F-P* relationship for the Ionic Flyers with triangular, square and hexagonal shape. The total perimeter length is a) *900mm, b) 1200mm*

5.3.6 The Lift-force Environmental Constant (K_f)

The performance of lift-force generation is expected to be affected by the environmental factors like temperature and pressure, etc. In the previous chapter, an electrical environment constant K_e is derived to characterize the current-voltage characteristic under standard temperature and pressure *STP* (i.e. 25^oC, $1atm$). The two parameters, the force gain J and the barrier voltage V_f, are also supposed to be sensitive to the environmental conditions. For the barrier voltage V_f of the Ionic Flyers, the proposition of Initial Power Dissipation has been derived based on the modified Peek's equation which consists of an air density factor (It is equal to one when the equation is applied under *STP*).

In the following discussion, we would define a lift-force related environment constant K_f for the force gain J by using the experimental results in previous sections of this chapter. By concluding the results from the experiments on the structural parameters, the force gain J of the Ionic Flyers can be summarized by the following equation:

$$K_f \cdot \frac{L}{d^{0.54}} \qquad \textbf{(5.3.5)}$$

where L and d are the electrode length and the gap distance in mm; K_f is the lift-froce related environmental constant which depends on the environmental conditions.

Similar to the previous chapter, the force gains have been plotted against $\frac{L}{d^{0.54}}$ as shown in Figure 5.20. A linear equation is used to fit the experimental data and the slope of the equation is equal to K_f under *STP*. It is indicated in the figure that the slope is equal to $0.005238 \ \ g/mm^{0.46} \cdot kV$. Again, this value reflects the changes of the environmental conditions and it should be valid under standard temperature and pressure. Recalibration of this value is needed if the environmental condition changes.

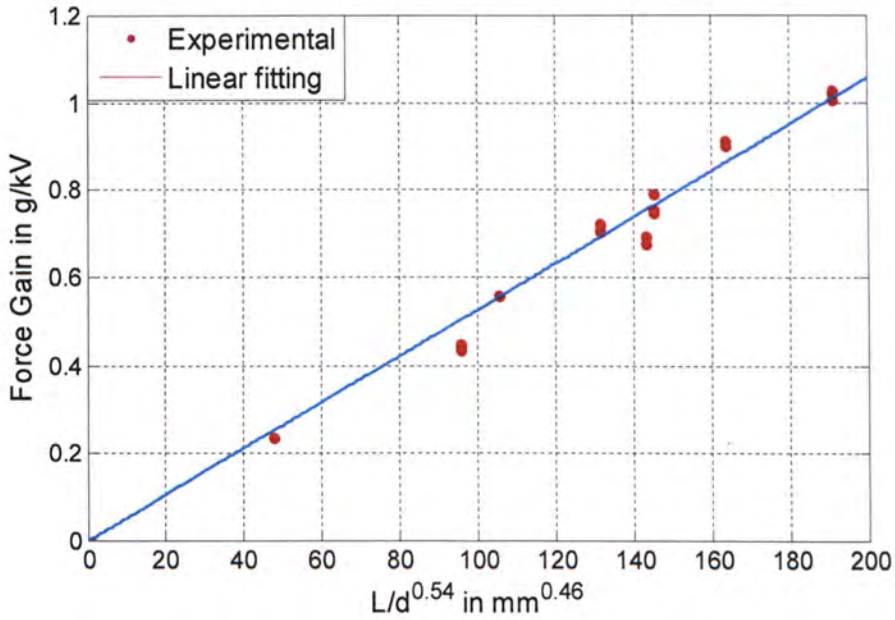

Figure 5.20: The experimental results on the force gain, which obtained in the previous sections, are plotted against $\frac{L}{d^{0.54}}$, with the corresponding electrode length L and gap distance d in mm. The data is fitted by a linear curve that is passing through the origin with the slope of $0.005238 g/mm^{0.46}.kV^2$.

5.4 Summary of the Experimental Derived Lift-force Model

By summarizing the experimental results of the five structural parameters, including L, d, r_w, h and A, a general lift-force model has been developed and presented in the following table.

Table 5.2: The experimental derived lift-force model for the Ionic Flyers

$$F = J(L,d)(V - V_f(V_0))$$

and

$$P = C(J^T F + V_f(V_0))(J^T F + V_f(V_0) - V_0)^2$$

with

$$J(L,d) = 0.005238\frac{L}{d^{0.54}}$$

and

$$V_f(V_0) \textit{ satisfy } CV_f(V_f - V_0)^2 = P_c$$

$$\text{where } P_c = 0.001259 \cdot L$$

The lift-force model (consists of the lift-force to voltage and the lift-force to power relationship) of the Ionic Flyer with wire-plate configuration working under standard temperature and pressure can be predicted within 10% variation by equations as state at Table 5.2.

5.5 Analysis on the Force/Power Ratio of the Ionic Flyers

Based on the power to voltage model (that is derived from the current to voltage model) and the lift-force to voltage model, an equation of the force/power ratio of the Ionic Flyer is derived as:

Table 5.3: The experimental derived force/power ratio for the Ionic Flyers

$$\frac{F}{P} = 2.98d^{1.46}\frac{(V - V_f(V_0))}{V(V - V_0)^2}$$

with

$$V_0(r_w, d) = G(r_w)m_0 g_0 \delta\left(1 + \frac{0.0301}{\sqrt{\delta \cdot r_w}}\right) r_w \cdot \ln\left(\frac{d}{r_w}\right)$$

$$\textit{where } G(r_w) = 1 + e^{-\left(\frac{r_w}{4x10^{-5}}\right)}$$

and

$$V_f(V_0) \textit{ satisfy } CV_f(V_f - V_0)^2 = P_c$$

$$\textit{where } P_c = 0.001259 \cdot L$$

It is indicated in the equation that the force/power ratio depends only on the gap distance and the applied voltage of the Ionic Flyer. Based on certain engineering requirements, Ionic Flyers with optimal force/power ratio can be obtained.

For example, given a variable *0kV* to *50kV* voltage input and the gap distance of the Ionic Flyer is limited in *30mm to 90mm*. The maximum force/power ratio is *0.9664* (see Figure 5.21) with the input voltage of *32kV* and gap distance of *90mm*. The electrode length can be obtained by concerning the output lift-force. For example, for the lift-force of *20g*, electrode length of *4658mm* is required.

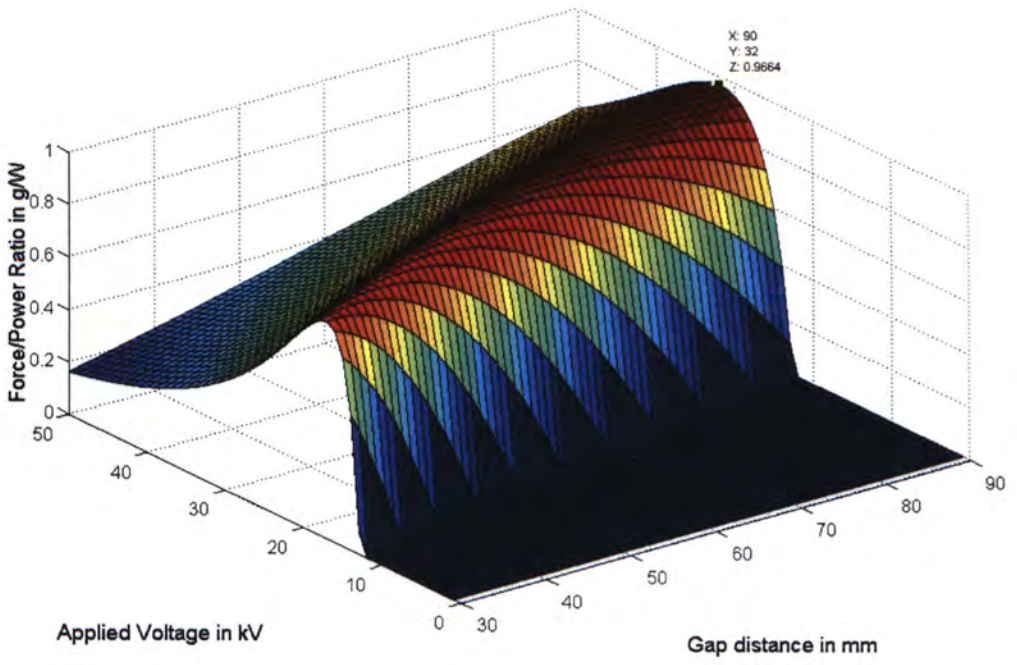

Figure 5.21: Variation of the force/power ratio with the applied voltage and gap distance of the Ionic Flyer. The gap distance is in the range of 30mm to 90mm and the applied voltage is in the range of 0kV to 50kV. The maximum force/power ratio is indicated at the peak of the surface.

Chapter 6

Further development of the Ionic Flyers

6.1 Multi-directional Force Generation

As we mention before, the working principle of the Ionic Flyer is generally electrohydrodynamics. Since the Biefeld-Bown effect propose that the force acting on the high-electric-field object is parallel to the gravitation field. Thereby, the force acting on the Ionic Flyers should be restricted in upward or downward direction only. However, this is not true based on our experimental results. We will demonstrate in this section that, the Ionic Flyer is not only a vertical lifting and landing machine, i.e., they can create force in different directions that is determined by the orientations of their electrodes.

We have already introduced that the Ionic Flyer is a composition of a metallic wire-emitter and plate-collector (The wooden frame is only presence for isolating he electrodes and theoretically not participating in generating force). For the electrodes in the usual orientation (like those illustrated in the previous chapters), the force acting on the Ionic Flyer is in upward direction. In the following discussion, we will further demonstrate the horizontal linear motion (forward and backward), and the rotational motion (rotation about the x, y and z axis of the body fame) of the Ionic Flyer. Therefore, verifying that the force acting on the Ionic Flyer can be in multi-directions. For the ease of explanation, the electrode direction is defined as the route/path from collector to emitter in the following in the following discussion.

6.1.1 Linear Motion

If the force acting on the Ionic Flyer is directed from the collector to the emitter, then horizontal linear motion can be achieved by orientating the electrode direction perpendicularly to the gravitational field. Figure 6.1 (a) shows a Hybrid Ionic Flyer that consisted of two identical "Vertical" Ionic Flyers (i.e. with vertical electrode direction) and a "Horizontal" Ionic Flyer. The two "Vertical" Ionic Flyers are electrically connected in parallel to a power supply. The "Horizontal" Ionic Flyer was constructed with the electrode direction in perpendicularly to the gravitational field. Also, it is connected independently to another power supply. Therefore, the two kinds of Ionic Flyers can work independently, with the "Vertical" Ionic Flyers corresponding to the vertical lift-up motion and the "Horizontal" Ionic Flyer corresponding to horizontal linear motion. Figure 6.1 (b) demonstrate that the Hybrid Ionic Flyer were lifting up when high-voltage power is supplied to the two "Vertical" Ionic Flyers and no horizontal linear motion is observed at this moment. Figure 6.1 (c) demonstrate that, when the "Horizontal" Ionic Flyer were activated, linear horizontal force were acting on the Hybrid Ionic Flyer. Therefore, it was moving forward in the mid-air. By using the same principle, the backward motion of the Hybrid Ionic Flyer can also be achieved by reversing the electrode direction of the Horizontal Ionic Flyer.

As indicated from the experimental results, the "Horizontal" and "Vertical" Ionic Flyer can work independently to provide component forces without interfering each others. It is apparent that multi-directional force can be achieved by orientating the electrodes pair in the desired directions. The force acting on the Ionic Flyer is generated by ions owing to the corona discharge. Also, the force is directed from the collector to the emitter and this is consistence with the electrohydrodynamic effect, but not the Biefeld-Bown effect.

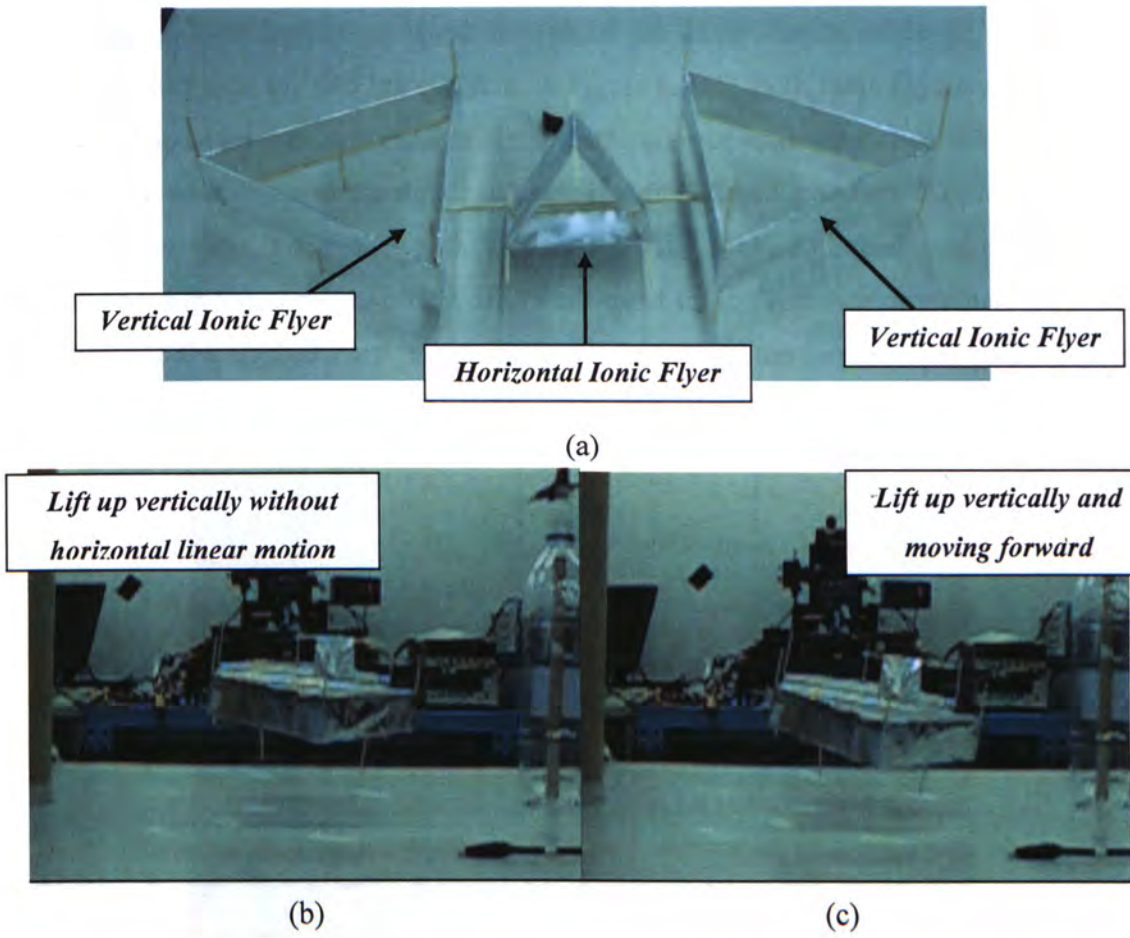

Figure 6.1: Demonstration of horizontal linear motion by a hybrid Ionic Flyer that consisted of one vertical Ionic Flyer and one horizontal Ionic Flyer. The two Ionic Flyers are powered by two independent power supplies. a) shows the prototype, b) shows that the vertical Ionic Flyer was powered up and the hybrid Ionic Flyer vertically lift up, c) shows that both vertical and horizontal Ionic Flyer were powered up and the hybrid Ionic Flyer moved forward in the mid-air

6.1.2 Rotation Motion

Besides linear motion, rotation motion of the Ionic Flyer will be demonstrated in the following. The experiments were carried out by investigating the "Lever" Ionic Flyer as described in Figure 6.2. The Lever Ionic Flyer is constructed by combining two "Vertical" Ionic Flyers with a wooden stick. Each "Vertical" Ionic Flyers is connected with its own power supply. Given the same applied voltage, they should have consistent working performance as they were constructed with the same structural parameters (i.e. L,

d, r_w, h, A). Therefore, the rotation motion of the Lever can be achieved by applying different voltage to the two Ionic Flyers. In Figure 6.2 (a), both Ionic Flyers were worked at *18kV*. The Lever was kept balance since identical force acted on its two sides. In Figure 6.2 (b), the Ionic Flyer in the right hand side is supplied with constant *18kV* while that in the left hand side is supplied with varying *17kV* to *18kV*. Anticlockwise rotation was observed when the applied voltage of the left-hand Ionic Flyer was dropping from *18kV* to *17kV*. As the applied voltage rose from *17kV* to *18kV*, the Lever balanced again. The result proved the feasibility of rotation motions of the Ionic Flyer.

(a)

(b)

Figure 6.2: An Ionic Lever that consisted of two identical Ionic Flyers which are connected to two independent power supplies. a) The Ionic lever is balance since both Ionic Flyers is applied with *18kV*, b) The Ionic Lever rotated clockwisely when the applied voltage to the Ionic Flyer in the left-hand side decreased gradually from *18kV* to *17kV*. The Lever can become balance again once the applied voltage raise to 18kV again.

6.2 Application of MEMS Motion Sensors and Wireless Signal Transmission

Application of MEMS motion sensors and wireless signal transmission is important in the future development of the Hybrid Ionic Flyer. However, it is believed that most electronic components would not able to work in the circumstance of high electric field because interference may exists and electrostatic charges may also cause damages to the MEMS sensors. It is expected that the high-strength electric field is concentrated in the gap between the electrodes of the Ionic Flyer. The inner space of the Ionic Flyer, that the sensors and the wireless modulus can be housed, is expected not to be insignificantly affected by the high-strength electric field. In this section, we will demonstrate the applications of MEMS motion sensors and Bluetooth wireless commumication in the Ionic Flyer.

The experimensts were carried out by investigating a *μ-IMU* that were housed on a Ionic Flyers. The *μ-IMU* is mainly consisted of an *Analog Device ADXL311* accelecrometer, a *Atmel ATmega32L* microcontroller and a *BlueRadio C30AH* Bluetooth module as shown in Figure 6.3. The accelerometer can sense the body frame accelerations and angular rates of the Ionic Flyer. The output signals of the accelerometer are measured directly by the A/D converter of the microcontroller. The serial Bluetooth tranceiver is implemented via a USART connection with MCU for wireless communications. The digital sample rate of the sensor unit is *200Hz* and the transmit baud rate is *57.6kbps*.

The experiments were partitioned into two sections. In the first section, we will demonstrate that the *μ-IMU* can work proporly under the high-strength electric field of the Ionic Flyer. The wireless signal of the accelerometer was first recorded (see Figure 6.4A) by putting the *μ-IMU* in a table (The signal represents that the sensor is stationary at normal condition). The *μ-IMU* was then housed in the *Ionic Flyer B* (refer to the previous chapter for the configurations of the *Ionic Flyer B*). When the *Ionic Flyer B* is applied with high voltage of *20kV*, the wireless signal was not blocked by the high-

strength electric field. The signal was then recorded and displayed in Figure 6.4B. Finally, the Ionic Flyer was subjected to vibration while it was operating at *26kV*. The sensory signal is shown at Figure 6.4C.

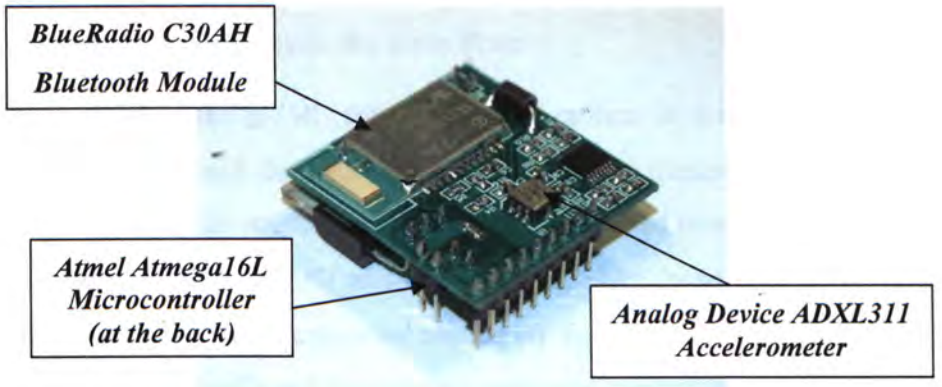

Figure 6.3: The *μ-IMU* which consists of an *Analog Device ADXL311* accelerometer, an *Atmel ATmega32L MCU* and a *BlueRadio C30AH* Bluetooth module.

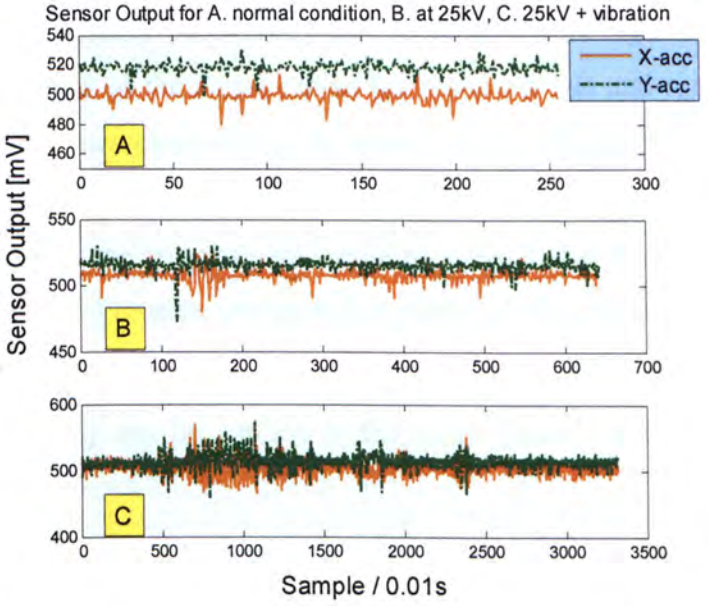

Figure 6.4: Wireless sensor signal of the *μ-IMU*. The *Ionic Flyer B* is: (A) stationary with zero applied voltage; (B) stationary with applied voltage of *20kV*; (C) vibration with applied voltage of *26kV*

The *Signal to Noise Ratio* (i.e. $SNR = 20\log(V_{signal} / V_{STDEV})$) for the two axis accelerations in (A) are *42.2dB and 42.3dB* respectively. While for the results in (B), the

SNR are *43.67dB* and *44dB*. So, it is apparent that the the high-strength electric field will not interfere or even block the wireless transmission as the *μ-IMU* is housed in the inner space of the Ionic Flyer. Moreover, as indicated in (C), the vibartions of the Ionic Flyer is well tracked by the accelerometer. Hence, commerical accerometers like *Analog Device ADXL311* can work properly inside the Ionic Flyer.

In the interest of using the *μ-IMU* for tracking the motion of the Ionic Flyers, a "Ionic Lever" was constructed and the experimental procedure is illustrated in Figure 6.5. The Ionic Lever has the similar structure as the one that described in section 6.1.2 except that it was fixed to a pivot. The *μ-IMU* was housed in the pivot to keep tracking the rotation of the Ionic Lever. The experiments were carried out by "rotating" the Ionic Lever at four angles (*15°, 20°, 30°* and *40°*) and the sensor signal was transmitted wirelessly to the host computer. The *μ-IMU* has been calibrated with the sensitivity of *145mV/g*. The experimental results are shown in Figure 6.6 with (a), (b), (c) and (d) corresponding to the angles of rotation of *15°, 20°, 30°* and *40°* respectively.

The sensor signals oscillate periodically as indicated in the figure. The oscillation amplitude and frequency of the signal reflect the rotation angle and speed respectively. As the Ionic Lever rotates clockwisely, the sensor signal falls to an amplitude $\Delta V-$; while it rotate anti-clockwisely, the sensor signal rises to an amplitude $\Delta V+$. As the rotation speed increases, the sensor signal oscillates with a higher frequency. As indicated in Figure 6.5, the angle of rotation can be well predicted by the sensor signal.

To conclude, MEMS motion sensors (like accelerometer) and wireless communication module (like Bluetooth) can be applied in the Ionic Flyers for motion tracking and wireless automating.

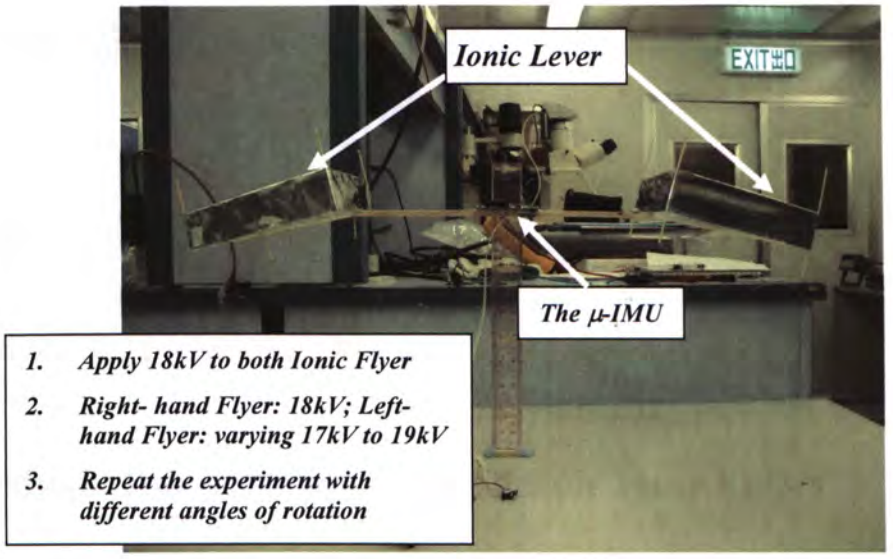

Figure 6.5: Experimental setup for the measurement of angle rotation of the Ionic Flyer by the application of the *μ–IMU*

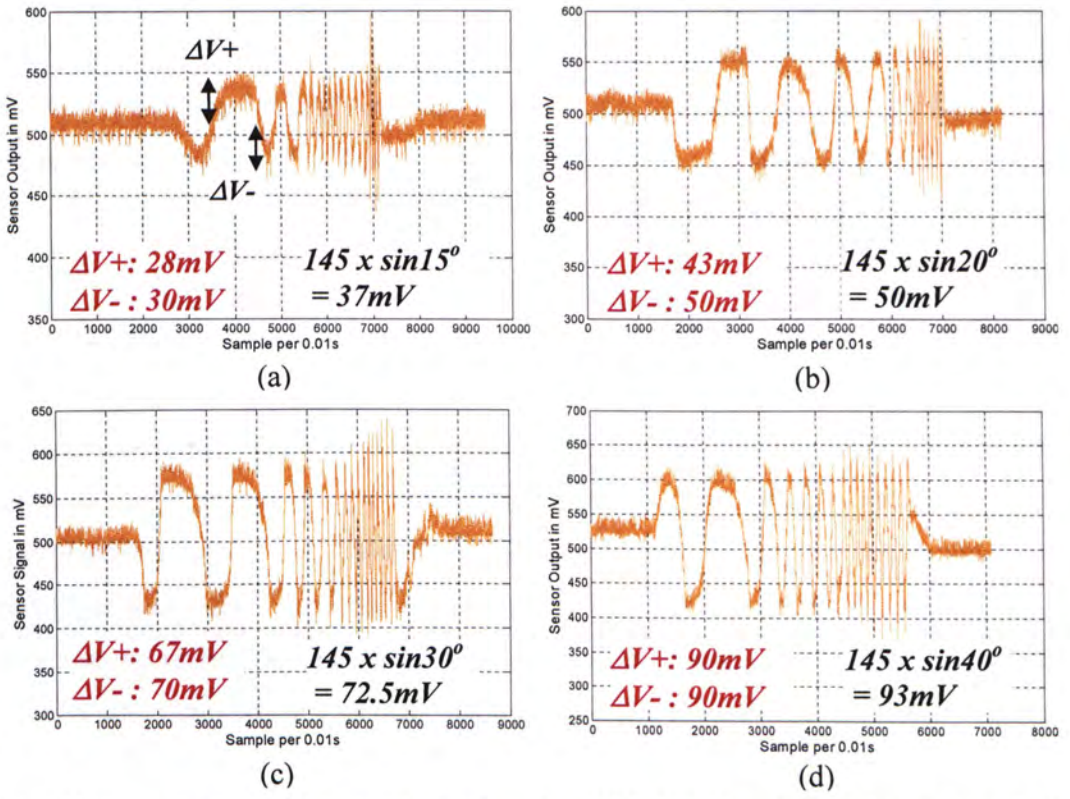

Figure 6.6: The wireless sensor signals from the *μ-IMU* which housed on the Ionic Lever. The Ionic Lever rotated at (a) 15^o ; (b) 20^o ; (c) 30^o and (d) 40^o

Chapter 7

Future Work

7.1 Single-Emitter-Multiple-Collector Ionic Flyers

The Ionic Flyer that is discussed in this dissertation has a single-emitter-single-collector configuration. We have already proved that the wire-emitter is more critical than the plate-collector in affecting the working performance, which is characterized by the *current gain*, *force gain*, *onset voltage* and *barrier voltage* of the Ionic Flyer. It is interested to develop Ionic Flyers with single-emitter-multiple-collector configuration by increasing the number of collectors. In this section, the feasibility of accomplishing a higher force/power ratio by the single-emitter-multiple-collector Ionic Flyer will be discussed.

It is preferable to maximize the magnitude of the vertical component electric force that acts on the ions. In this case, single-emitter-multiple-collector configuration may take this advantage when compare to single-emitter-single-collector configuration. An online shareware *Electromagnetic Kinetic Analyzer* [38] is applied to simulate the basic ion flow in the electrode gap for a single-wire-single-collector and the single-wire-double-collector Ionic Flyer under the same applied voltage. Although the simulation does not take into account some reality factors, like diffusion or space charge effects, it can simulate the basic ion cloud movement and flow distribution. Figure 7.1 shows the simulation results, the double-collector flyer display a better electric field contour than the single-collector flyer because comparatively more ions go along vertical path.

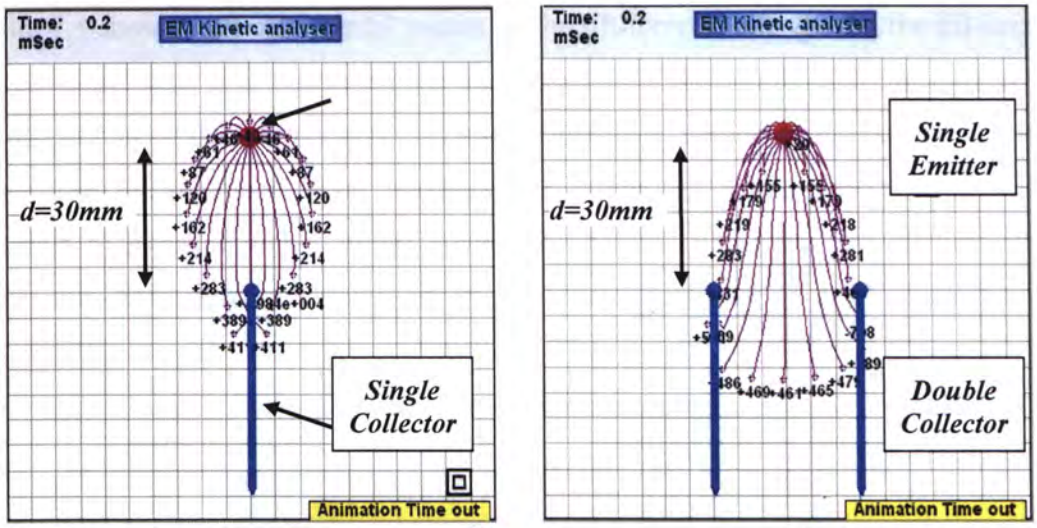

Figure 7.1: Simulations by the *Electromagnetic Kinetic Analyzer* [38] on the ion flow between the electrode gap of the Ionic Flyer with a) single-emitter-single-collector configuration and b) single-emitter-double-collector configuration.

Based on the simulation results, an Ionic Flyer with single-emitter-double-collector configuration were constructed as shown in Figure 7.2. As indicated in the figure, it has the wire length L_w of *660mm*, the outer collector length L_1 of *900mm,* the inner collector length L_2 of *480mm*, the gap distance d of *30mm* and the collector height of *40mm*. For the single-collector flyer, the emitter length is equal to the collector length (as well as the electrode length). However, the emitter length of the double-collector flyer is much smaller than the total collector length. In Figure 7.3, we have compared the *I-V* characteristics of the double-collector flyer with two single-collector flyers that have *L=600mm (comparable to the emitter length of the double-collector flyer)* and *L=1350mm (comparable to the collector length of the double-collector flyer)* respectively. As indicated in the figure, the current gain C and onset voltage V_0 of the double-collector flyer are $0.001406mA/kV^2$ and *5.804kV* respectively. Obviously, its *I-V* relationship is closer to the *600mm-length* single-collector flyer. On the other hand, its onset voltage can still be well predicted by the modified Peek's formula. Since the wire-emitter governs the ion generation, it is reasonable that the current consumption of the double-collector flyer is close to that of single-collector flyers that have the same emitter length.

Figure 7.4 shows the experimental results on the lift-force to voltage and the lift-force to power relationship. It is interesting that the force gain of the double-collector flyer is very similar to that of the *1350-length* single-collector flyer. However, the barrier voltage is larger than the predicted value. As indicated in Figure 7.4 (b), although the double-collector flyer has a higher Initial Power Dissipation (*IPD*), the force/power ratio is higher than the single-collector flyers as the power input reaches *12W*. In the future, I suggest others to carry out more experiments on it.

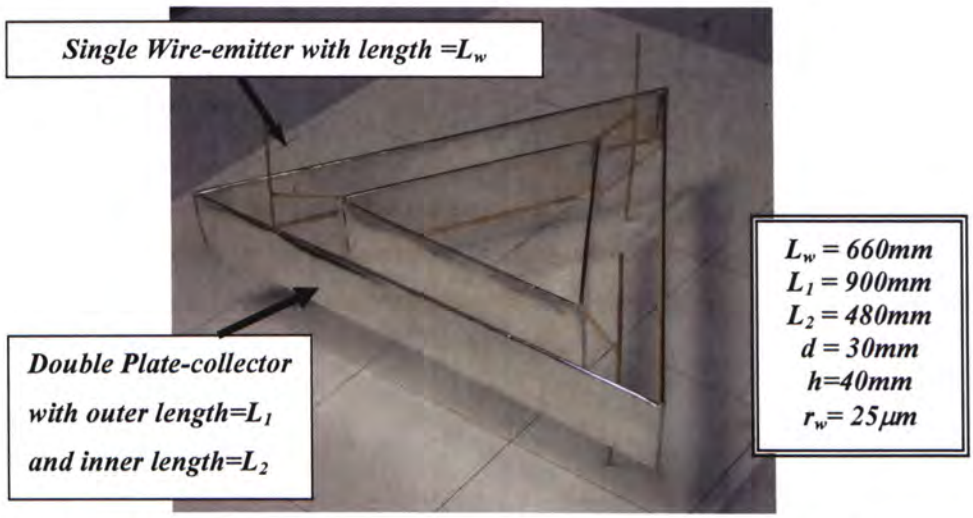

Figure 7.2: A Ionic Flyer has single-emitter-double-collector configuration.

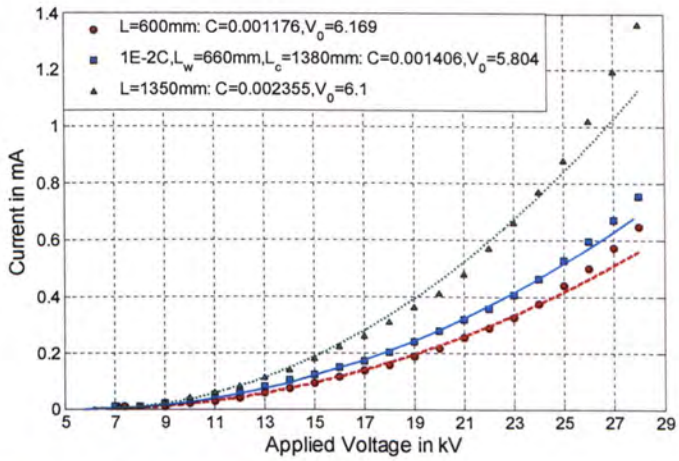

Figure 7.3: Experimental (square points) and derived (blue solid line) current to voltage relationship for the single-emitter-double-collector Ionic Flyer as described in Figure 7.2. The other two curves are the results of the two single-emitter-single-collector Ionic Flyer with *L=600mm* and *L=1350mm* respectively

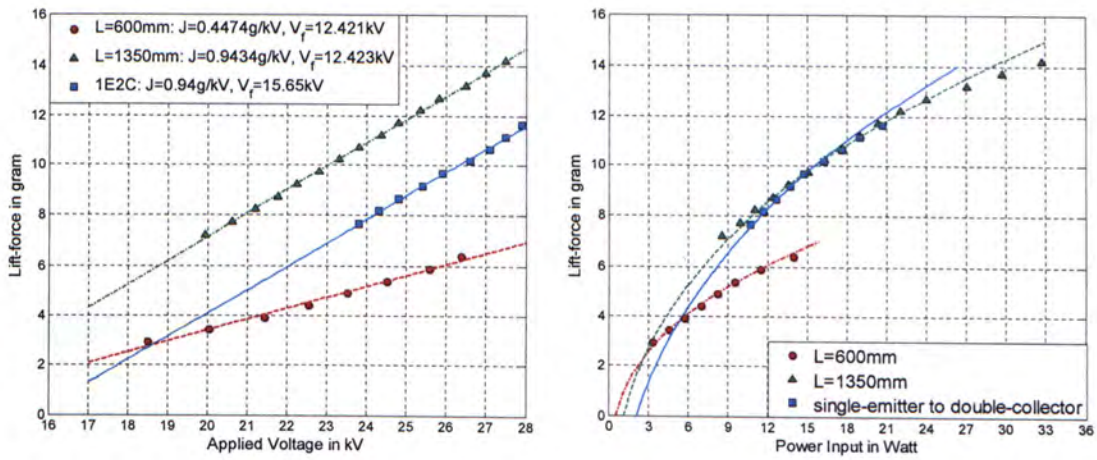

Figure 7.4: Experimental (square points) and derived (blue solid line) (a) lift-force to voltage and (b) lift-force to power relationship for the single-emitter-double-collector Ionic Flyer as described in Figure 7.2. The other two curves are the results of the two single-emitter-single-collector Ionic Flyer with *L=600mm* and *L=1350mm* respectively.

7.2 Development of Miniaturized High-voltage Power Supply

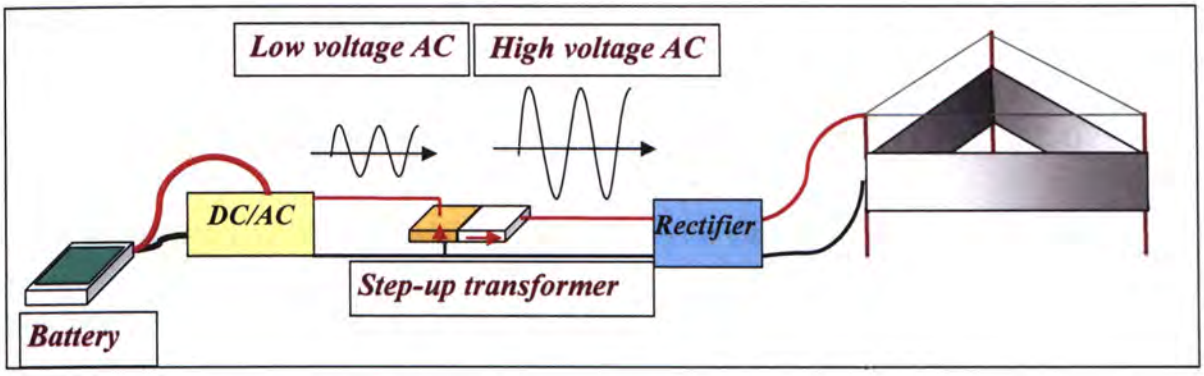

Figure 7.5: The schematic representation of the on broad power supply

Development of miniaturization power supplies is a major concern in the future development of the Ionic Flyer (see Figure 7.5). Recent research activities in the piezoelectric transformers indicate a trend to replace the conventional electromagnetic transformers in high voltage power supplies. Piezoelectric transformers utilize piezoelectric effect to generate high voltage. Since it is constructed from a ceramic bar and does not include any magnetic material, potential benefits over conventional electromagnetic transformers include reduced size, inflammable and free of leakage of magnetic flux. This section discusses the feasibility of using piezoelectric transformers to develop a high voltage power supply for the Ionic Flyer.

The developed high voltage power supply is composed of the piezoelectric transformer, a Cockcroft Walton Multiplier and a MCU-controlled driver circuit as presented in Figure 7.6 (the circuit schematic is given in Appendix A). The total weight of the circuit is *64 gram* including 31-gram lithium-ion batteries. The piezoelectric transformer employed is manufactured by Kong Hong [39]. It has a resonance frequency of $47 \pm 2kHz$ and maximum voltage step-up ratio of $120 \pm 5kHz$. The maximum output voltage and power is *3.2kV* peak to peak and *8.5W* respectively. The piezoelectric transformer is driven by an oscillating wave and this is accomplished by the MCU-controlled driver circuit. The amplified voltage at output terminals of the piezoelectric transformer is then further amplified and rectified by the six-stage Cockcroft Walton Multiplier. The output is in an

ideal case equal to the amplitide of the input voltage multiplied by six times (i.e. *18kV)*. The output loading R_{load} that connect to the output of the Cockcroft Walton Multiplier is related to the input imperdance R_{in} by [40]:

$$R_{in} = \frac{R_{load}}{8n^2} \qquad \textbf{(7.2.1)}$$

where n is the number of stages which is equal to 6 in the circuit.

Since the optimal loading for the piezoelectric transformer is about $350k\Omega$. To achieve the optimal performance of the piezoelectric transformer (i.e. maximum step up ratio and power output), the output loading of the Cockcroft Walton Multiplier is $100M\Omega$ based on equation (7.2.1). By using a resistor of $100M\Omega$ to test the performance of the circuit, a current of *0.18mA* is obtained. Thus the output voltage of the circuit is about *18kV* and the output power is *3.24W* at the loading of $100M\Omega$. Based on the *I-V* and lift-force models of the Ionic Flyer, the high voltage circuit is able to lift-up a *2.1-gram* triangular Ionic Flyer with $L = 600mm$, $d = 30mm$, $r_w = 25mm$ and $h = 40mm$. However, the circuit (including the battery) is still too heavy to be carried by the Ionic Flyer.

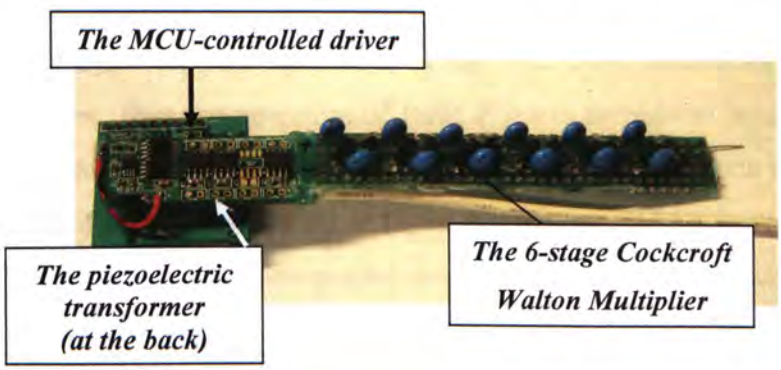

Figure 7.6: The high voltage power supply consists of a piezoelectric transformer, a MCU-controlled driver circuit and a 6-stage Cockcroft Walton Multiplier

Chapter 8

Conclusion

A novel indoor flyer, called the Ionic Flyer, which does not contain any mechanical moving parts and uses only high-voltage electrical energy to produce thrust has been developed. The Ionic Flyer, as demonstrated in our laboratory, could be levitated in mid-air, operates without any moving parts, and produces no noise during its flight. Experimental studies have been parametrically carried out to understand and evaluate the working performance of the Ionic Flyer with wire-plate configuration.

8.1 The Electrical Current to Voltage Model

This dissertation presents an experimental derived electrical current to voltage model of the Ionic Flyer. The wire-plate electrodes of the Ionic Flyer have substantially different radii of curvatures, thus the operation of Ionic Flyer is dominated by corona discharge. Experimental studies show consistence properties between the corona discharge and the current-voltage relationship of the Ionic Flyer. A quadratic current to voltage relationship is derived experimentally and the equation is characterized by two parameters: the current gain C and the onset voltage V_0. Six structural parameters of the Ionic Flyer, including the electrode length (L), the gap distance between the wire-emitter and the plate-collector (d), the wire-emitter radius (r_w), the collector height (h) and the electrode enclosed area (A) have been investigated systematically on how they affect the current gain and the onset voltage. The current gain C is derived experimentally to be proportional to the electrode length and in inverse-square relationship to the gap distance. The onset voltage is proved experimentally can be well predicted by the Peek's equation with a modification factor.

Finally, an environmental constant K_e is determined to concern the environmental conditions, thus a general *I-V* model is obtained. The current to voltage relationship of Ionic Flyers with wire-plate configuration can be predicted by the general *I-V* model in stand temperature and pressure with a variation of less than *10%* guarantee.

8.2 The Mechanical Lift-force to Power Model

Based on the *I-V* model, the power consumption of the Ionic Flyers with different configurations of the structural parameters can be predicted. Experiments were carried out to further study the lift-force to input power relationship of the Ionic Flyer. A linear equation, characterized by the force again J and barrier voltage V_f is obtained to describe the lift-force to voltage relationship. Based on the *I-V* model and the lift-force to voltage relationship, a third-order equation on the lift-force to power relationship is derived. The five structural parameters are systematic evaluated on the relationship to the lift-force to power relationship. Based on the results, the power requirements and the corresponding lift-force acting on the Ionic Flyers with different configurations can be predicted

8.3 The Force/Power Ratio Model

Based on the power input to applied voltage relationship and the lift-force to applied voltage relationship, an equation describing the force/power ratio of the Ionic Flyer is derived. Based on our results, we proved that Ionic Flyers based on engineering requirement and optimal force/power ratio can also be realized by using the derived models.

Appendix A

Circuit Schematics

1. The μ-IMU
2. Driver circuit for pizeo-transformer

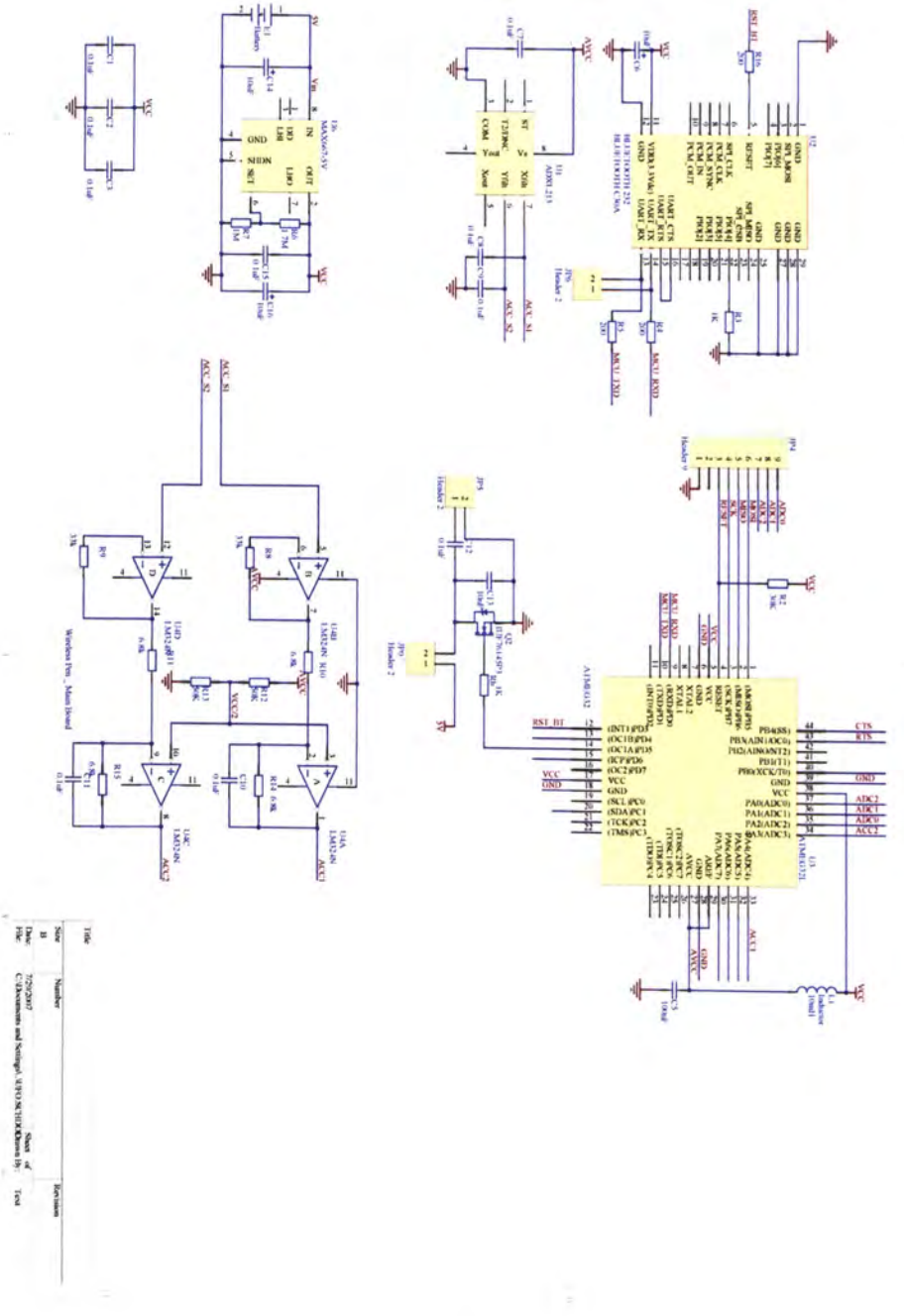

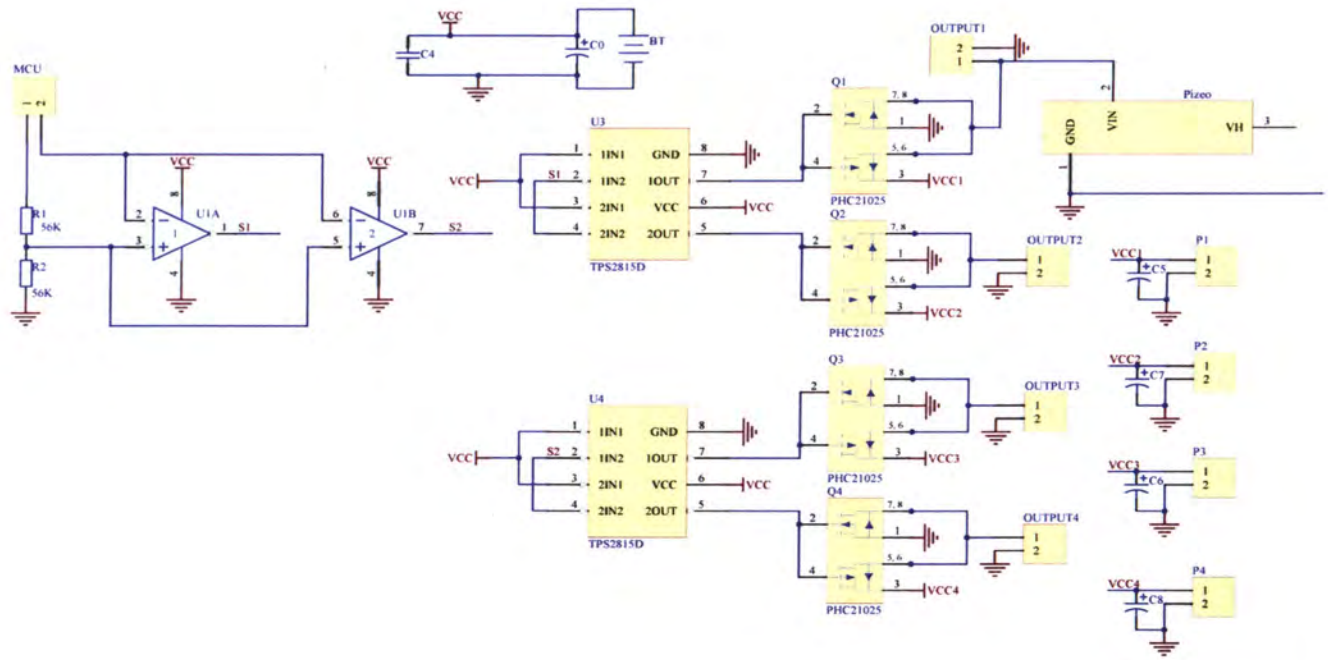

Title		
Size: A4	Number	Revision
Date: 7/29/2007	Sheet of	
File: C:\Documents and Settings\..\Design3.SCHDOC	Drawn By:	

Bibliography

[1] Aerodynamics, *http://en.wikipedia.org/wiki/Aerodynamics*.

[2] J. Gordon Leishman, *Principles of Helicopter Aerodynamics, Second Edition*, Cambridge University Press

[3] William R. Davis, Jr., Bernard B. Kosicki, Don M. Boroson and Daniel F. Kostishack, Micro Vehicles for Optical Surveillance, *The Lincoln Laboratory Journal*, vol.9, no.2, 1996

[4] T. Nick Pornsin-sirirak, Y. C. Tai, H. Nassef and C. M. Ho, Titanium-alloy MEMS Wing Technology for A Micro Aerial Vehicle Application, *Sensors and Actuators*, vol.A89, no.1-2, pp.95–103, 2001.

[5] J. Nicoud and J. C. Zufferey, Toward indoor flying robots, *Proceedings of IEEE/RSJ International Conference on Intelligent Robots and Systems*, pp. 787– 792, 2002.

[6] Closed Quarter Aerial Robotic, *http://www.pages.drexel.edu/~weg22/CQAR.html*

[7] Jean-Christophe Zufferey, Adam Klaptocz, Antoine Beyeler, Jean-Daniel Nicoud and Dario Floreano, A 10-gram Microflyer for Vision-based Indoor Navigation, *Proceedings of the 2006 IEEE/RSJ International Conference on Intelligent Robots and Systems*, Beijing, pp. 3267 – 3272, 2006

[8] Srikanth Saripalli, David J. Naffin, and Gaurav S. Sukhatme, Autonomous Flying Vehicle Research at the University of Southern California, In Multi-Robot Systems: From Swarms to Intelligent Automata, *Proceedings of the First International Workshop on Multi-Robot Systems*, A. Schultz and L. E. Parker (eds.), pp. 73-82, Kluwer Academic Publishers, 2002

[9] Wei Wang, Gang Song, Kenzou Nonami, Mitsuo Hirata and Osamu Miyazawa, Autonomous Control for Micro-Flying Robot and Small Wireless Helicopter X.R.B, *Proceedings of the 2006 IEEE/RSJ International Conference on Intelligent Robots and Systems*, Beijing, pp 2906 – 2911, 2006

[10] J.C. Zufferey and D. Floreano, Fly-inspired visual steering of an ultralight indoor aircraft, *IEEE Transactions on Robotics*, vol. 22, pp. 137–146, 2006.

[11] James Lighthill, A general introduction to aeroacoustics and atmospheric sound, *Presented at the ICASE/NASA Langley Research Center Workshop on Aeroacoustics*, 6-9 Apr. 1992

[12] *Alexander P. de Seversky, "Ionocraft," U.S. Patent 3 130 945, April 28, 1964.*

[13] Hans Fantel, Major De Seversky's Ion-Propelled Aircraft, August 1964, *http://www.rexresearch.com/desev/desev.htm*

[14] The JLN Labs, *http://jnaudin.free.fr*

[15] Blaze Lab Research, *http://www.blazelabs.com/l-intro.asp*

[16] JLN Labs Groups, *http://tech.groups.yahoo.com/group/Lifters/*

[17] AmericanAntigravity Groups, *http://tech.groups.yahoo.com/group/americanantigravity/*

[18] W. Stein and J. Rusek, Electrokinetic Propulsion for Exoatmospheric Applications, *Int. Conf. on Green Propellant for Space Propulsion*, European Space Research and Technology Center, June 2001.

[19] T. C. Lober, III, Outside the Box Space and Terrestrial Transportation and Energy Technologies for the 21st Century, *AIAA Paper*, pp.2002-1131, 2002.

[20] Takaaki Musha, The Possibility of Strong Coupling Between Electricity and Gravitation, *Infinite Energy Magazine Issue 53,* pp. 61-64, Jan-Feb 2004.

[21] M. Tajmar, Biefeld-Brown Effect: Misinterpretation of Corona Wind Phenomena, *AIAA Journal*, vol. 42, No. 2, pp. 315-318, February 2004.

[22] E. Kuffel, W.S. Zaengl and J. Kuffel, *High Voltage Engineering: Fundamentals, Second Edition*, Oxford, Boston, Newnes, 2000

[23] F. W. Peek, Jr., *Dielectric Phenomena in High Voltage Engineering, 3rd edition.,* New York, McGraw-Hill Book Company

[24] L. B. Loeb, *Electrical Coronas*, University of California Press, London, England, 1965.

[25] J. D. Cobine, Gaseous Conductors, *Dover*, New York, 1958

[26] R. Morrow, The Theory of Positive Glow Corona, *J Phys D: Appl. Phys*, 1997, 30(22): pp 3099-3114

[27] T. Musha and I. Abe, Biefeld-Brown Effect and Electro-gravitic Propulsion by High Potential Electric Field, *Proceeding. of the 24th JSASS Annual Meeting*, JSASS, pp.189-192 (in Japanese), 1993

[28] A. M. Howatson, *An Introduction To Gas Discharge, 1st edition*, Oxford, New York, Pergamon Press, 1965

[29] J. S. Townsend, *Electricity in Gases*. Oxford Press, 1914.

[30] Stand Temperature and Pressure:
http://en.wikipedia.org/wiki/Standard_temperature_and_pressure

[31] F. W. Peek, Jr., 1911, *Trans. AIEE.* 30 1889

[32] R. S. Sigmond, 1982 *J. Appl. Phys.* 53 891

[33] R. T. Waters and W. B. Stark, 1975 *J. Phys. D: Appl. Phys.* 8 1652

[34] J. E. Jones, A. Boulloud and R. T. Waters, 1990 *J. Phys. D: Appl. Phys.* 23 1652

[35] The MathWorks Documentation, Curve Fitting Toolbox,
http://www.mathworks.com/access/helpdesk/help/toolbox/curvefit/bqxosqu.html#f1-57616

[36] A. Boulloud and J. Charrier, 1981 *J. Phys. D: Appl. Phys.* 14 207

[37] Dan Rafiroiu, Ilie Suarasan, Roman Morar, Pierre Atten, L. Dascalescu, Inception of Corona Discharge in Typical Electrode Configurations for Electrostatic Processes Applications, *Industry Applications Conference, 1999. Thirty-Fourth IAS Annual Meeting.* Conference Record of the 1999 IEEE, vol. 1, pp. 387 – 392

[38] Xavier Borg, Electromagnetic Kinetic Analyzer, Blaze Labs Research,
http://www.blazelabs.com/l-emk.asp

[39] Piezoelectric Ceramics Transformer, Model: MPT3608A85L0, Xi'an Kong Hong New Materials Sci-tech Co.,Ltd, *http://www.konghong.com*

[40] M. Imori, T. Taniguchi and H. Matsumoto, A Photomultiplier High Voltage Power Supply Incorporating a Piezoelectric Ceramic Transformer, *IEEE Transactions on Nuclear Science*, 43(1996) pp.1427-1431.